University of Pannonia

Doctoral School of Chemical Engineering and Material Sciences

Submitted for the degree of
Doctor of Philosophy
of the University of Pannonia, Hungary

Author: Zixiang Gao

DOI:10.18136/PE.2024.889

Supervisor(s): Dr. habil. Gusztáv Fekete and Dr. András Kovács

Dissertation Title: Towards improved Understanding of Running Fatigue and Gait Asymmetry

Veszprém
2024

Towards improved Understanding of Running Fatigue and Gait Asymmetry

Thesis for obtaining a PhD degree in the Doctoral School of Chemical Engineering and Material Sciences of the University of Pannonia

in the branch of Bio-, Environmental- and Chemical engineering

Written by
Zixiang Gao

Supervisor: **Dr. habil. Gusztáv Fekete**
Co-supervisor: **Dr. András Kovács**

propose acceptance (yes / no)

…….……...……
(Supervisor)

propose acceptance (yes / no)

…….……...……
(Co-supervisor)

As reviewer, I propose acceptance of the thesis:

Name of Reviewer: ……..……...…….……yes / no

…….……...……
(reviewer)

Name of Reviewer: ……..……...…….……yes / no

…….……...……
(reviewer)

The PhD-candidate has achieved ….....% at the public discussion.
Veszprém,

…….……...……
(Chairman of the Committee)

The grade of the PhD Diploma …..... (…….. %)
Veszprém,

…….……...……
(Chair of the UDHC)

Content

Towards improved Understanding of Running Fatigue and Gait Asymmetry

Abstract

The popularity of long-distance running as an easily accessible and promoted sport has increased within the last four decades. However, the incidence of musculoskeletal injuries caused by running has also increased rapidly, especially in the lower extremities of amateur runner. It should, however, be noted that the etiology of running fatigue-induced injuries is multifactorial and complex. Fatigue-induced changes in the symmetry of the lower limbs may be one of the major causes of unilateral limb overloading.

The first research question of this thesis: Fatigue gait risk is associated with shifts in the distribution of bilateral plantar pressure. Therefore, human activity recognition (HAR) methods based on wearable sensors and deep learning algorithms have been widely developed in the last decade. Despite significant strides in gait and biomechanics analysis, research into automated fatigue gait recognition with data-driven models remains insufficient. Force plates or insoles with force transducers are easy to use relative to other biomechanical data collection methods, saving time in experimental setup data collection. Therefore, this study intends to use a deep learning algorithm based on bilateral plantar pressure data for the early identification of fatigue gait.

The first objective of this thesis: Detecting fatigue at the early stages of a run could aid training programs in making adjustments, thereby reducing the heightened risk of injuries from overuse. The study aimed to investigate the effects of running fatigue on plantar force distribution in the dominant and nondominant feet of amateur runners. The Convolutional Long Short-Term Memory Network (ConvLSTM) model will be used in this study on the ground that it transforms the structure of recurrent neural networks into a convolutional structure, thereby preserving the spatial and temporal information of plantar pressure.

The second research question of this thesis: Although many studies have investigated the acute effects of long-distance running on gait symmetry, they have mainly focused on exploring pre- and post-fatigue comparisons. One gap is the lack of understanding of how symmetry changes during various stages of long-distance running. In addition, researchers have utilized various techniques from chaos theory and information theory to enhance their understanding of the intricacies of gait behavior. Although nonlinear evaluation is important in the quantification of gait stability, there is a lack of research on gait asymmetry.

The second objective of this thesis: This part focuses on understanding the variations in gait symmetry during a prolonged running activity. Specifically, the question seeks to unravel how the dynamic stability of gait symmetry, as quantified by the Largest Lyapunov exponent (LyE), alters across different stages of a 10-kilometer run among amateur male runners. The results of present study could provide a towards improved understanding of the symmetry of long-distance running.

The third research question of this thesis: Understanding the internal load characteristics of the knee joint is essential for investigating unilateral knee injuries associated with running. previous studies on fatigue and differences in load between limbs haves not precisely addressed the distribution and extent of the load on the knee joint's internal tissues, potentially missing key insights into the causes of unilateral limb injuries.

The third objective of this thesis: The aim of this study is to determine whether there are differences in the location and magnitude of von Mises stress in the internal structures of both knee joints during the stance phase of gait, and to investigate the effects of running at the submaximal speed for 10 kilometers on these internal structures. The findings enhance our understanding of the impact of running-induced fatigue on bilateral knee joint loading. It provides a detailed analysis of factors leading to unilateral knee overload during extended running. These insights are essential in formulating targeted strategies to reduce injury risks.

In summary, this study investigates the biomechanical implications of long-distance running, focusing on the potential relationship between running-induced fatigue and the risk of musculoskeletal injury in amateur runners. It delves into three key areas: using deep learning algorithms to detect fatigue gait through changes in bilateral plantar pressures, analyzing nonlinear changes in gait symmetry during long-distance running, and exploring internal knee loading characteristics to understand unilateral knee injury mechanisms. This study aims to provide new insights into the prevention and management of running-related injuries by comprehensively analyzing gait dynamics and joint loading at different stages of long-distance running.

Abbreviations

HAR: human activity recognition
LyE: Largest Lyapunov exponent
DS: Dynamic stability
CNS: central nervous system
OA: Osteoarthritis
SA: symmetry angle
GRF: ground reaction force
IMU: Inertial Measurement Unit
HAR: Activity Recognition
SVM: support vector machine
CNN: Convolutional neural network
LSTM: Long Short-Term Memory Network
NMS: neuromuscular skeletal
EMG: electromyographic
RRA: Residual Reduction Algorithm
CMC: Computed Muscle Control
FE: finite element
LCL: lateral collateral ligament
MCL: medial collateral ligament
ACL: anterior cruciate ligament
PCL: posterior cruciate ligament
PT: patellar tendon
ConvLSTM: Convolutional Long Short-Term Memory Network
H: Hallux
OT: Other toe
M1-M5: Metatarsal 1-5
MF: Midfoot
HM: Medial heel
HL: Lateral heel
API: Application Programming Interface
IC: initial contact
FP: first peak
MS: mid-stance
SP: second peak
TO: Toe-off
SF: Symmetry Function
MRI: magnetic resonance imaging
SPM1d: statistical parameter mapping 1d
SD: Standard Deviation
HSD: Honest Significant Differences
RMS: root mean square
MVC: maximum voluntary contraction

List of Figures

List of Tables

1. Introduction

1.1 The structure and functions of human lower limbs

1.1.1 The structure of human lower limbs

The human lower limb locomotor system is constructed by three important components: skeletal tissue, joints and skeletal muscles. In this system, the femur and tibia play a major supporting role in human gait tasks[1]. Bones are connected to each other by ligaments to form joints as the pivot of movement, which in the lower limbs mainly include the hip, knee and ankle joints[2]. The hip joint is a pestle and mortar joint consisting of two components, the head of the femur and the acetabulum. It is an essential joint that connects the body's abdomen to the lower thigh and is the most deeply located joint in the body[3]. The anatomical structure of hip joint is depicted in Figure 1.1.1.

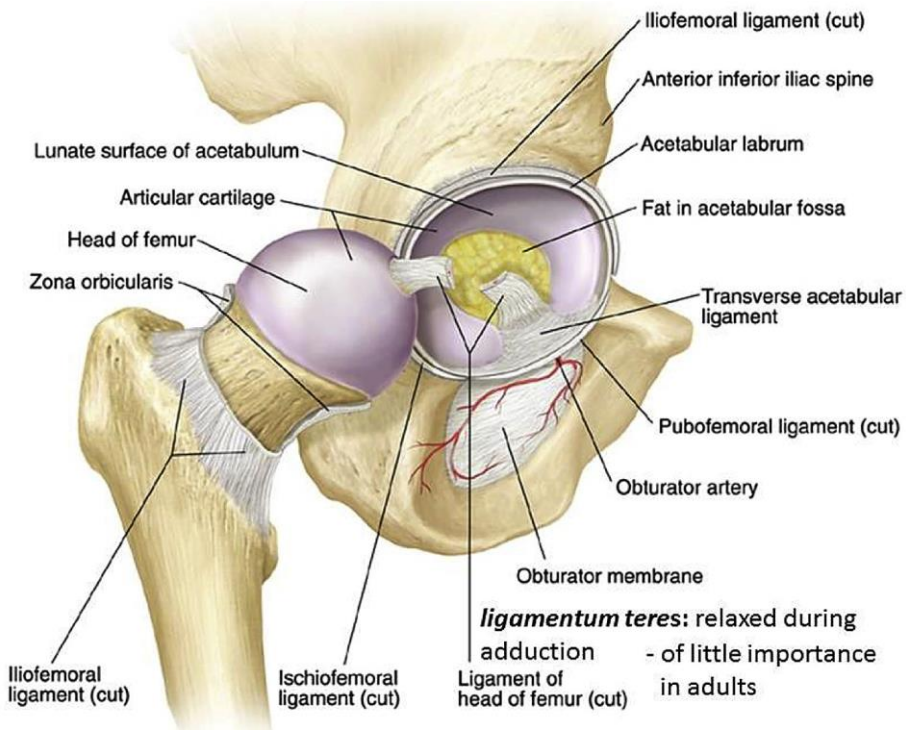

Figure 1.1.1 Anatomical structure of the hip joint[4]

The spherical femoral head can rotate in all directions in the socket-like acetabulum during movement, and their surfaces are covered with a thick layer of cartilage, which functions to reduce friction, absorb impact, and dampen vibrations[5]. In addition, the hip joint possesses a robust and thick articular capsule along with intricate ligaments that serve a supportive role. The function of the iliofemoral ligament is to limit overextension and adduction of the thigh to prevent joint

dislocation, the function of the pubofemoral ligament is to limit excessive abduction and external rotation of the joint, the function of the is chi femoral ligament is to limit excessive adduction and internal rotation, the function of the transverse acetabular ligament is to compensate for the notch in the acetabulum, and the function of the ligament of the femoral head is to limit joint flexion, adduction, and external rotation, maintaining the stability of the femoral head[6]. The hip joint also possesses well-developed muscles, which can participate in various types of movement tasks such as walking, running, and jumping. Movement of the hip joint revolves around three fundamental anatomical axes, encompassing flexion and extension about the coronal axis, adduction and abduction about the sagittal axis, and internal and external rotation around the vertical axis.

The knee joint, encompassing the tibiofemoral and patellofemoral joints, stands as one of the most intricate and fragile human joints. The knee joint is the largest and most complex joint in the human body. The primary function of the knee joint is to bear the weight of the body and support the main movements of flexion, internal and external rotation, and inversion and eversion in daily life[7]. Anatomically, the bony structure of the knee joint consists of four main bones: the distal femur (thigh bone), the proximal tibia (shinbone), the patella (kneecap), and the fibula. The soft tissue structure of the knee joint includes the femoral cartilage, tibial cartilage, medial and lateral menisci, anterior and posterior cruciate ligaments, medial and lateral collateral ligaments, and the patellar ligament[8]. The anatomical structure of knee joint is depicted in Figure 1.1. 2.

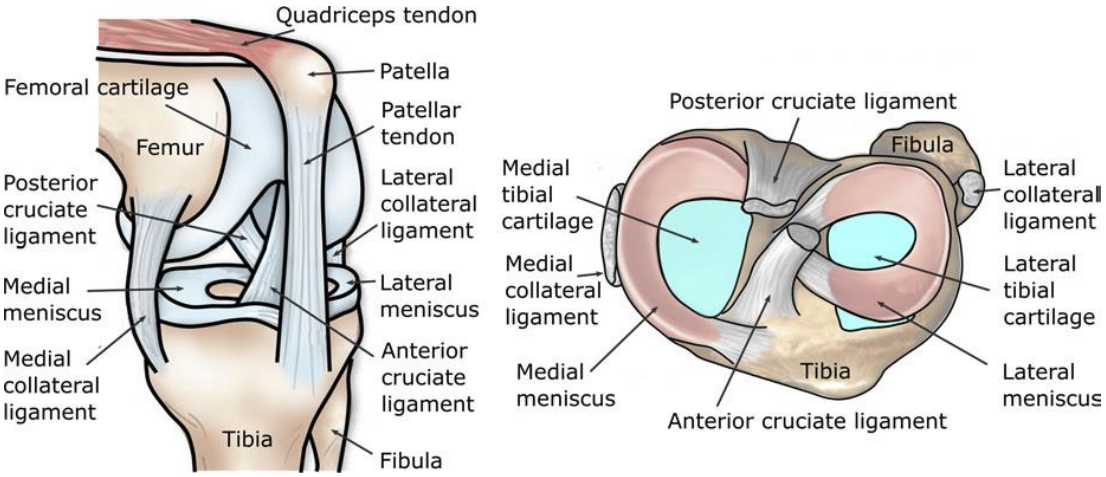

Figure 1.1.2 Antero-medial (left) and axial (right) view of the knee joint.[9]

At the back of the distal end of the femur, there are two rounded prominences known as the medial and lateral femoral condyles. The tibial plateau is the term for the tibial condyles found on the upper surface of the tibia. Research has shown that the femur undergoes sliding and rolling over the tibia to facilitate bending movements when the lower limb walks, with the bending axis

roughly corresponding to the line connecting the medial and lateral femoral condyles. The axis line is defined as the line connecting the most prominent point of the lateral femoral condyle and the deepest concavity of the medial condyle[10].

The articular cartilage, affixed to the femur, tibial plateau, and patella, is a translucent thin layer of connective tissue predominantly made up of cartilage cells and intercellular matrix. The articular cartilage offers a smooth surface for facilitating motion, enabling the femoral condyles to glide on the tibial plateau and preventing wear of the contact area. The meniscus, a vital part of the knee joint, is a fibrocartilaginous pad with a thick outer rim and a thin inner margin. Positioned on the joint surface of the tibial plateau, it is categorized into the medial and lateral menisci[11]. Serving as a shock absorber during bodily movements, the meniscus's role is to distribute the load between the femur and tibia, thus diminishing cartilage surface wear. Clinically, the meniscus is anatomically segmented into three parts: the anterior horn, the body, and the posterior horn[12]. The five major ligaments of the knee joint (anterior cruciate ligament, posterior cruciate ligament, medial collateral ligament, lateral collateral ligament, patellar ligament) play a crucial role in maintaining stability during its physiological movements[13, 14]. The anterior and posterior cruciate ligaments restrict the movement of the tibia relative to the femur, while the medial and lateral collateral ligaments control the knee's varus and valgus movements, as well as internal and external rotation[15, 16]. Additionally, the periphery of the knee joint cartilage is attached to the joint capsule, which acts as a lubricant, with fat filling the spaces. These tissue structures ensure that the knee joint stably performs a wide range of flexion and extension movements, as well as slight varus and valgus, and internal and external rotational movements.

The ankle joint is an essential joint that connects the leg to the foot and has a complex anatomical structure consisting mainly of bones, ligaments, tendons, and a joint capsule[17]. Bone structures include the tibia, fibula, and talus, which together form the joint that allows the foot to perform a variety of movements. Ligamentous structures, such as the anterior talofibular ligament, posterior talofibular ligament, medial collateral ligament, and lateral collateral ligament, provide stability to the ankle joint, limiting excessive motion and preventing injury. Tendons, especially the Achilles tendon, connect the calf muscles to the heel bone and play a key role in ankle motion[18]. In addition, the joint capsule and synovium surround the ankle joint and secrete synovial fluid to minimize friction and provide nourishment. The anatomical structure of knee joint is depicted in Figure 1.1. 3.

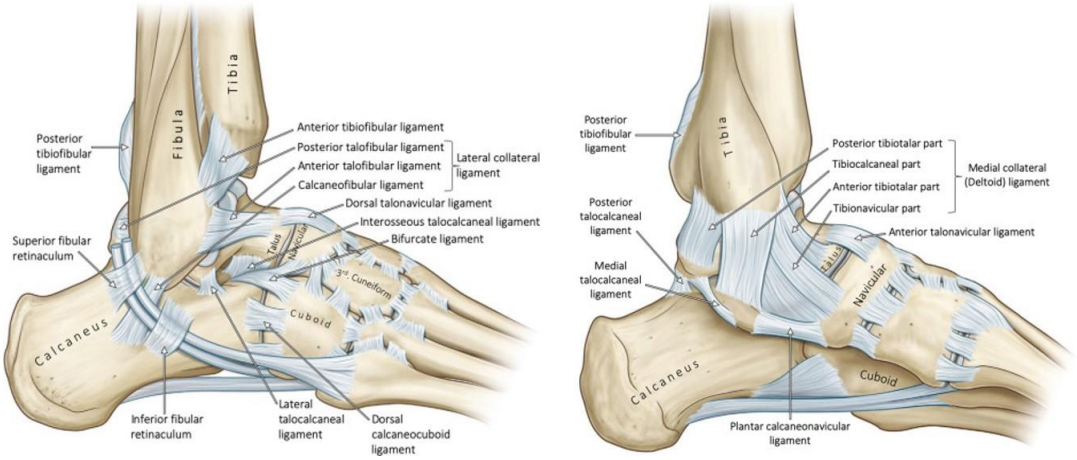

Figure 1.1.3 Medial collateral ligaments (right) and Lateral ligaments of the ankle and midtarsal joints (left) of the Ankle joint.[19]

Gait movement in the human body is facilitated through the ankle joint's interaction with the ground[17]. This involves active movements such as dorsiflexion (upward rotation of the foot around the joint's coronal axis) and plantar flexion (downward rotation of the foot around the joint's coronal axis) on the sagittal plane, inversion (inward rotation of the foot around the joint's sagittal axis) and eversion (outward rotation of the foot around the joint's sagittal axis) on the coronal plane, and internal (inward rotation of the foot around the joint's horizontal axis) and external rotation (inward rotation of the foot around the joint's horizontal axis) on the horizontal plane.

1.1.1 The functions of human lower limbs

During sport tasks, the thigh moves around the knee joint and the lower leg around the ankle joint, creating sliding and rotating motions. The hip, knee, and ankle joints are closely connected through bones, ligaments, and muscles, supporting and influencing each other, collectively coordinating the fundamental and important movement behavior of advancing the leg forward, thereby propelling the body forward. The task of gait consists of repetitive lifting and landing of both lower limbs, with these movements occurring at relatively consistent times. Analyzing phase division and parameter characteristics in the gait process is crucial before delving into lower limb movement, as it lays the groundwork for summarizing the general patterns and individual variations in human gait tasks. The full gait cycle is divisible into two phases: the stance phase and the swing phase. The stance phase is the period from heel contact to toe-off, where the foot is in contact with the ground and bears weight, constituting approximately 60% of the gait cycle. The swing phase describes the duration from when the support leg lifts off the ground and steps forward until it touches the ground again, making up roughly 40% of the gait cycle. While

walking, there are two instances when both feet contact the ground simultaneously, termed the double support phase, generally comprising 20% of the gait cycle, with the other stages characterized by single foot support, known as single support phases. The stance phase of gait can be subdivided into initial contact, loading response, mid-stance, terminal stance and push-swing phases, each named for the position of the ipsilateral foot. Conversely, the swing phase encompasses an initial swing phase, mind swing phase and terminal swing phase (Figure 1.1.4).
In the acceleration phase of the swing, the lower limbs swing forward, catching up and surpassing the torso. Conversely, during the deceleration phase, the lower limbs prepare for heel strike, setting the stage for the ensuing stance phase. However, the intricacies of human walking gait far exceed this simplified division. This categorization of the gait cycle, while a general simplification, provides a convenient and broadly accepted framework for analyzing muscle contraction changes in the lower limb joints throughout the gait cycle.

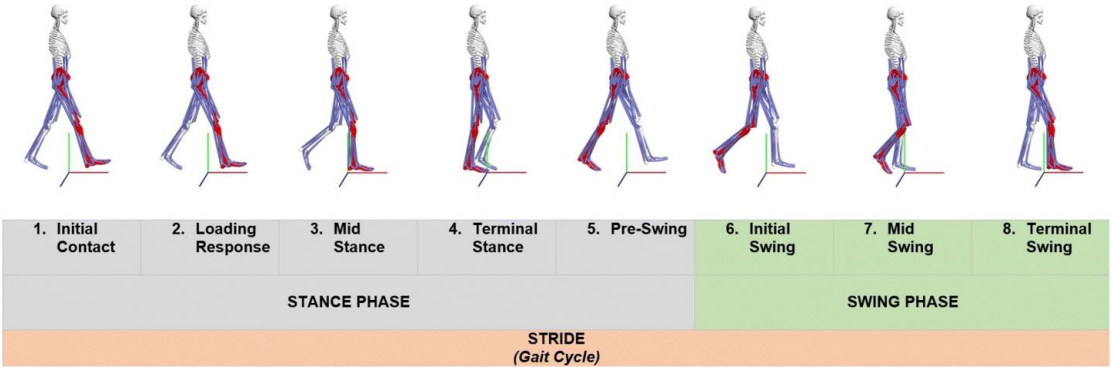

Figure 1.1.4 Pictorial representation of a one complete gait cycle [20]

The lower limbs of the human body experience a combination of ground reaction forces, muscle forces, and gravity when performing gait tasks. The knee joint, while walking, primarily manages weight bearing and flexion-extension movements, driving the body forward. Besides its own weight, the knee joint is influenced by the combined forces of muscle contraction and dynamic loading, underscoring the significant role of muscle force in walking. During extension movement of the knee joint, the lateral, medial, and intermediate vastus muscles, as well as the vastus medialis oblique and rectus femoris, are mainly active. During flexion, the hamstring muscles, gastrocnemius, and hamstring tendons (semimembranosus, semitendinosus, and biceps femoris) predominantly function. Maintaining motion balance in the knee joint depends on the interplay of these forces, and considering the complexity of muscle force coordination, simplified resultant forces and torque at the knee joint are typically used for mechanical calculations.

1.2 Biomechanics analysis of long-distance running

1.2.1 Running biomechanical analysis

Running biomechanics has received widespread attention from runners, coaches and researchers for the past 30 years [21, 22]. In the realm of recreational and amateur sports, running stands as a quintessential and accessible form of physical activity, garnering attention not only for its cardiovascular benefits but also for the biomechanical intricacies underlying its execution[23]. The decrease in athletic performance associated with running fatigue is partly due to inadequate central nervous system (CNS) drive of motor neurons and poor muscle executive function [24]. Exercise results from a combination of biomechanical and neurophysiological factors[25]. Long-term movement produces motor variability, therefore increasing exercise duration can result in neuromuscular fatigue. Similar studies have shown that running fatigue can reduce the body's control over posture and change lower limb biomechanical parameters[26].

However, fatigue caused by long-distance running may affect the neuro-muscular control of lower limb stability [27]. Thus, it is relevant to study the gait stability in athletes and numerous studies have reported that the symmetrical movement patterns exhibited by proficient runners are postulated to reflect not only efficient energy transmission but also underlying neuromuscular control mechanisms[22]. In addition, running is a cyclical exercise, and every step is not exactly the same from a biomechanical perspective [28]. Small internal or external perturbations may impact the neuromuscular and motor systems. Traditionally, Linear methods are frequently employed to analyze the stability of running gait, such as limb kinematics and Kinetic data [29, 30]. Approximately thirty years ago, scientific evidence emerged to demonstrate that the implementation of non-linear methods, grounded in dynamic systems theory, served as a plausible enhancement to the analysis of human locomotion[31]. Dynamic stability (DS) reflects the compensatory ability of the neuromuscular system to small perturbations[32].Therefore, in the study of human walking, the evaluation of gait stability has frequently relied on the analysis of DS [32]. The DS or running stability can be calculated through nonlinear time series analysis [28]. The largest Lyapunov exponent can be used to quantify the degree of response of a sports system to these small perturbations at different stages of long-distance running. Running-relevant injury, such as stress fracture of tibia induced by repetitive monotonous loads, may occur with lower DS and poor ability of compensatory the small perturbations[33]. Therefore, DS testing is an important method for analyzing gait signal characteristics. Running stability can be affected by neuromuscular and central fatigue, decreased of gait symmetry, running experience. A study on the 5000m running reported that stability increases with the increase of running distance[34]. In addition, elite runners with more running experience have higher gait stability compared to

recreational runners[34]. Previous research has reported that the gait of older adults is characterized by lower levels of DS in the trunk and lower limbs[35]. The loss of DS and regular kinematics in the gait cycle is a potential mechanism for injury and fall occurrence[36]. Within the field of studying DS of fatigue gait, there are numerous parameters that necessitate analysis[37]. A study by Hollander et al. [38] using an inertial sensor attached to the tibia found decreased running stability during a 15-min run. Previous study found that the running fatigue can change the temporal dynamics[23]. In addition, Schutte et al. have shown that run-induced fatigue increases the complexity of the pace and the complexity of trunk acceleration[39, 40].

1.2.2 Running-related injury

It is estimated that more than 35 million Americans participate in long-distance running as part of their daily physical activity[41]. Previous studies have shown that individuals with a long distance running habit can reduce the risk of cardiovascular-related death by 45%-70%[42]and cancer-related death by 30-50% [43]. However, fatigue from long distance running is also associated with a higher rate of injuries[44]. Hulme et al.[45] reported that 2.5-33.0 running-related injuries occurred per 1000 hours of running, and more than 79.3% of injuries occurred in knee joints. In addition, changes in muscle strength, cognitive function, and proprioception can be caused by fatigue[46], besides, stress, strain, shear force, and impact force on the lower limb joints also increase during fatigue [47]. The incidence of musculoskeletal injuries caused by running has also increased rapidly, especially in the lower extremity[48]. The tendons, muscles or bones of the lower extremities during long-distance running are repeatedly subjected to chronic submaximal loading over a long period of time[49]. As a consequence, overuse injuries are considered to be the most common running injury[49]. It should, however, be noted that the etiology of running fatigue-induced injuries is multifactorial and complex[50]. Fatigue from long-distance running can shift foot mechanics, potentially causing structural overload [51, 52]. Investigating the relationship between fatigue and the load distribution pattern during running gait has garnered increased interest [53]. A consensus is that an increase in peak metatarsal head pressure occurs after running fatigue[54, 55]. However, inconsistent results have been reported for the influence of running fatigue on the middle foot and heels[49, 54]. Weist et al. demonstrated a significant increase in midfoot pressure and the impulse in the medial heel after performing a running-induced fatigue protocol[56]. Nevertheless, the study by Bisiaux et al. [57] found a reduction in pressure and impulse in the midfoot under similar conditions. Willson and Kernozek [58] observed a significant reduction in peak heel pressure after 30 minutes of high-intensity running. In addition, more laterally directed roll-off and inadequate pronated heel strikes has been demonstrated to be the

potential triggers for lower limb overuse injuries[59]. Previous studies have reported that midfoot, metatarsal and medial heel loading increases after running-induced plantar muscle fatigue while loading on the lateral toes decreases[49]. Similar studies have reported that running fatigue causes a reduction in the medial longitudinal arch, which significantly increases mid-toe pressure[60]. In addition, excessive plantar forces of the forefoot lateral were identified as a potential cause for gait-related Achilles tendinopathy[54]. Most of the studies mentioned above did investigate changes in unilateral plantar pressure distribution after fatigue, especially the dominant side.

The mechanical loading within the knee joint is a dynamic interplay between motion and contact mechanics[61]. The knee joint's capacity to endure high mechanical loads is formidable, yet knee injuries are becoming more prevalent with the increasing number of runners. Annually, 37% to 56% of runners incur at least one running-related injury[62]. The knee is one of the joints most prone to pain in runners [63]. Prolonged repetitive mechanical loading may damage the knee joint, such as cartilage degeneration and additional chondrocyte apoptosis[64]. Osteoarthritis (OA), meniscal and ligament injuries are significant contributors to these pathologies. A previous study reported that the adduction moment is a pivotal factor in OA progression during the stance phase of gait[65]. Peak forces are concentrated in the lateral compartment of the knee during the initial contact and terminal stance, while the medial compartment bears the most weight during mid-stance [66]. OA primarily affects the articular cartilage but also impacts surrounding structures [67, 68]. Miller et al. [69] found that the knee load of per unit distance during running is comparable to walking, suggesting that runners' compensatory mechanisms (stride length adjustments and reduced ground contact time) effectively mitigate overall load. Nonetheless, rapid force is exerted on the articular cartilage during instances of unanticipated high-impact or substantial joint loading, which is incapable of adequate force dispersion [67]. Consequently, this leads to matrix damage and irreversible cartilage disruption, serving as a potential initiating factor for post-traumatic OA. In addition, a recent systematic review on prospective evidence for running related injury found only limited evidence for increased asymmetry in ground contact time and decreased asymmetry in vertical impact peak as being related to running injury[70]. Consequently, the presence of bilateral lower limbs asymmetry may be one of the potential causes of injure. Especially when one side of the limb load is more than the other side, suggesting that the unilateral injures may occur [71]. For example, healthy recreational runners have significantly higher Achilles tendon loads in the dominant lower limbs than in the non-dominant lower limbs [71].

1.3 Limb dominant and asymmetry evaluation

1.3.1 Limb dominant and Asymmetry in sports biomechanics

Symmetry has long been regarded as a synonym for health in sports training[72], therapy[73] and daily practice[74]. However, the movement and posture of human does not conform to the concept of complete symmetry[75]. Asymmetry may be widespread even in high-performance sports[76]. Movement symmetry is an essential technical parameter in some competitive sports, such as sprint running[77], walking race[78] and rugby[79]. In addition, most athletes have dominant limbs for certain tasks, and these preferences may be determined by different motor tasks[76]. Asymmetry of athletes is one of the main causes of musculoskeletal diseases, sports injuries and poor performance[80]. Although bilateral asymmetry is widely believed to be detrimental to sports performance of athletes, previous studies does not fully support this association[81]. Therefore, the athletes and coaches would benefit from an biomechanical examination of quantitative asymmetry of the bilateral movement or posture, rather than depending exclusively on subjective determination during daily training [76]. Quantification of bilateral asymmetries has been widely examined in the available studies as well as the quantification method is not uniform[80]. The literature reports that the associated symptoms may occur only when the degree of asymmetry exceeds certain thresholds [80]. Previous studies have shown a potential relationship between athletes' limb asymmetry greater than 15% and the occurrence of sports injuries[82, 83]. In addition, other researchers have set asymmetry of less than 10% as the goal for discharge and returning to the sport of athletes with unilateral limb injury[84, 85]. Trivers et al.[86] reported that symmetry can be identified as one of the indicators of early talent recognition in athletes. A long-term Jamaican study observed that the athletes' knee asymmetry at age 8 could predict their sprint performance 14 years later[86]. On the other hand, opponents argue that musculoskeletal coordination forms the basis for the symmetry of an athlete's static and dynamic movements[87]. In practice, interpreting motor coordination is more complex than classical biomechanical measurements[88]. Therefore, athletes performing an action with bilateral asymmetry may cause a decrease in biomechanical parameters of one or both sides. For example, water rowing is widely evaluated by bilateral continuous variables of force symmetry rather than coordination[81]. These findings suggest that asymmetry is an adaptive consequence magnified with long-term physical activity participation [76]. One of the causes of bilateral asymmetry is an abnormality of the spine[89]. The pressure generated during movement is transferred to the spine to stabilize the upper body and keep it balanced and upright. Therefore, biomechanical assessment of athletes' bilateral symmetry is the main method to develop recovery strategies to restore normal function in clinical practice.

Limited literature suggests that greater than 10% power and force asymmetry of the bilateral lower extremity can reduce the change of direction speed times[90] and jumping performance[91], indicating that increased asymmetry can impair athletic performance. Tomkinson et al [92] have reported that the athletes who are symmetrical can improve the sport performance. Although further research is needed into the relationship between symmetry and athletic performance, the potential applications of this research should also be considered. On the other hand, opponents argue that bilateral asymmetry may negatively affect athletic performance [76]. Loturco and colleagues[93] analyzed the relationship between vertical asymmetry and basal performance in high level female soccer players and they found that bilateral countermovement jump performance was significantly associated with strength on sprinting and squat tests, while asymmetry of unilateral squat jump was not associated with athletic performance. Within the previous studies, a stronger topic surrounding patients or rehabilitated people to have been explored then the participants of athletes. Asymmetry of the bilateral body has been evidenced to be indicative of movement function [94]. Therefore, The symmetry of biomechanical parameters were often used in the clinical and motion capacity assessment, which was important for restoration of abnormal function through appropriate of treatment strategies[73, 75]. Increased symmetry is considered by clinicians to be a sign of successful recovery and can increase the confidence of athletes to return to sport safely and effectively[80]. The degree of asymmetry determines whether an athlete may have a potential injury risk[74, 95]. Asymmetry of bilateral loading can contribute to the increase of unilateral limb damage such as ACL injuries, especially in female athletes[96, 97]. The non-contact injury rates in soccer were 68% in non-dominant limbs for females and 74% in dominant limbs for males[98]. Similarly, Brown and Brughelli [99] used symmetry of lower limbs as a decisive factor in assessing rugby players' return-to-sport status. Schache et al. [100] observed a soccer player with a unilateral hamstring strain due to a 5.7° difference in peak knee extension between legs and a 7% vertical peak force during the swing. However, the methods used to assess symmetry vary greatly, so caution should be exercised when establishing a correlation between asymmetry and injury[76]. Previous research has shown that when asymmetry exceeds a certain threshold, it can negatively impact an athlete's health, although it may be beneficial for specific athletic performance[81]. However, these thresholds are still an unsolved problem in current studies and may vary between individuals and individual states. Therefore, these complex explanations should be considered in future studies. By better understanding of the effects of limbs asymmetry on athletes' physical activities can provide an important basis for coaches and athletes to design training strategies and rehabilitation testing.

The asymmetry of human body structure will cause the asymmetry of bilateral limb function. Similarly, asymmetrical movement over a long period of time can promote structural asymmetry.

This potentially vicious cycle may have a negative impact on athletes' training efficiency, so exploring the causes of asymmetry should be the focus of future research. Previous studies have reported that dexterity is one of the important causes of upper extremity gross anatomical asymmetry[101]. Oyama et al.[102]assessed the asymmetry of bilateral scapular position and orientation in 3 groups of healthy overhead athletes (13 tennis players,15 baseball pitchers and 15 volleyball players). More internally rotated ($p<0.01$) and anteriorly tilted ($p<0.01$) of the scapula was showed on the dominant side of the overhead athletes and a more protracted of the scapula position occurred on the dominant side of the tennis players($p<0.05$). These results indicate that the cause of the asymmetry may be related to the athletic attributes of the athletes, and clinicians should be cautious in evaluating the asymmetry of the upper limbs in such athletes. However, the authors did not analyze the correlation between asymmetry and exercise experience, and more future research would be required to confirm this suggestion. More definite conclusion has been described for the Paralympic powerlifting athletes. Dalla Bernardina and colleagues[103] analyzed functional asymmetries during different submaximal intensities (50% and 90% of the one-repetition maximum, 1RM) using linear velocity. Powerlifting performed symmetrically at 50% of 1RM. In comparison, significant asymmetry in favor of the dominant limb occurred at 90% of 1RM. By comparing the sensitivity of ANOVA and FANOVA to body asymmetry, the authors found that the latter is the most suitable for examining the asymmetry of the performance of paralympic weightlifters. However, Further research is needed to confirm the relationship between bilateral asymmetry and weightlifting performance. Similar disparate findings have been reported for racing wheelchair propulsion. Goosey[104] reported that no statistical difference was found in the elbow height, elbow angular displacement and propulsion phase of the racing wheelchair athletes.

For sports requiring a high level of the unilateral upper extremity, such as archery, previous studies have shown that the nature of the movement leads to an asymmetry in skin temperature. The authors point out that the asymmetry of different temperatures can reflect the muscle activation of archers and make an important contribution to their posture. The influence of exercise experience on skin temperature needs to be further explored in combination with neuromuscular signal analysis. Asymmetry is generally thought to affect athletic performance negatively, but the scientific evidence to support this claim is insufficient. In addition, asymmetric types are usually not defined. Warmenhoven et al.[88] noted that high-level rowers are more likely to use adaptive asymmetric strategies for rowing, suggesting that asymmetries have a functional role in a rowing movement. However, more scientific evidence is needed to determine whether asymmetry boosts rowing performance. Gender differences is also widely believed to be an important reason for individual differences in asymmetric parameters. Male pole vaulters with

greater explosive power have greater step length and step frequency asymmetry during competition. This gender difference could be attributed to the athletes' physical condition and pole characteristics. Gray et al.[105] By comparing abdominal muscle thickness asymmetry in fast bowling players with and without low back pain, athletes with low back pain had more symmetrical abdominal muscle size. However, whether this phenomenon has clinical significance remains unclear. A systematic review on the application of symmetry in competitive sports was reported by Gao, which shown that the application of symmetry angle (SA) is the most symmetrical evaluation measure in competitive sports (Figure 1.3.1). As shown in Figure 1.3.1 (B), the author identified 6 studies on the variables of asymmetry on sprinter and 4 on multifarious sports. The number of analyzed the variates of kinetic and kinematics asymmetries was the highest among all the included studies, 14 and 13, respectively. 9 studies analyzed the asymmetry of spatiotemporal variables (Figure 1.3.1 (C)). In addition, SA was used as an assessment tool for asymmetry in 8 studies, and 6 studies used the method of SI (3 studies) and two side differences (3 studies), respectively. 5 of 22 articles used general statistical check approaches to identify bilateral asymmetries, ANOVA (2 studies), N-K procedures (1 study), FANOVA (1 study), W M-Pairs Signed (1 study) and Separate analyses of variance (1 study), as shown in Figure 1.3.1 (D). The results show that the Inter-limb asymmetry appears to have a positive effect on physical performance in upper limb movement, while it may cause injury to occur and have a detrimental effect on performance in gait related sports. However, the evidence pertaining to inter-limb asymmetry in ball athletes and different athletes is less conclusive. Mixed results were also found in a specific sport, suggesting that the effects of bilateral limbs asymmetry on different athletes may be task-specific.

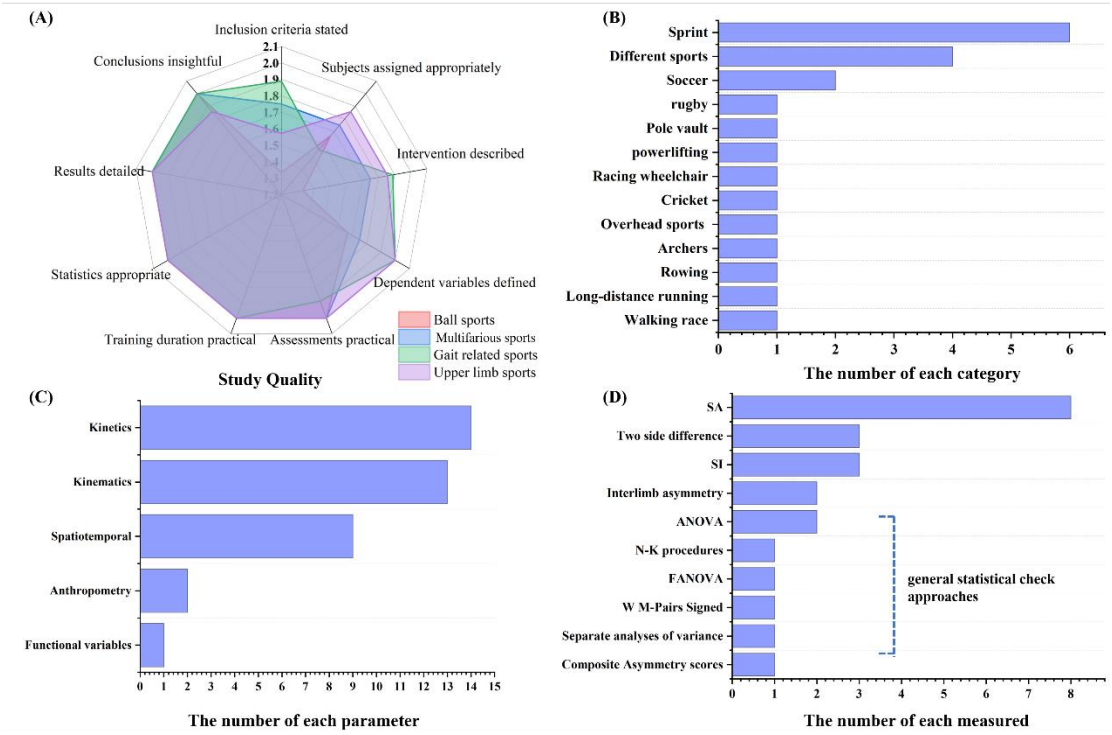

Figure 1.3.1 The Effect of Application of Asymmetry Evaluation in Competitive Sports[22]; (A) Study Quality assessment. (B) The number of each sport category. (C) the number of each test parameter. (D) The number of each asymmetry metrics measured.

Limited data are available on the effect of motor tasks on limb asymmetry. Further studies in a broad population of athletes are needed to clearly determine whether various body asymmetries are associated with motor tasks. Liu and Jensen[106] calculated asymmetry of kinematics and kinetics in 56 athletes who underwent ACLR and found that asymmetries in sagittal plane knee moments at initial contact during the landing phase of a DVJ are strong predictors of second ACL injury. This prediction model only applies to the prediction of secondary ACL injury in athletes who have experienced ACLR, and further research is needed for the prediction of injury risk in healthy athletes. A similar study assessed changes in lower extremity symmetry in athletes who had experienced ACLR after return to sports criteria and found that patients used hip, pelvis, and trunk compensatory strategies to address inter-limb differences in knee function[107]. A further consideration for the inducement of asymmetry would be the Athletic level. Minimal literature has focused on the difference in biomechanical symmetry of lower limbs in athletes of different sports levels. Morishige et al. (2016) compared the leg asymmetry between 23 female collegiate and 19 recreational athletes during the landing phase of a DVJ, and the results showed that the asymmetry of bilateral knee abduction Angle was opposite in the two groups. However, further evidence is needed to determine whether this interesting phenomenon is related to the injury. The presence of biomechanics asymmetries within athletes has been reported for several decades. Investigations

had previously reported that an increased asymmetry of bilateral lower limbs was one of the potential causes of spinal abnormalities. However, investigation of the ameliorating interventions of asymmetry has only recently been examined. Alvarenga et al.[108] reported that the intervention of lumbar SMT can improve the immediate static asymmetry of athletes, more interventions related to dynamic asymmetry need to be explored in the future.

1.3.2 Limb dominant and asymmetry in running biomechanics

Since the human body is a large and complex system, consequently, gait motion can be realized in many different ways. For example, the muscle group of the normal leg can compensate for the other leg with the weak muscle group during gait movement[109]. Therefore, Gait asymmetry can increase the workload of one limb. By analyzing the gait variability and symmetry of 35 race walkers, Tucker and Hanley reported the asymmetrical step lengths were persistent in individual athletes, which may be caused by the underlying gait imbalance[78]. Further data has also linked gait asymmetries to sprint running performance. Brown et al[79] used acceleration and maximal velocity sprinting to assess athletic performance in thirty male rugby athletes (development-level). Trivial to small correlations was proved between the Vmax and symmetry angle of vertical and horizontal force in both acceleration (R^2 = 0.021 and 0.100) and maximal velocity sprint phases (R^2 = 0.179 and 0.0002), while the correlations between the symmetry angle in acceleration and maximal velocity sprint phases were 0.459 for vertical force and 0.721 for horizontal force. These results suggesting that the asymmetry of vertical and horizontal force may be the crucial components for acceleration performance in sprinting. However, the relationship between athlete performance with asymmetries is not clearly stablished. Another similar case study indicated that asymmetry was negatively associated with a lower risk of injury and high sprinting performance[72]. On the other hand, opponents argue that the symmetry of kinematic parameters during the stride cycle was no relationship with sprinter sports performance and the prevalence of injury[77].

In addition, Exell and colleagues used asymmetry composite scores to quantify the intra-limb asymmetry in eight male sprint athletes and reported that asymmetrical measures exist for inter-participant differences[110]. A similar study compared and evaluated the spatiotemporal parameters and GRF asymmetries of 18 elderly and 17 young walkers and found that although there was no overall mean asymmetry, the individual analysis found asymmetries of several athletes(SA≥1.2%)[78], This is somewhat supported by Girard who highlighted the relatively large range of asymmetries between individuals should be taken into account in the analysis[111]. Therefore, these findings should be interpreted with caution, significant asymmetrical variables may be athletes specific, and therefore, intra-limb variability should be included in asymmetrical

analyses to avoid misleading results[112]. In addition, Previous studies have hypothesized that gait asymmetry may be due to running fatigue[79]. Girard and colleagues have examined whether inter-limb asymmetry in lower limb mechanics increases with fatigue and found that similar fatigue rates exist in bilateral lower limbs during sprinting exercise[113]. Consequently, the cause of bilateral lower extremity asymmetry should be the focus of future research.

Typically, the mean value of bilateral variables [26, 114] or the default complete symmetry of both limbs [52, 115] was widely used in running biomechanical research. Although these methods mentioned above can describe the motion well, it also ignores the false claims and misleading interpretations caused by the asymmetry of bilateral variables [116]. Neuromuscular asymmetry is a widespread phenomenon occurred in functional tasks [117]. Few previous studies have considered that the biomechanical asymmetry of running gait [116, 118, 119], even though this phenomenon is common among healthy people [21, 52]. Quantitative gait characteristics (e.g., parameters of time and parameters of space) and qualitative gait characteristics (e.g., gait variability and gait asymmetry) are related to running-related injuries, especially among amateur runners [120, 121]. Similarly, the effects of gait asymmetry are also an important consideration for motor performance[122]. Previous studies have shown that a 10% increase in asymmetry of vertical ground reaction force (GRF) leads to a 3.5% increase in net metabolic power during running[116]. Another finding was that increased foot contact time asymmetry was associated with increased metabolic costs of running[116]. Zifchock et al. [123] found that the asymmetry was 49.8% and 37.5% at the running speed of 3.65 m/s by evaluating the peak lateral and medial GRF of bilateral lower limbs in the running process of healthy individuals, similarly by Williams et al.[124] reported that 13.8% and 20.2% asymmetry of peak lateral and medial GRF at the speed of 5.36m/s, suggesting that greater symmetry is associated with faster running speeds. The same conclusion regarding walking gait was reported by previous. Asymmetry between limbs refers to the phenomenon that one limb difference of function, physical strength, and other parameters relative to the other limb[25]. Moreover, Seeley et al.[125]found that impulses from dominant limbs were significantly larger than those from non-dominant limbs during the push-off phase during fast walking, suggesting that the dominant limb contribute more to gait propulsion. Likewise, previous studies also have reported that the non-dominant foot showed more stable Foot Balance Index Range during running gait [52]. Likewise, Gao et al. [52] reported that a Running-Induced Fatigue Protocol caused knee flexion angle, hip flexion angle, hip extension angle, and the hip flexion moment to be more asymmetrical. However, the biomechanical changes of human movement usually occur in three anatomical planes[126]. Therefore, the effect of fatigue on the symmetry of coronal and horizontal biomechanical parameters is less known. Previous studies have widely shown that fatigue gait risk is associated with shifts in the distribution of bilateral plantar pressure [48, 51, 53, 58].

The quest for optimal stability often intersects with the pursuit of gait symmetry, as deviations from symmetry may not only impede performance but also predispose individuals to overuse injuries and musculoskeletal imbalances[116]. Therefore, research on the symmetry of running gait mainly involves investigating biomechanics[29], athletic performance[116], or outcomes related to injuries over the past few decades [127]. However, the ultimate conclusions regarding its benefits or harms are still pending. Although many studies have investigated the acute effects of long-distance running on gait symmetry, they have mainly focused on exploring pre- and post-fatigue comparisons. One gap is the lack of understanding of how symmetry changes during various stages of long-distance running. In addition, researchers have utilized various techniques from chaos theory and information theory to enhance their understanding of the intricacies of gait behavior. Although nonlinear evaluation is important in the quantification of gait stability, there is a lack of research on gait asymmetry. Therefore, the existence of asymmetries is often assumed to be unstable without clear evidence. Mechanisms of the central and peripheral nervous systems may be involved in the phenomenon of fatigue in a complex manner[128]. Therefore, the effect of this gait symmetry may not be easily quantified by linear methods during running. And inferring symmetry information from kinematic and kinetics data can be challenging. Therefore, more sophisticated tools are especially important to probe fatigue-induced symmetry changes. In the present study we investigated the temporal gait variability associated with gait asymmetry running 10km running.

In addition, stress during exercise tasks gives rise to specific joint dynamics, and investigations of stressful activities can help to understand the biomechanisms of forces generated by joint loading. The menisci, crucial in load distribution and shock attenuation, withstand significant shear, tensile, and compressive forces[129]. Composed of fibrocartilaginous material, they are essential in the effective transmission and dispersion of mechanical loads[130]. Notably, 5% of runners sustain meniscal injuries[131]. Meniscal tears are common and often disrupt circumferential fibers, leading to extrusion, displacement, and intra-articular constriction under axial stress[132]. Running fatigue has been reported to increase tibial stress in past studies[133]. However, the research related to whether this phenomenon exists in the context of internal tissue stress in the knee is still insufficient. In addition, the ligaments of the knee joint are significant contributors to the DS of gait, as they prevent excessive extension or rotation of the knee with the assistance of muscular strength. Prolonged running may lead to decreased muscle strength, resulting in an overuse load on the ligaments[44]. Therefore, the health of the ligaments is crucial for maintaining a healthy gait posture. Numerous studies in gait biomechanics presuppose entirely symmetrical gait patterns and only examine unilateral variables, encompassing both the experimental analysis and numerical simulation [129, 134, 135]. However, Sadeghi and colleagues[25] observed that

asymmetry in lower limb gait is present even in healthy individuals. The stronger limb typically compensates for its counterpart to address biomechanical shortcomings in the gait during long-distant running[136]. However, running-related injuries commonly occur in a unilateral limb[137]. Approximately half of recreational runners sustain an injury annually, with many being recurrent and side-specific[138]. Despite extensive research into factors contributing to injuries, the mechanisms underlying side-specific injuries are not well understood[139, 140].

1.4 Running gait investigations using modelling technology

1.4.1 Machine learning modelling technology

Machine learning approaches have been widely utilized in gait biomechanics studies in the past decades[141, 142]. Utilizing learning-driven sensor data, machine learning and deep learning methodologies can facilitate real-time gait monitoring, offer recommendations for running equipment, and provide insights for running injury prevention. Understanding the implementation of machine learning techniques in lower limb running biomechanics through the exploration of wearable sensor data is essential. Recent advancements in artificial intelligence provide novel opportunities for analyzing variations during exercise and estimating fatigue levels.

Uhlrich and colleagues[143] reported that a new approach of integrating physical and machine learning models into a unified model could be a popular topic in future biomechanics research. These models can be trained on smaller data sets and achieve higher accuracy. There are three common application methods (Figure 1.4.1):

(1) The application of musculoskeletal models to generate training data for machine learning models, particularly those utilizing sparse inputs like data from a limited number of Inertial Measurement Units (IMUs) or acoustic emissions from joints, is a strategic approach in biomechanical studies.[144, 145]

(2) Incorporating elements of the physical system into machine learning models is an effective strategy. For instance, using physics simulations can notably enhance the accuracy of a deep learning-based pose estimation model [146, 147]. Additionally, integrating physics-based terms into the loss function can effectively regularize neural networks, ensuring that their predictions adhere more closely to physical principles[148].

(3) An alternative strategy involves employing physical models for well-understood elements of a system, while training machine learning models for the less understood components. For instance, through reinforcement learning, a network can learn a model of sensory-motor control, which is inherently challenging to model mechanistically. This approach enables a musculoskeletal model to effectively navigate complex environments[149].

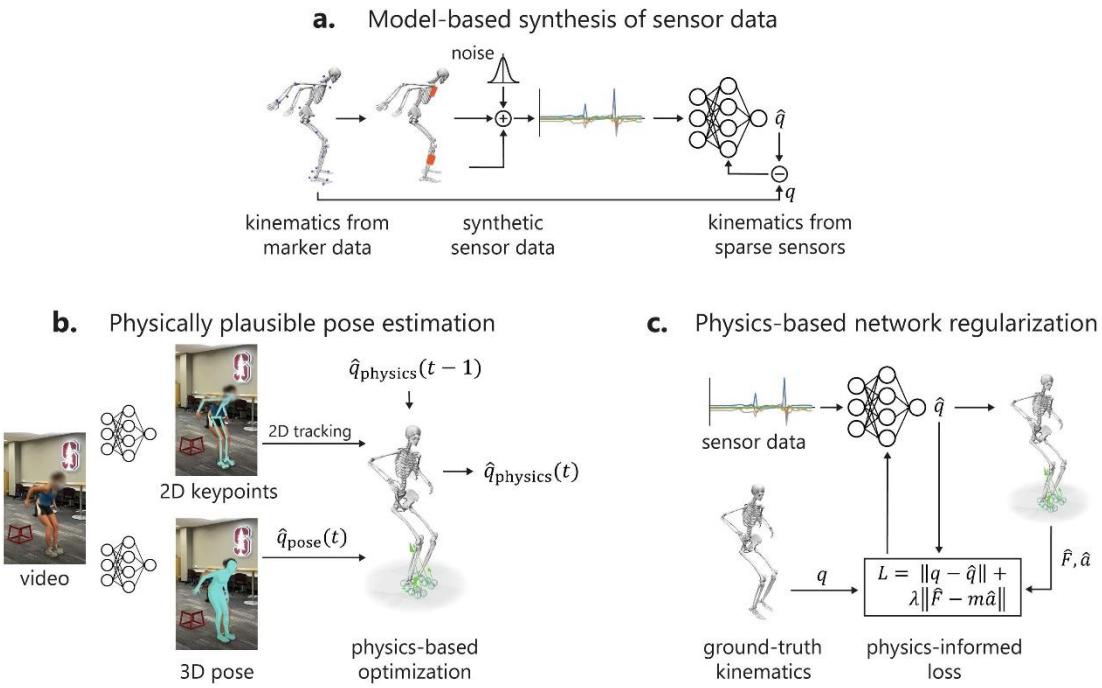

Figure 1.4.1 Approaches to combining physics-based modeling and machine learning[143]. (a) Musculoskeletal models can be used to synthesize inputs to machine learning models[144, 145]; (b) Physics-based optimization can improve the accuracy of deep-learning-based pose estimation[146, 147]; (c) Physics terms can regularize the loss function of a deep learning model, helping to reduce overfitting[148].

Coaches and runners can avoid the occurrence of overuse injuries by monitoring fatigue levels in the context of competitive and recreational sports. In addition, excessive fatigue may affect runners' performance and cause secondary injuries to the runner[150]. Therefore, human Activity Recognition (HAR) methods based on wearable sensors and deep learning algorithms have been widely developed in the last decade [151]. Despite significant strides in gait and biomechanics analysis, research into automated fatigue gait recognition with data-driven models remains insufficient [141, 152]. Typical techniques to detect fatigue are surface electromyogram -based collection of muscle activity signals and optical motion capture-based collection of joint kinematics[29, 153]. However, the limited data collection area and the location of the marker attachments make monitoring limited. On the contrary, Force plates or insoles with force sensors are easy to use and save time in the experimental setup for data collection. Therefore, this study intended to use a deep learning algorithm based on bilateral plantar pressure data for early identification of fatigue gait. Nonetheless, these methods can be both computationally and data intensive. A systematic review by Xiang[154] and colleagues on the application of machine learning algorithms in running biomechanics reported that deep learning algorithms account for 57% of the total number of machine learning methods, while traditional machine learning algorithms

make up 43%. The specific application distribution is shown in Figure 1.4. 2.

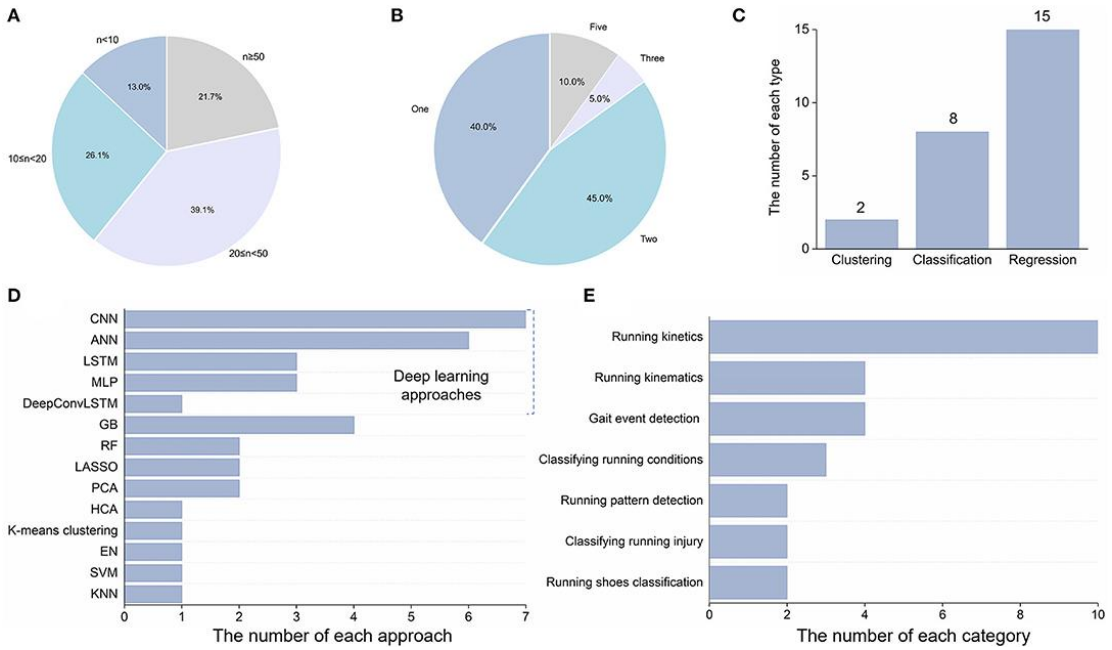

Figure 1.4.2 Recent Machine Learning Progress in Lower Limb Running Biomechanics With Wearable Technology.[154] (A) sample size; (B) the number of sensors; (C) types of machine learning algorithms; (D) machine learning approaches; (E) purpose of machine learning.

The previous study demonstrated that the support vector machine (SVM) has a high generalization ability for dichotomous data[155]. The optimal separating hyperplane was created by maximizes the distance of separation in SVM model[155]. Moreover, it can transform the matrix into a higher dimensional space for classification by setting the different types of kernel functions[155]. SVM algorithms was widely used in gait patterns recognition, such as differences of young and elderly populations[156], competitive and recreational runners[157], barefoot and shod population[141]. Mundt et al.[158], for instance, expanded their measured inertial sensor dataset with simulated IMU data to enhance the estimation of walking and running biomechanics.

Supervised machine learning and deep learning techniques have been developed for classifying fatigue status, with deep learning offering the advantage of autonomously extracting features without the need for specific domain knowledge, leading to state-of-the-art outcomes[159]. Contemporary research predominantly assesses fatigue by analyzing sensor-derived data through person-specific statistical and data mining techniques. The evaluation approaches of running gait symmetry have been widely utilized in biomechanical studies in past decades[117, 123, 160]. Traditional person-dependent fatigue recognition systems necessitate user-specific labeled data to train classifiers. This process, involving the induction of a fatigue state for data collection, is both

time-consuming and labor-intensive. Currently, only a limited number of studies have successfully generalized fatigue classifiers across different participants. Buckley and colleagues [161] explored the efficacy of a single IMU in distinguishing between non-fatigue and fatigue states utilizing both subject-dependent and subject-independent classifiers. Their findings indicated superior accuracy with the subject-dependent classifier (100%) compared to the subject-independent one (75%). They highlighted that fatigue is a multifactorial condition influenced by various factors such as sleep disorders, pain, and alterations in affective and cognitive states. The majority of data augmentation techniques applied to time series data rely on random transformations of the training dataset. Khandakar et al.[162] recently addressed the challenge of identifying construction activities using a LSTM network, employing augmented IMU data. By integrating four data augmentation techniques—jittering, scaling, rotation, and time warping—the model's accuracy was substantially enhanced from 63.5% to 97.9%.

Since larger spatial dependencies exist in the pressure data of each plantar region throughout the gait cycle[163], the CNN model has been reported to be better at extracting to local spatial features[164]. Similarly, time series data-based plantar pressure data are considered to possess time dependence[165]. However, the plantar pressure distribution data based on time series features may be regarded as static spatial data by the CNN model, and the time-dependent information within the series is lost. Previous studies have shown that Long Short-Term Memory Network (LSTM) models perform better for the prediction of long-time dependence and nonlinear dynamic changes in a time series[166]. However, LSTM models are less effective in handling spatial relationships of data. The spatial characteristics of the pressure distribution in different plantar regions and the dynamic time characteristics of the variation with time should be considered in the model selection for this study. Therefore, the ConvLSTM model, which integrates the advantages of CNN and LSTM, was used in this study because it converts the structures in the recurrent neural network into convolutional structures, thus preserving the spatial-temporal information of plantar pressure.

1.4.2 Musculoskeletal modeling technology

Scientists working in biomechanics have recently developed numerous computational tools for analyzing the neuromuscular skeletal (NMS) system, grounded in a joint-multibody system framework. In order to foster the progress of sports science, researchers aspire for computational modeling and simulation tools to transcend disciplines like anatomy, physiology, neuroscience, kinematics, mechanics, robotics, and computer science, thereby facilitating easier motion analysis[167]. Utilizing mathematical and physical algorithms, these tools facilitate the biomechanical analysis and quantification of internal variables during human movements,

including analyses of kinematics and kinetics, muscle fiber length, muscle force, joint force, and reaction forces of muscles/joints. Analysis tools such as LifeMod, SIMM, Visual 3D, AnyBody, and recent open-source tools like OpenSim are employed to simulate human motion, compute muscle strength and muscle activation, and are extensively applied in gait analysis[168]. The software encompasses all essential computational components, crucial for deriving motion equations in dynamic systems, conducting numerical integrations, and addressing constrained nonlinear optimization challenges.

A dynamic simulation framework, incorporating models that detail the neuromusculoskeletal system's anatomy and physiology along with the mechanics of multi-joint movements, offers a comprehensive approach. These muscle-driven dynamic simulations augment experimental methods, furnishing estimates of critical but experimentally elusive variables such as muscle and joint forces. Additionally, they facilitate the elucidation of causal relationships and permit hypothetical analyses. In these analyses, modifications to a muscle's excitation pattern can be implemented, enabling observation and analysis of the consequent motion[169]. In the latest five decades an increasing number of biomechanical researchers have chosen to use opensim for musculoskeletal modeling and simulation investigations, and Figure 1.4.3 shows the number of relevant published studies.

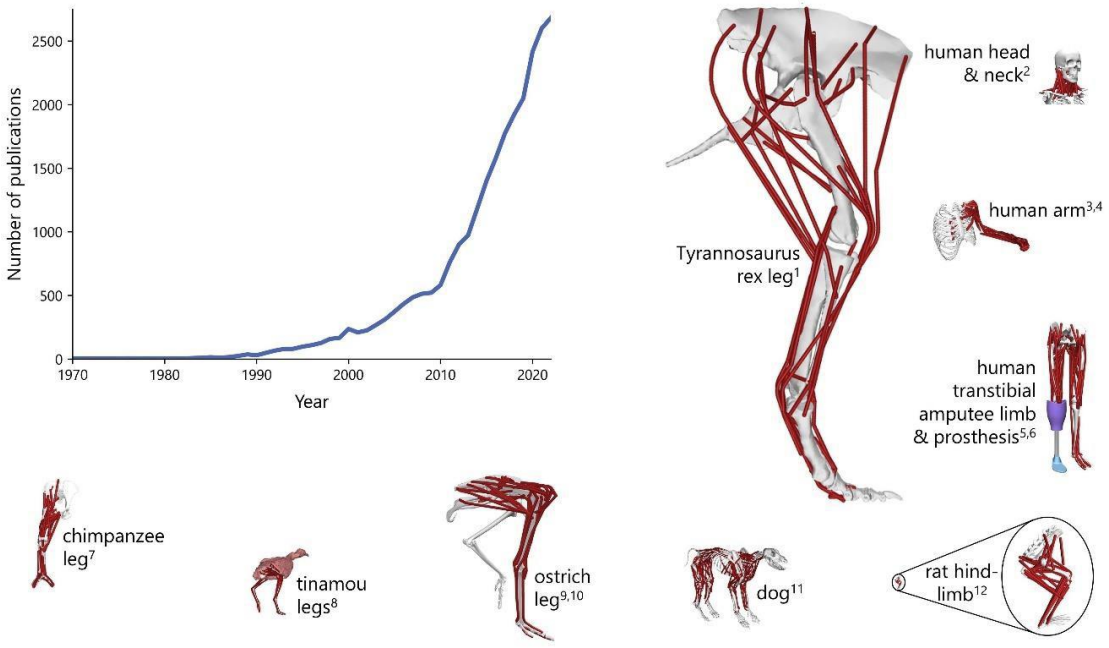

Figure 1.4.3 Growth of musculoskeletal modeling and simulation[143], Annual PubMed publications in “(musculoskeletal simulation) OR (musculoskeletal model*)” have grown by three orders of magnitude since 1970. Over the past two decades, many musculoskeletal models have been developed and shared publicly on SimTK.org for use in simulation research. Examples of shared models, shown to relative scale, have been provided by 1

Hutchinson et al. (2005), 2 Mortensen et al. (2018), 3 McFarland et al. (2019), 4 Saul et al. (2015), 5 Rajagopal et al. (2016), 6 Willson et al. (2020), 7 O'Neill et al. (2013), 8 Bishop et al. (2021b), 9 Hutchinson et al. (2015), 10 Rankin et al. (2016), 11 Stark et al. (2021), and 12 Johnson et al. (2008).

OpenSim users are capable of fully utilizing the open-source model library to create and augment new models, as well as engage with other users in exchanging simulation research outcomes and develop and share novel model data and plugins through a vibrant developer community. Consequently, after a thorough analysis of factors like operating environment, precision of muscle control, extent of errors, software price, and the capability for whole-body human modeling, as well as inverse and forward kinematic and dynamic simulations, OpenSim has been selected from the mainstream human motion simulation software as the musculoskeletal modeling and simulation tool for our research. Lerner and colleagues[170] developed an OpenSim full-body model that includes a quantitative function for medial and lateral contact forces between the tibia and femur in the knee joint(Figure 1.4.4(A)). They validated it using a model with geometric parameters and found that the model has high predictive accuracy (Figure 1.4.4(C)). In addition, As shown in Figure 1.4.4 (D), Delp et al.[169] utilized a 12-segment, 29 degree-of-freedom (DOF) musculoskeletal model to construct their simulation. This model featured actuation in the lower extremity and back joints through 92 musculotendon actuators. In the simulation, muscle color serves as an indicator of the activation level, ranging from fully activated (represented in red) to fully deactivated (depicted in blue) (Figure 1.4.2.2(E)), the results shown that the quadriceps and plantar flexors are the major contributors to acceleration of the body mass center during running[171].

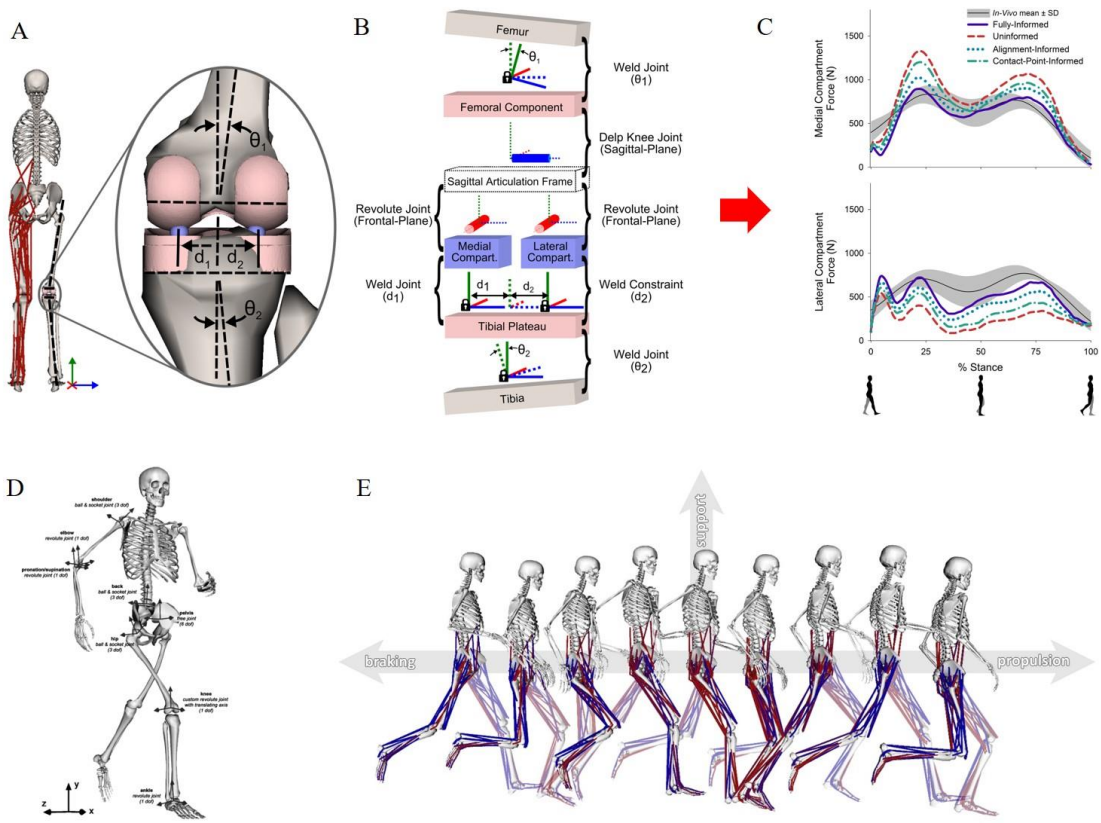

Figure 1.4.4 Graphical (A) and schematic (B) depictions of the medial/lateral compartment joint structures in Lerner et al musculoskeletal model, (C) Medial (top) and lateral (bottom) compartment tibiofemoral contact forces during stance[170];(D) Joint definitions for the 12 segment, 29 degree-of-freedom musculoskeletal model created by Hamner et al, (E) Snapshots from a simulation of the running gait cycle[171].

The verification of a simulation typically hinges on the consistency between its outputs and experimental measurements of kinematic, kinetic, and electromyographic (EMG) activities. Upon successful performance and validation, the simulation can be analyzed to evaluate muscle contributions to body movement and the effects of simulated treatments. The primary challenge in developing a dynamic simulation for coordinated movement lies in identifying a suitable set of muscle excitations. Advancements in computer science and robotic computed muscle control technology have now significantly expedited the determination of muscle excitation levels. Creating a dynamic musculoskeletal model in OpenSim simulation software is divided into the following 5 steps (Figure 1.4.5).

（1） Utilizing motion capture devices to design experiments and gather data, a suitable OpenSim generic musculoskeletal model is scaled to create a personalized model aligned with individual traits.

（2） Inverse kinematic analysis is applied to align the experimental kinematics with the

measured motion data, ensuring that the experimental model is consistent with the actual human motion posture.

（3） The Residual Reduction Algorithm (RRA) method is utilized to rectify residuals resulting from model minimization and inaccuracies in marker data processing. This is achieved by combining ground reaction forces with human body inertia parameters, thereby limiting the calculation errors from inverse dynamics to a smaller scope, dynamically converging towards ground reaction force data, and fulfilling the aim of static optimization.

（4） Forward dynamics involves altering muscle parameters such as activation level and maximum isometric contraction force through Computed Muscle Control (CMC). Optimal simulation results are achieved through a combination of these parameters and static optimization.

（5） Ultimately, through the forward dynamics process, the results of simulation calculations are achieved, replicating the process of actual movement, and obtaining related data such as joint reaction forces and joint reaction moments generated relative to the ground, considering muscle activity.

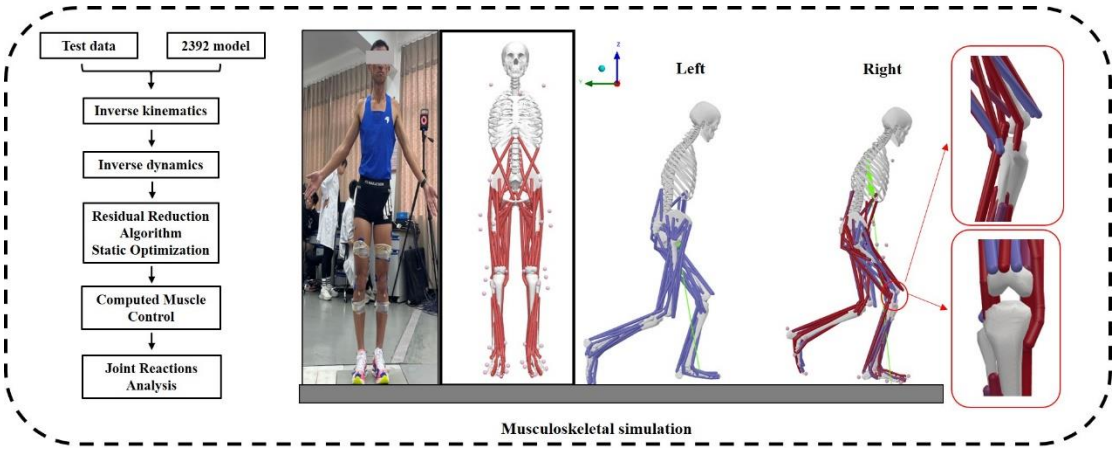

Figure 1.4.5 The process of musculoskeletal modeling simulation in Opensim software

1.4.3 Finite element modelling technology

The finite element (FE) analysis is a computer simulation technique, where its built-in algorithms can divide larger and more complex mechanical problems into smaller elements that can be solved in relation to each other[172]. Moreover, finite element analysis for examining the biomechanical characteristics of the knee joint is a mainstream tool in engineering and medical research[173]. Previous research on knee joint finite element analysis primarily concentrated on four areas: predicting the knee joint's mechanical properties[172], comprehending the stress conditions it endures[174], investigating the mechanisms of joint injury, and simulating the stress-strain

relationship between knee joint prosthetics and bones[175]. FE analysis primarily excels in its ability to model intricate geometries, varied material properties, and complex boundary and loading conditions. When integrated with experimental methodologies, it effectively uncovers the internal states of bony structures under various scenarios.

Alterations in knee mechanical load can influence OA-induced knee pain[176]. Tibiofemoral joint contact forces arise from the combined action of muscles and ligaments[177]. Direct JCF quantification is invasive and ethically complex[135, 178]. Therefore, MS and FE modeling are widely used as non-invasive alternatives to simulate dynamic loads. MS models estimate muscle and joint forces using kinematic and kinetic data, but the tissue response during KOA progression or the factors influencing cartilage degeneration cannot be fully evaluated[67]. FE modeling, on the other hand, can provide intuitive graphical results to elucidate the distribution and magnitude of localized loads induced by biomechanical changes in the knee joint[179]. Running-related knee injuries are caused by the complex interplay of tissues such as the meniscus, cartilage, ligaments, and muscles, even if they may be due to fatigue or an asymmetric gait[44]. Nonetheless, previous studies on fatigue and differences in load between limbs has not precisely addressed the distribution and extent of the load on the knee joint's internal tissues, possibly missing key insights into the causes of unilateral limb injuries[29].

As described by the author in the previous section (1.4.2), musculoskeletal modeling, which relies on motion measurement data, has been demonstrated to offer relatively accurate predictions of muscle activities throughout the human body. A static optimization algorithm is commonly employed to address the muscle redundancy problem, enabling the estimation of muscle activities either throughout the entire body or in specific local areas of the body. Muscle activities play a significant role in influencing joint kinematics, which can alter the deformation of cartilage and other soft tissues. These deformations, in turn, may modify the joint's secondary kinematics. Such changes are critical as they can significantly impact muscle length and the muscle moment arm, thereby affecting the accuracy of muscle activity estimations[169]. However, traditional musculoskeletal models are predominantly developed within the framework of multibody dynamics, where the skeletal structure is modeled as a rigid body. In these models, joints are typically represented as simple rotational joints with specific degrees of freedom.

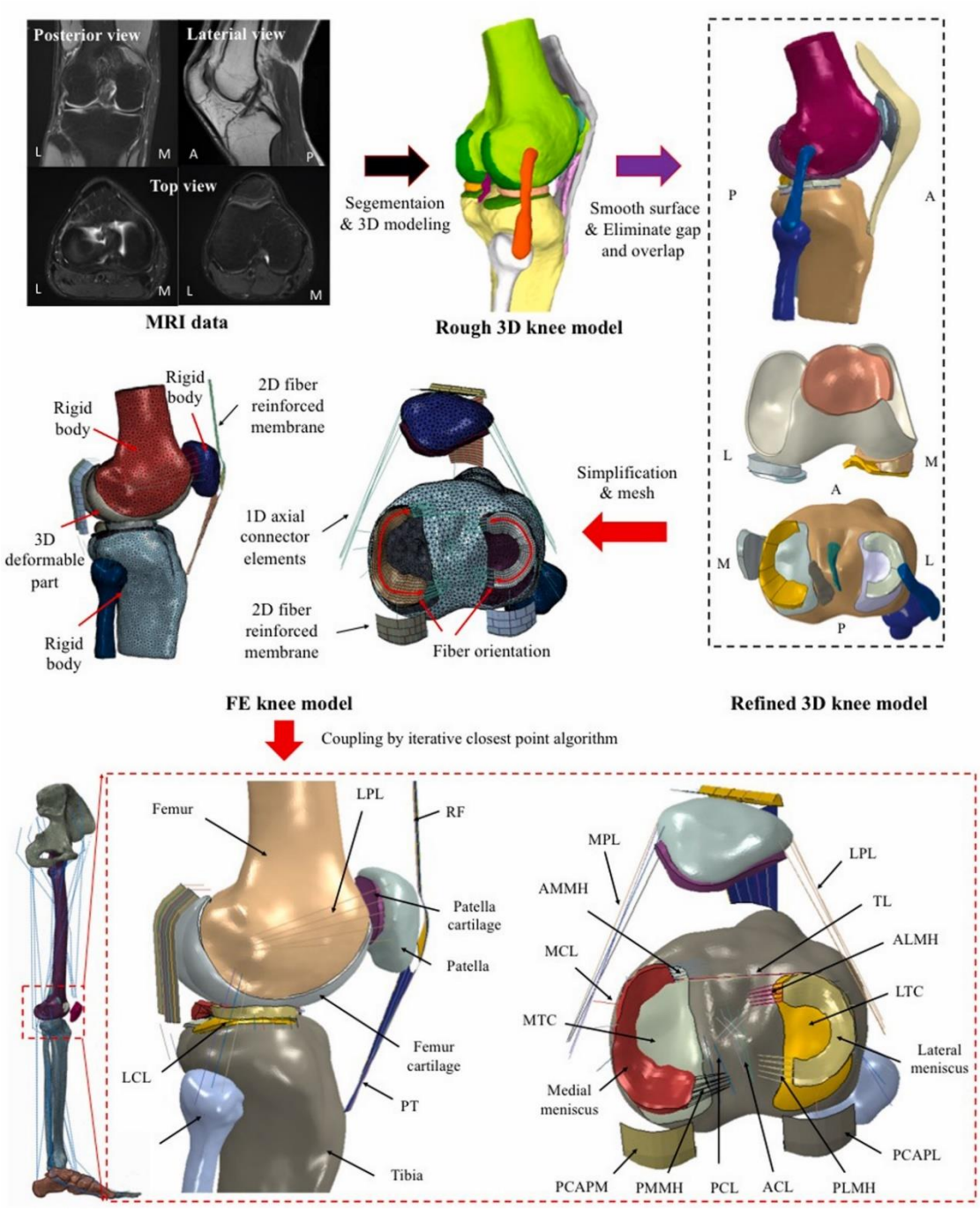

Figure 1.4.6 Subject-specific FE MS model with high-fidelity intact FE knee joint[180] (LCL: lateral collateral ligament; MCL: medial collateral ligament; ACL: anterior cruciate ligament; PCL: posterior cruciate ligament; PT: patellar tendon; RF: Rectus femoris; MPL: medial patellofemoral ligament; LPL: lateral patellofemoral ligament; TL: transverse ligament; AMMH: anterior medial meniscus horn; ALMH: anterior lateral meniscus horn; PMMH: posterior medial meniscus horn; PLMH: posterior lateral meniscus horn; MTC: medial tibial cartilage; LTC: lateral tibial cartilage; PCAPM: medial posterior capsule; PCAPL: lateral posterior capsule).

Through FE analysis, individual tissues are divided into finite, independent elements, each of which is assigned material properties corresponding to the tissue it represents. Material models of bone, cartilage and ligaments have been validated under laboratory conditions[181]. Therefore, by applying forces, moments, rotations and/or translations from MS models as boundary conditions, it helps to non-invasively estimate the stresses and strains in bones, cartilage and ligaments during everyday activities such as gait[182]. The study of Halonen and colleges[183] used a combination of MS and FE modeling to simulate the biomechanical effects of different gait styles on knee stresses, and they demonstrated that this method is also effective for analyzing the stress and load on the internal tissue of the cartilages of knee joint. Similarly. Shu et al. used MRI data to establish a 3d knee joint model and assess detailed joint kinematics and contact mechanics during the gait cycle (Figure 1.4.6). The methodology included analysis of the tibiofemoral and patellofemoral joints, cartilage, meniscus, and ligaments, and the results showed that inter cartilages contact carries the majority of the load of the joint[180]. An accurate three-dimensional model of the knee joint is a prerequisite to ensure that its finite element model simulation is close to reality. The construction of a knee joint model mainly involves developing a comprehensive knee geometry model that encompasses the femur, tibia, patella, fibula, femoral and tibial cartilage, medial and lateral menisci, anterior and posterior cruciate ligaments, medial and lateral collateral ligaments, and the patellar ligament. The finite element model of knee joint established in this study is mainly divided into the following four steps: Model construction, Material property assignment, Boundary and loading condition and Model validation. Detailed modeling and analysis steps are described separately in the Methods section of this study.

1.5 Aims and hypothesis

1.5.1 Plantar pressure and fatigue gait recognition

Fatigued gait is common one of the risk factors for run-related injuries. Therefore, the research on wearable sensor equipped with automatic gait recognition system for fatigue risk has a wide application prospect. Most of the existing fatigue gait recognition methods in the literature require the participation of others, so they are difficult to be used in this scenario.

The ConvLSTM model will be used in this study on the ground that it transforms the structure in recurrent neural networks into the convolutional structure, thereby preserving the spatial and temporal information of plantar pressure [184]. To verify the performance of ConvLSTM model for fatigue gait recognition, we used a CNN model to compare the performances. Two hypotheses were proposed: 1). The metatarsal, midfoot, and heel pressures increased in the dominant and non-dominant feet after the fatigue intervention, with more significant changes in the non-dominant foot; 2) The ConvLSTM model has better performance than the CNN model for automatic recognition of fatigue gait.

1.5.2 Dynamic stability

Long-distance running usually causes discomfort or injury in one limb, partly due to bilateral lower limb asymmetry. Previous studies have shown that asymmetry between lower limbs or imbalance between limbs greater than 10-15% is associated with an increased incidence of injury. Therefore, the stage at which asymmetry occurs and worsens the most may be a potential factor in the occurrence of running-related injuries.

The effect of repeated test conditions period of running symmetry stability has been investigated in present study. Although the specific physiological mechanisms that influence running stability are not yet clear, it can be hypothesized that as running distance increases, the DS of symmetry in recreational runners may decrease. Therefore, this study aims to determine the nonlinear biomechanical effects of running distance on symmetry capacity. The stability of symmetry capacity is represented by the LyE of the kinematic time series symmetrical function. This exponent, which encapsulates the rate of divergence of initially close trajectories in a dynamical system, offers a unique vantage point to discern the DS of symmetry function amidst the temporal flux of a prolonged running task. Although the specific physiological mechanisms that influence running stability are not yet clear, it can be hypothesized that as running distance increases, the DS of symmetry in recreational runners may decrease.

1.5.3 Joint stress response

Excessive internal load of the knee joint is one of the causes of common musculoskeletal diseases in long-distance runners. However, current biomechanical studies on long-distance running mainly report the kinematic characteristics of the lower limbs and focus on unilateral limb analysis, while there are few comparative studies on internal load of the bilateral knee joint.

Therefore, the aim of this study was to employ coupled person-specific musculoskeletal with finite element models to explore inter-limb variations in internal knee joint loading and assess the effects of a long-distance running event on these variables. We hypothesize that: (1) differences in the loading distribution of the menisci, tibial cartilage, and ligaments on both sides will be observed at the peak value phase, both pre- and post-fatigue states; (2) disparities in the loading magnitude of the menisci, tibial cartilage, and ligaments on both sides will be observed throughout the gait support phase in both states; (3) the loading on the knee will increase with fatigue and be greater on the non-dominant side than the dominant side due to the different fatigue tolerance of the two limbs during the whole gait support phase.

2. Materials and methods

2.1 Participant

2.1.1 Plantar pressure and fatigue gait recognition

Thirty healthy amateur runners (males) were enlisted from universities and local running clubs for this study. The anthropometric information of the participates is presented in Table 2.1.1. The inclusion criteria for the current study were that the dominant extremity side was the right extremity side (preferred leg when kicking a ball), the absence of any lower extremity or pelvic musculoskeletal pain in the last six months, and running at least 2-3 times per week and for < 45 minutes or <10 km at per running event. Ethics Committee at Ningbo University approved the study (code: RAGH20210827), and all subjects signed the informed consent.

Table 2.1.1 Anthropometric characteristics of the recruited participants

Information	Mean	S.D.
Age (year)	24.27	1.36
Height (cm)	177.00	4.33
Weight (kg)	69.80	8.46
BMI (kg/m^2)	22.20	1.7

2.1.2 Dynamic stability

Seventeen male amateur runners were recruited for the study and the Table 2.1.2 shown that the demographic information. Amateur runners are required to have the ability to run 10 kilometers in 45-50 minutes [185]. All participants were determined to have their right limb as the dominant limb and have had no injuries or abnormalities in the lower limbs and pelvis in the past six months. The subjects have provided written consent for all aspects of the experiment, and the Ethics Committee of Ningbo University has approved this testing protocol (code: RAGH20220218).

Table 2.1.2 Descriptive characteristics of 17 participants

Information	Mean	SD
Age (year)	22.4	2.58
Height (cm)	177.4	4.77
Weight (kg)	71.29	7.16
BMI (kg/m^2)	22.61	1.82

2.1.3 Finite element model

A 20-year-old healthy male amateur runner was enlisted for this study, with a body weight of 72 kg and a height of 178 cm. Dominance in the right limb and a rearfoot strike pattern were noted,

alongside an absence of pelvic or lower limb injuries in the preceding six months. The amateur runner are required to be able to run 10 kilometers in 45-50 minutes[185]. Ethical approval for the study protocols was conferred by the Institutional Ethics Committee, with the assurance that all methods adhered to the Declaration of Helsinki. Furthermore, the Ethics Committee at Ningbo University (code: RAGH20230315) sanctioned all procedures.

2.2 Experimental protocol and Data collection

2.2.1 Plantar pressure and fatigue gait recognition

Subjects were guided by the experimental operator to familiarize the experimental environment (Includes ground running tests with barefoot before and after the running induced fatigue protocol) and process and participated in a 10-minute jogging warm-up on a treadmill (Satun h/p/cosmos, Nussdorf- Traunstein, Germany) in advance. A previously identified and validated protocol was employed for building a running-induced fatigue model [186]. With reference to our previously built approach [52], A heart rate sensor band (Polar RS100, United States) and Borg RPE scale (6–20 scales) were utilized for monitoring fatigue during running [187]. Every participant commenced walking on a treadmill at a velocity of 6 km/h. The pace of gait was augmented by 1 km/h every 2 minutes until an exertion level of 13 on the Borg scale was attained. Participants sustained the running pace at the established equilibrium until achieving a Borg rating of 17 or 90% of their maximum heart rate (maximum heart rate = 220-age), at which juncture they persisted in running for an extra 2 minutes. New neutral running shoes were given to every participant for the protocol involving running-induced fatigue.

Pedobarographic data collection was done before and after the running induced fatigue protocol. Dynamic plantar force data were measured during running using a FootScan pressure plate (Size:2m×0.4m, frequency:480Hz, RsScan International, Olen, Belgium) embedded in the middle of a 20-m runway. The pressure plate is calibrated using the individual's body weight prior to measurement to avoid errors. Two sets of infrared photocells were placed on either side of the data collection area to monitor the running speed. All participants were required to run barefoot over the data collection area at a speed of 3.3 m/s±5%[187]. Participants were instructed to use the non-dominant foot as the first step on the force plate and to ensure that two consecutive steps were recorded for each trial. Attempts to change the operating mode to strike the pressure plate were ruled out until three valid trial data points were measured before and after running-induced fatigue protocol.

2.2.2 Dynamic stability

XSENS MVN (Xsens, Enschede, Netherlands) represents a portable inertial motion capture system designed for comprehensive analysis of human body movements. The sensors within the system encompass accelerometers, gyroscopes, and magnetometers. As shown in Figure 2.3.4, seven sensors were individually affixed to the subject's sacrum, bilateral dorsal surfaces of the feet, shins, and thighs, in order to construct a lower limb skeletal model. The initial calibration process was carried out in accordance with the manufacturer's instructions. As shown in Figure 2.3.4 (A), this calibration data was utilized to initiate the analysis within the Xsens MVN software (version

2023, Xsens, Enschede, Netherlands) in order to fit a 7-segment half-body kinematic model to the data captured by the inertial sensors with 60Hz sampling. Prior to conducting this experiment, participants were thoroughly acquainted with the surroundings and underwent a 10-minute treadmill (Satun h/p/cosmos, Germany) warm-up session of walking or running and to confirm a submaximal speed range[30, 188].

The participants completed a 10km running on a treadmill at a submaximal speed (approximately 12 kilometers per hour, 80% of their personal best pace) [189]. Data were collected for 60s at 1000, 2000, 3000, 4000, 5000, 6000, 7000, 8000, 9000 and 10000m, which allowed for at least 100 steps can be collected during each sampling period. The participants were accustomed to using treadmills and all of them donned standard running footwear provided by the laboratory.

2.2.3 Joint stress response

Data collection was divided into four parts: (1) MRI scans, (2) ground running test before and (3) after a 10km treadmill run, and (4) treadmill running at submaximal speed for 10km. The (2) and (3) sections employed the same testing procedure (Figure 2.3.4 (A)).

2.2.3.1 Medical image acquisition

A 3.0 T clinical MRI scanner (General Electric Healthcare, Milwaukee, WI, USA), equipped with a 12-channel knee joint transmit-receive RF coil, was employed for the acquisition of magnetic resonance data. The participant was oriented in a supine, non-weight-bearing posture, with the right knee under investigation centrally aligned within the coil. The MRI data was collected in the morning to avoid the day-long load bearing in the knee joint[190].

2.2.3.2 Experimental data collection

For the 10 km treadmill running (Quasar, h/p Cosmos®, GmbH, Germany), the participant wore standardized lab-provided running footwear and maintained a submaximal speed of approximately 11.5 km/h, 80% of their personal best, to represent a casual running pace [30].

Our data were collected in the ground running test before and after the 10km treadmill run. The participant was allowed to acclimate by running on the track in the data collection area before the ground running tests to mitigate the influence of conscious gait adjustments. Subsequently, a total of 38 retroreflective markers were affixed in alignment with a pre-established protocol[191]. The marker trajectory and Ground reaction forces (GRFs) were synchronously collected using an eight-camera Vicon 3D motion capture system (Vicon Metrics Ltd.,200Hz, Oxford, United Kingdom) and an AMTI force platform (AMTI, 1000Hz, Watertown, Massachusetts, USA), respectively. The velocity for the ground running tests was consistently monitored at 3.33 m/s using photocells. Five successful trials meeting the criteria for proximity to the target speed and step location within the force plate area were chosen for subsequent MS and FE analysis[192].

In addition, muscle activity from the rectus femoris, biceps femoris, tibialis anterior, medial gastrocnemius, and lateral gastrocnemius of the dominant limb was synchronously captured using a 16-channel surface electromyography system (Delsys, 1000 Hz, Boston, Massachusetts, US). Prior to the testing procedures, maximum voluntary contraction (MVC) levels for these muscles were also recorded to establish a baseline for activity assessment.

2.3 Data processing

2.3.1 Plantar pressure and fatigue gait recognition

For each trial, 10 plantar anatomical regions were identified by the FootScan application. To avoid recognition errors, the pixels of each area was manually calibrated by an operator. These areas were defined as the Hallux (H), Other toe (OT), Metatarsal 1-5 (M1-M5), Midfoot (MF), Medial heel (HM) and Lateral heel (HL). Time-series attributes of force information for each region and the sum area were interpolated to 101 frames using linear interpolation for statistical comparison. In order to reduce the effect of individual weight and gait speed differences on the data, all data in this study were annotated using Zavg (total force over the entire support period divided by the total number of frames)[165]. As shown in Figure 2.3.1, To preserve asymmetric information of bilateral limbs before and after fatigue, the plantar force data of the non-dominant and dominant foot were stitched longitudinally to obtain the bipedal force distribution information of one gait cycle for machine learning training[163].

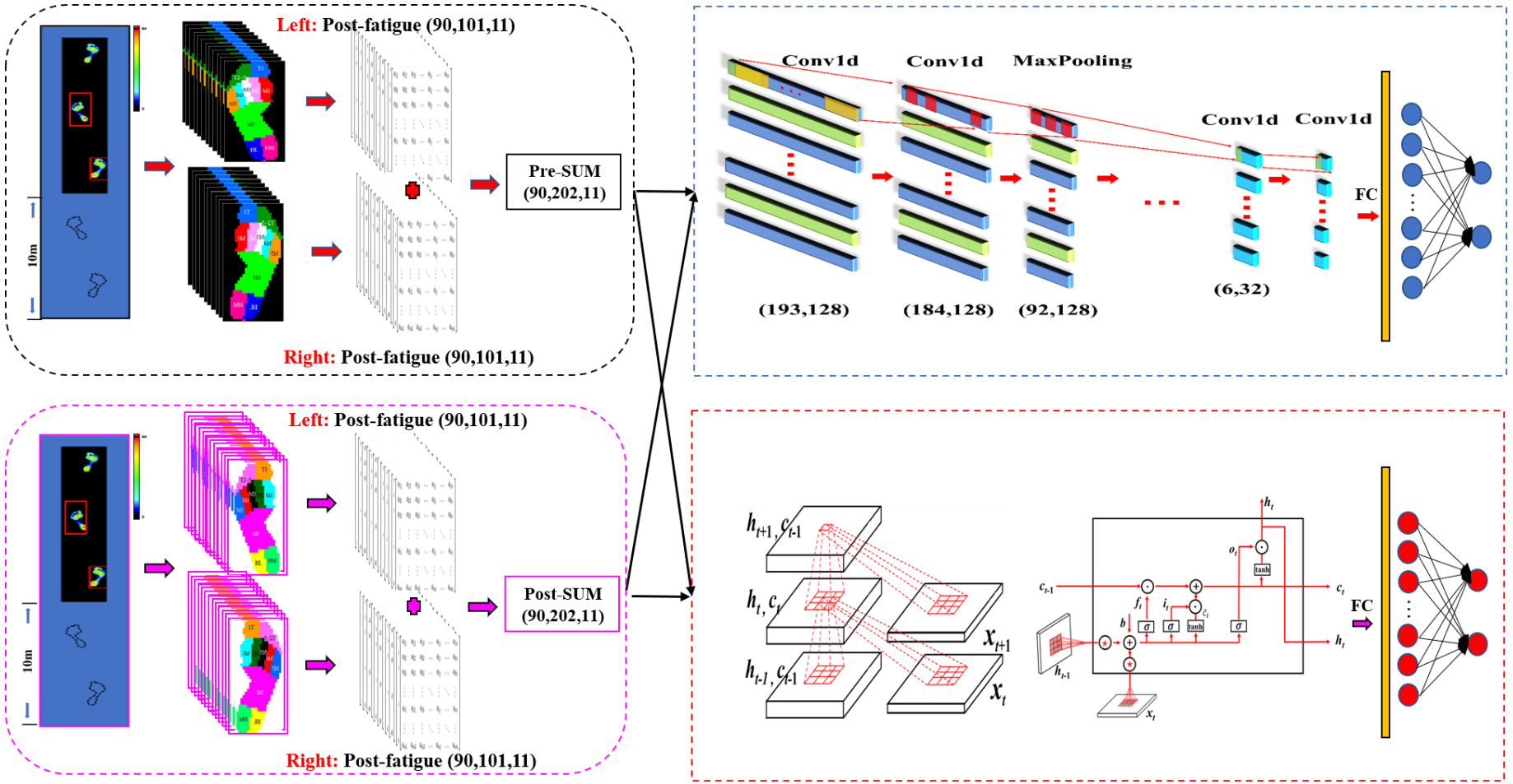

Figure 2.3.1 Data collection and analysis process. Note: Non-dominant side: left foot; Dominant side: right foot; H: Hallux, OT: Other toe; M1-5: Metatarsal 1-5; MF: Midfoot; HM: Medial heel; HL: Lateral heel.

2.3.1.1 CNN model building

The current study uses the Keras Application Programming Interface (API) in python 3.8.8 for CNN and ConvLSTM model building. CNN models have good performance for feature extraction of input data through convolutional operations of different topological structures kernels. The convolution layer in the model preserves the spatial relationships of the data by using the same convolution operation for each position of the original data in turn. Each type of feature that is extracted generates a feature matrix *Z*. Therefore, after k times convolution calculations, the corresponding output matrix Z_k can be represented by Equation (1). In addition, the convolution operation for one-dimensional time series data is also a nonlinear transformation of the original series. Applying a convolution kernel of length l to a univariate time series *X* of length *T*, Equation (2) is obtained.

$$Z_k = f(W_k * X + b) \tag{1}$$

$$C_t = f\left(w * X_{t-l/2:t+l/2} + b\right) \mid \forall t \in [1, T] \tag{2}$$

Where W_k and k are the convolution kernels (Size: $k_1 \times k_2$) and the number of convolution kernels, respectively. b is biased, and the convolution operator is defined as $*$. f is the activation function that performs a nonlinear transformation in the convolution layers.

As shown in Figure 2.3.2, The optimal convolution neural network model for the recognition of fatigue gait is obtained through repeated debugging parameters. We used a total of eight convolutional layers, three maximum pooling layers, one average pooling layer, one Dropout layer and one Dense layer to build the convolutional neural network model. The number of convolution kernels is set to (128, 128, 128, 128, 64, 64, 32, 32). The time step settings are (10, 10, 10, 10, 10, 10, 4, 4). In addition, 'RELU' and 'Softmax' are set as the activation functions for the convolutional and Dense layer, respectively.

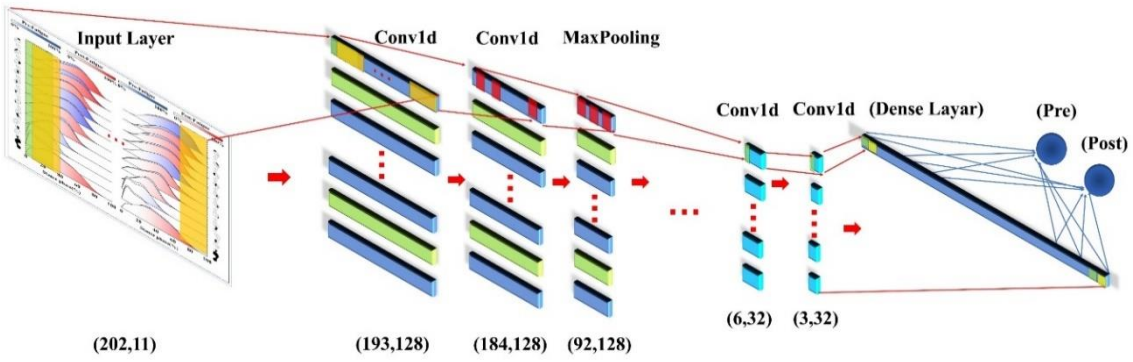

Figure 2.3.2 Diagram of the internal structure of CNN model in this study

2.3.1.2 ConvLSTM model building

The convolutional layer extracted the temporal characteristics from the pressure data, while the LSTM layer handled the spatial characteristics (Figure 2.3.3 (B)). In our ConvLSTM model, operations are depicted by Equations (3-8), where $*$ symbolizes the convolution process, and $\circ$ denotes the Hadamard product.

$$f_t = \sigma\left(W_{xf} * x_t + W_{hf} * h_{t-1} + b_f\right) \quad (3)$$

$$i_t = \sigma(W_{xi} * x_t + W_{hi} * h_{t-1} + b_i) \quad (4)$$

$$\tilde{c}_t = \tanh(W_{xc} * x_t + W_{hc} * h_{t-1} + b_c) \quad (5)$$

$$c_t = f_t \circ c_{t-1} + i_t \circ \tilde{c}_t \quad (6)$$

$$o_t = \sigma(W_{xo} * x_t + W_{ho} * h_{t-1} + b_o) \quad (7)$$

$$h_t = o_t \circ \tanh\left(c_t\right) \quad (8)$$

Where i_t, f_t, and o_t are the input gate, oblivion gate, and output gate, respectively, in the proposed model; x_t represents the data input at the current moment, while h_{t-1} refers to the output from the hidden layer at the preceding moment. c_t denotes the cell state.

Figure 2.3.3 (A) shows the framework for building the ConvLSTM model in the current research. In this study, we try to make l choose a variety of different division lengths, such as 51, 101, 151, 202, etc., for modeling, and finally find that the model's classification performance is optimal when the subsequence length is l = 101. The optimal ConvLSTM for the recognition of fatigue gait is obtained through repeated debugging parameters. We sequentially set up a ConvLSTM layer (Number of convolution kernels=64, kernel size= (1,5)), A dropout layer (Random Discard Ratio= 0.5), a Flatten layer and two dense layers (first: units=50, activation='RELU'; Second: units=2, activation= 'Softmax') in the final model.

In order to ensure fast convergence during the training of the binary classification model, the cross-entropy loss function was chosen as the loss function for the current study, as shown in Equation (9).

$$L = -\frac{1}{N}\sum_{i=1}^{N}\left[y^{(i)}\log\left(\hat{y}^{(i)}\right) + \left(1 - y^{(i)}\right)\log\left(1 - \hat{y}^{(i)}\right)\right] \quad (9)$$

where N is the number of samples and $y^{(i)}$ and $\hat{y}^{(i)}$ are defined as the true and predicted values.

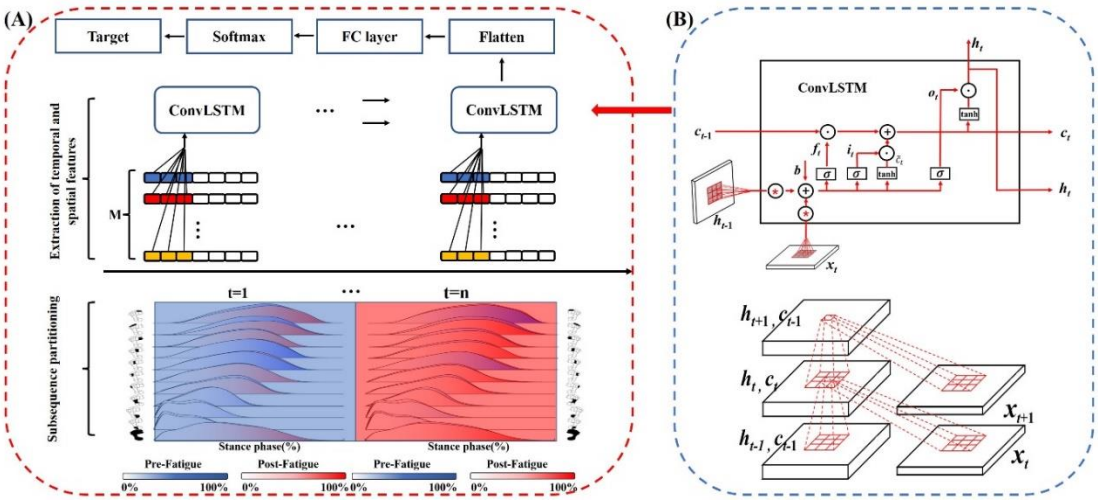

Figure 2.3.3 Diagram of the internal structure of ConvLSTM model in this study. (A) Frame diagram of the ConvLSTM model. (B) Structure diagram of the ConvLSTM model.

2.3.2 Dynamic stability

Each recorded running measurement underwent post-processing within the Xsens MVN software, employing the corresponding calibration file. This post-processing was executed using the 'High Definition' mode and the "no-level" processing scenario. In addition, the built-in algorithm of software was used to calculate the angle information of the mannequin's knee, hip, and ankle joints on three anatomical planes of the same space coordinate system. Additional post-processing steps for the angle and acceleration data were carried out using a custom Python script written in Visual Studio Code version 1.59.0.

Successive gait cycles (comprising 50 cycles in this investigation, collected from the 35th cycle to calculate LyE) were discerned, with each gait cycle delineated as the interval between successive ground contacts of the same foot. The methodology employed for stride identification through resultant acceleration inertial data form a IMU attached in foot back (Figure 2.3.4 (B)) is detailed elsewhere[193]. First, we calculate the resultant acceleration of the IMU data (As show in Eq 10, resultant acceleration is calculated by taking the square root of the sum of the squared individual components of acceleration in these three axes). The peak resultant acceleration points were defined as initial contact (IC) and two adjacent IC are identified as one complete gait cycle of one side. The threshold of 2g (g= gravitational acceleration) was identified as Toe-off (TO). Previous studies have shown that errors caused by axis misalignment can be minimized because of the resultant acceleration applied to the method[194, 195].

For each participant and each side total of continuous 50 cycles were selected from the collected data. Following this, the dataset was temporally standardized to comprise 5050 data points for

each side, which on average corresponded to approximately 101 data points per side of individual gait cycle.

$$\text{Resultant acceleration } = \sqrt{x^2 + y^2 + z^2} \tag{10}$$

The degree of asymmetry of each complete gait cycle was assessed using the dynamic Symmetry Function (SF). The specific calculation method is shown in eq. (11):

$$SF(t) = 2 \cdot \frac{x_{right}(t) - x_{left}(t)}{\text{Range}\left(x_{right}(t)\right) + \text{Range}\left(x_{left}(t)\right)} \tag{11}$$

Where, the overarching structure of SF encompasses a function of time (t) and articulates the percentage disparity between the implicated right (x_{right}) and left (x_{left}) facets relative to an average range of change[196]. Then the SF data of 50 continuous gaits were spliced to facilitate the DS calculation.

DS was determined based on the LyE, The computation of LyE was performed using the algorithm outlined in the publication by Rosenstein et al.[31], This approach assumes that each stride feature has the potential to be identical to any other stride feature. The variations observed in SF measurements in gait are attributed to minor perturbations. Consequently, SF variability can serve as a means to assess the system's stability by monitoring the recovery of a perturbed gait cycle toward the mean. Since the calculated SF has the characteristics of a one-dimensional time series vector. Therefore, a new n-dimensional state space should be created for determine dynamic perturbations. A SF in n-dimensional space would calculate as eq. (12):

$$X(t) = [x(t), x(t + \tau), x(t + 2\tau) \ldots, x(t + (n - 1)\tau)] \tag{12}$$

Where, For the determination of time delay (τ), the initial minimum of mutual information was identified in accordance with the approach proposed by Fraser and Swinney in 1986[197]. Likewise, the selection of an appropriate number of dimensions (n) involved the utilization of the global false nearest neighbor technique[198], as shown in Figure 2.3.5. In addition, the embedding dimensions and time delay settings for present study are shown in Table 3.2.1 & Table 3.2.2.

Following the reconstruction of the state-space, the quantification of the Lyapunov exponent (λ) was conducted utilizing the algorithm delineated by Rosenstein et al.[31]. To achieve this, the Euclidean distance between the initially proximate neighbors of every point within the state-space was meticulously monitored. Elevated values of λ are indicative of diminished DS. Therefore, the DS can be created using the following formula (eq. (13)):

$$\ln\{d_i(t+t)/d_i(t)\} = \lambda_{max}\, t. \qquad (13)$$

The $\ln\{d_i(t+t)/d_i(t)\}$ denotes the logarithm of dispersion, di(t), which is calculated as the average across all pairs of nearest neighbors, i. The λ_{max} represents the slope of this line, which measures the average rate of divergence among initially adjacent trajectories across the dimension that is considered the least stable.

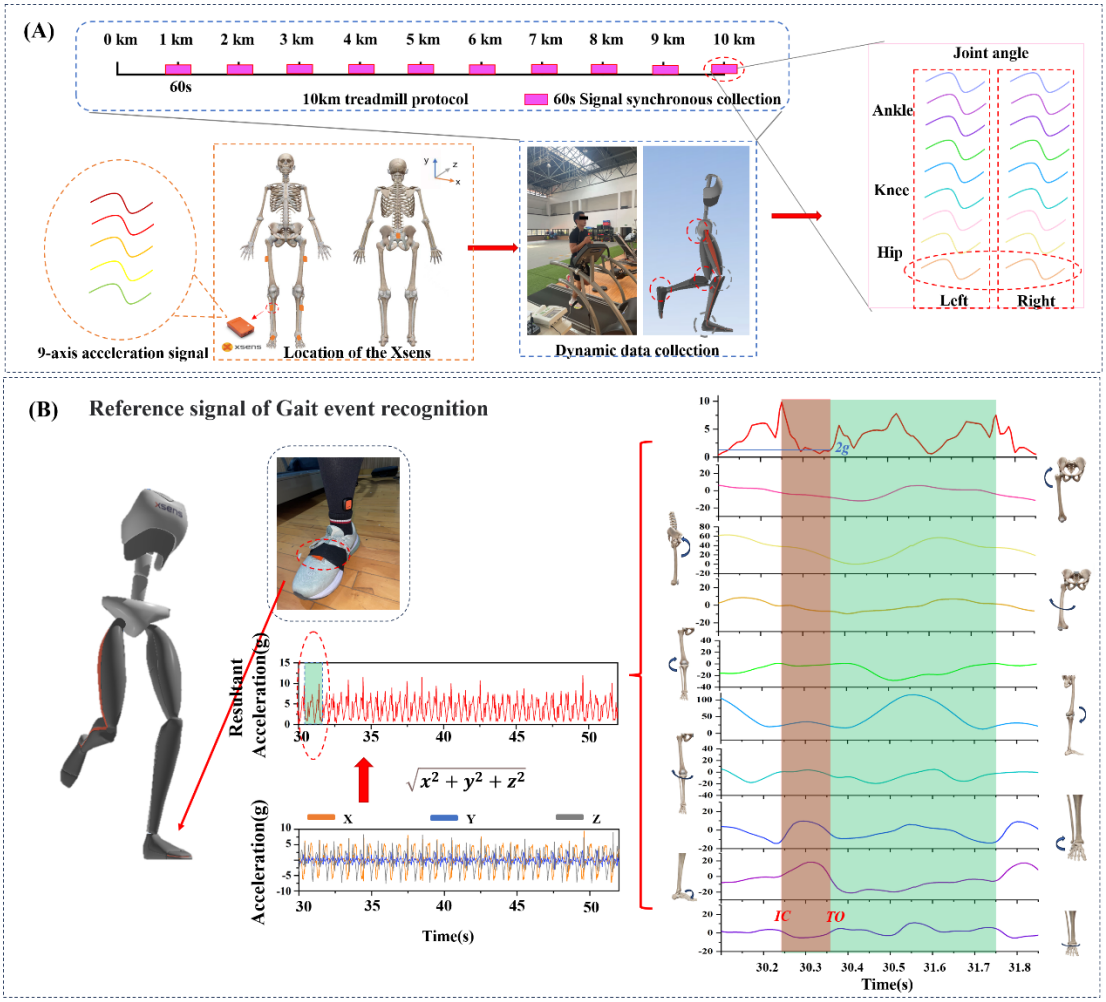

Figure 2.3.4 Illustrating (A) 10km running protocol and the location of the IMU. (B) Process of gait data detection. (C) Evaluation of the local dynamic running stability

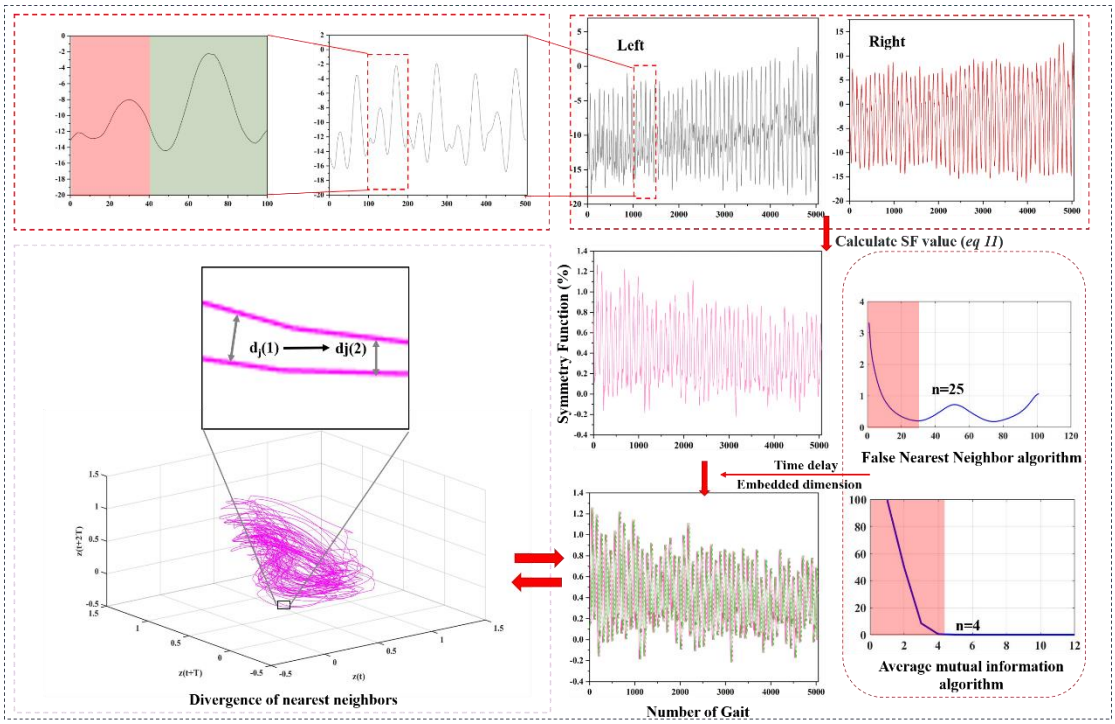

Figure 2.3.5 Illustrating of evaluation of the dynamic stability of SF of running gait.

2.3.3 Joint stress response

2.3.3.1 Musculoskeletal model

The Opensim (National Center for Simulation in Rehabilitation Research, Stanford, USA) gait 2392 generic musculoskeletal model was chosen and scaled in the context of real experiments to establish a personalized model that aligns with individual characteristics[169]. Figure 2.3.5 (A)). An inverse kinematic analysis was then conducted to align the experimental biomechanics with the acquired motion data. The residual reduction algorithm (RRA) was employed to address minimization errors in the modeling and marker data processing. This application ensured that any computational inaccuracies in inverse dynamics remained within acceptable limits, allowing for a dynamic alignment with GRF data, culminating in static optimization. Finally, joint reactions analysis (JRA) was used to calculate the knee reaction forces for the muscle activation scenario and the joint reaction moments relative to the ground.

2.3.3.2 Finite element modeling

Knee Joint Reconstruction and Segmentation

Figure 2.3.6 (B) presents the structured framework outlining the sequential phases for reconstructing FE models. The three-dimensional reconstruction was carried out using MIMICS 21.0 software (Materialise, Leuven, Belgium). Segmentation of magnetic resonance imaging (MRI)

data facilitated the delineation of the anatomical boundaries of the articular cartilages (femoral, tibial, and patellar), menisci (medial and lateral), and ligaments (ACL, PCL, MCL, LCL, and PTL). To assure the accuracy of the FE model, manual segmentation of non-osseous elements was meticulously performed under the guidance of experienced orthopedic and radiological experts, attaining a precision of 0.1 mm[199]. The tissues reconstructed in great detail were exported as STL files and further refined for model representation in Geomagic Studio 2021 (Geomagic, Inc., Research Triangle Park, NC, United States), where any problematic surfaces were identified and rectified. The final geometries were then assembled using SolidWorks 17 software (SolidWorks Corporation, MA, United States), completing the model construction.

Model Assembly and Material Allocation

Material properties were allocated to each specific tissue to authentically model the biomechanical variations within the knee joint. The stance phase of running gait, characterized by a comparatively brief load application, permits the characterization of all cartilage tissues under quasi-static conditions using an instantaneous elastic model [200-202]. For the sake of computational efficiency without compromising accuracy, ligaments were modeled as transversely isotropic, nearly incompressible materials using the Neo-Hookean approach[200]. Table 2.3.1 enumerates the attributes and values of material constants for each geometric entity. In accordance with the knee joint's anatomy and the specifics of the stance phase in running, modeling, meshing, and boundary conditions setting for this finite element knee model were established in Workbench 2021 R1 (ANSYS Inc., Canonsburg, Pennsylvania, USA). The distal portions of the tibia and fibula were fully constrained, immobilizing all shifts and rotations.

Model Validation

By setting boundary conditions for the model, the rotation center (The midpoint of the trans-epicondylar line[203]) of the femur is used to find the translational displacement values for the knee joint. The two values for rotation are based on how the tibial moves (the average rotation angles of the MCL and LCL attachment points on the tibia and fibula in relation to the tibial plateau reference point). We compared the displacements in the antero-posterior, proximal-distal, and medial-lateral directions of the knee model of the present study (under conditions of 0° and remote displacement of 15° and 30° knee flexion and 134N afterload on the center of rotation of the femur) with the finite element simulation results of Song et al.[204] (0°) and cadaveric experiments of Gabriel et al.[205] (0°, 15° and 30°).

Running Gait Simulation

The stance phase was divided into five stages (initial contact, first peak, mid-stance, second peak,

and toe-off) based on the vertical GRF data. The knee rotation center was used to apply the knee flexion angle (the translational displacement), joint reaction force, and joint reaction moment calculated by the MS model to the corresponding five gait moments (Figure 2.3.6 C1 & C2). Constraints on femoral rotations were imposed only when specific flexion angle-related loads were applied, leaving other directional movements unconstrained. Through binding commands, cartilage and ligament tissues were rigidly attached to their corresponding skeletal points of origin. The meniscus and tibial cartilage were also bound together in the same way. Five discrete contact pairs were featured within the knee joint model, each facilitating surface-to-surface interactions: between the femoral cartilage and the medial meniscus, the lateral meniscus, the medial tibial cartilage, the lateral tibial cartilage, and the patellar cartilage. A frictionless, finite sliding approach was employed to address the minimal friction between joint cartilage surfaces[206], as shown in Figure 2.3.6.

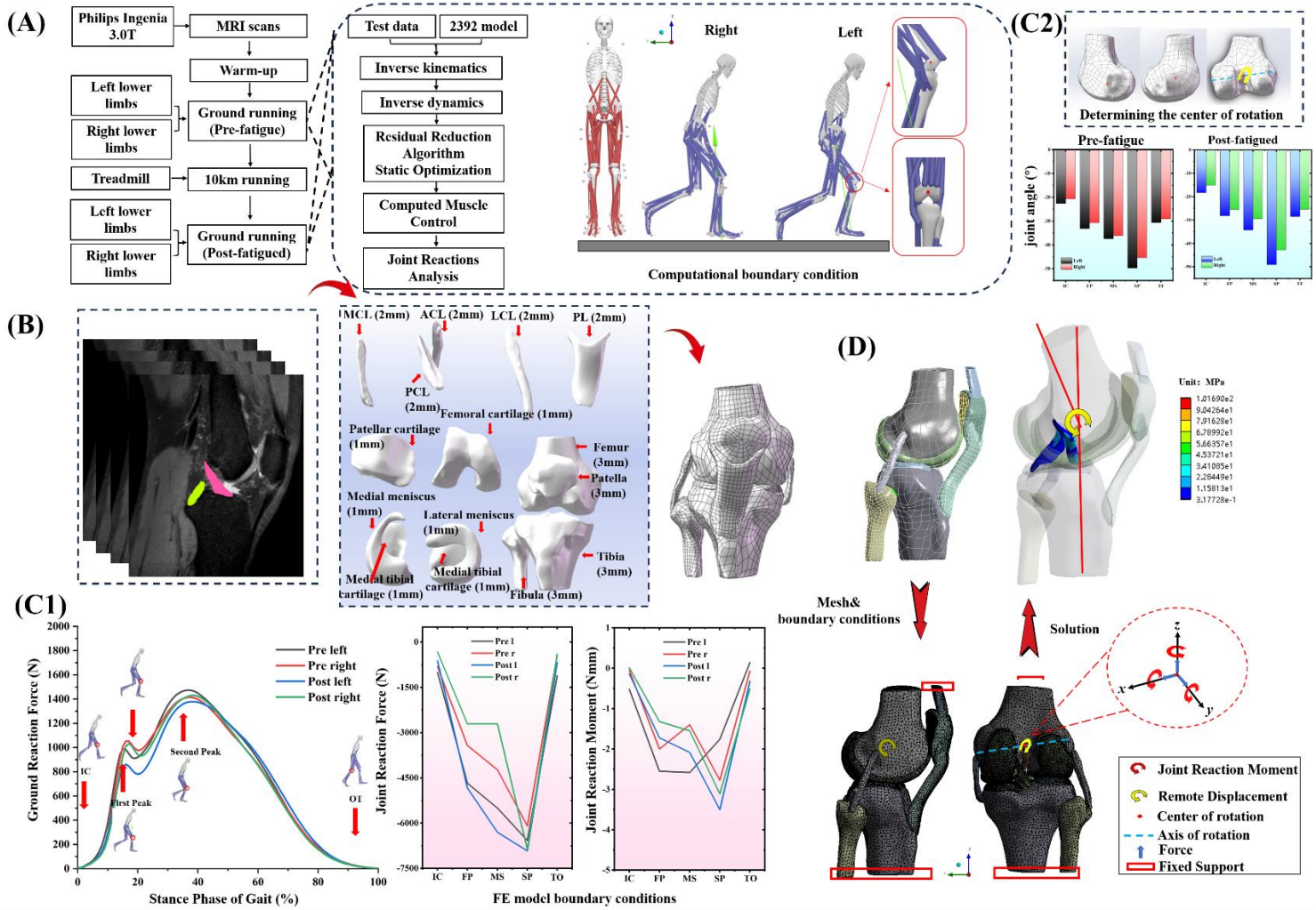
(A)
Philips Ingenia 3.0T
MRI scans
Warm-up
Left lower limbs
Right lower limbs
Ground running (Pre-fatigue)
Treadmill
10km running
Left lower limbs
Right lower limbs
Ground running (Post-fatigued)
Test data
2392 model
Inverse kinematics
Inverse dynamics
Residual Reduction Algorithm Static Optimization
Computed Muscle Control
Joint Reactions Analysis
Right
Left
Computational boundary condition
(C2)
Determining the center of rotation
Pre-fatigue
Post-fatigued
joint angle (°)
(B)
MCL (2mm)
ACL (2mm)
LCL (2mm)
PL (2mm)
PCL (2mm)
Femoral cartilage (1mm)
Patellar cartilage (1mm)
Femur (3mm)
Patella (3mm)
Medial meniscus (1mm)
Lateral meniscus (1mm)
Tibia (3mm)
Medial tibial cartilage (1mm)
Medial tibial cartilage (1mm)
Fibula (3mm)
(D)
Unit: MPa
1.01690e2
9.04264e1
7.91628e1
6.78992e1
5.66357e1
4.53721e1
3.41085e1
2.28449e1
1.15813e1
3.17728e-1
Mesh& boundary conditions
Solution
Joint Reaction Moment
Remote Displacement
Center of rotation
Axis of rotation
Force
Fixed Support
(C1)
Ground Reaction Force (N)
Pre left
Pre right
Post left
Post right
IC
First Peak
Second Peak
OT
Stance Phase of Gait (%)
Joint Reaction Force (N)
Joint Reaction Moment (Nmm)
Pre l
Pre r
Post l
Post r
IC FP MS SP TO
FE model boundary conditions

Figure 2.3.6 Musculoskeletal Modeling and Finite Element Modeling and Analysis. (A) Typical flow of motion simulation of OpenSim. (B) Optimized three-dimensional model of the knee joint. (C1) GRFs, joint reaction forces, and joint reaction moments correspond to the 5 phases of the stance phase; (C2) the center of rotation of the knee joint is determined, and knee flexion angles correspond to the 5 phases of the stance phase. (D) Knee joint model after meshing and solutions. Note: Pre left: left leg before 10km running. Pre right: eight legs before 10km of running. Post left: left leg after 10km running. ACL: anterior cruciate ligament, PCL: posterior cruciate ligament, MCL: medial collateral ligament, LCL: lateral collateral ligament, PTL: Patellar tibial ligaments. IC: initial contact; FP: first peak; MS: mid-stance; SP: second peak; TO: Toe of

Table 2.3.1 Material properties and element types used in the knee joint FE models to represent different components.

Part name		References	Element number	Model assumptions	Element Type	Material assignment			
						Young's modulus (MPa)	Poisson's ratio	C1	D1
Bone	Femur	Song et al.,[204]	51809	Linearly elastic	Tetrahedral solid	11000	0.3		
	Tibia		43673						
	Fibula		5935						
	Patella		8062						
Meniscus	Medial	Li et al., 2001[202]	24313	Linearly elastic		59	0.49	\	\
	Lateral		22276						
Cartilage	Femoral	LeRoux et al., 2002[201]	133537	Linearly elastic		55	0.46		
	Medial tibial		4780						
	Lateral tibial		5373						
	Patellar		11524						
	Tibiofibular		3521						
Ligament	ACL	Li et al., 2001[202]	1602	Neo-Hookean	Tension-only Tetrahedral solid	\	\	1.95	0.00683
	PCL		1902					3.25	0.0041
	MCL		1441					1.44	0.00126
	LCL		1959					1.44	0.00126
	PTL		18163					3.25	0.0041

Note: ACL: anterior cruciate ligament, PCL: posterior cruciate ligament, MCL: medial collateral ligament, LCL: lateral collateral ligament, PL: Patellar ligament.

2.4 Statistical analysis

2.4.1 Plantar pressure and fatigue gait recognition

In this study, a total of 90 cases were sampled, and 80% of the samples were set as the training set and 20% as the test set, where 20% of the training samples were set as the validation set for cross-validation. Therefore, the training set validation set and test set samples in the current study are 72, 14 and 18. In order to avoid the occurrence of model underfitting, the number of model iterations was set to 300. The current study uses Accuracy, Sensitivity and Specificity as quantitative metrics for the performance of two classification models. We used fatigue gait as positive samples and normal gait as negative samples. Thereinto, ***Acc*** (14) was used to assess the overall classification capability of the models. ***Sen*** (15) and ***Spe*** (16) were used to evaluate the classification capability of negative samples and positive samples of the models, respectively.

$$Accuracy = \frac{TP+TN}{(TP+FN+FP+TN)} \times 100\% \quad (14)$$

$$Sensitivity = \frac{TP}{(TP+FN)} \times 100\% \quad (15)$$

$$Specificity = \frac{TN}{(FP+TN)} \times 100\% \quad (16)$$

Where TP, TN are the number of samples correctly identified as fatigue gait and normal gait, respectively, and FP and FN are the number of samples incorrectly identified as fatigue gait and normal gait, respectively. In order to avoid accidental error, each model is run five times on the test set, and the corresponding classification results are collected.

The Shapiro-Wilk test was performed to check the normality of the data distribution. The paired sample T-test of open-source statistical parameter mapping 1d (SPM1d) was used to check the differences between pre- and post-fatigue time-series force at dominant and non-dominant foot. The discrete values of the percentage of time of peak force were checked using paired sample T-test in python 3.8.8 with the SciPy library. The significance levels were set at 0.05.

2.4.2 Dynamic stability

Statistical analyses examined the effects of different running stages within 10 km on the DS of the angular symmetry of each joint of the lower limbs. Descriptive statistics are presented in the form of Mean± Standard Deviation (SD). All data underwent normality assessment through the examination of Q–Q plots and the application of Shapiro–Wilk tests. The one-way repeated measures analysis of variance(one-tail) and Tukey's Honest Significant Differences (HSD) was performed to assess significant differences among groups of Lye of SF. Analyses were performed

using SciPy library of Python 3.8.8 using a statistical significance level of $p < 0.05$.

3 Results

3.1 Plantar pressure and fatigue gait recognition

3.1.1 Force development in toe and metatarsal areas

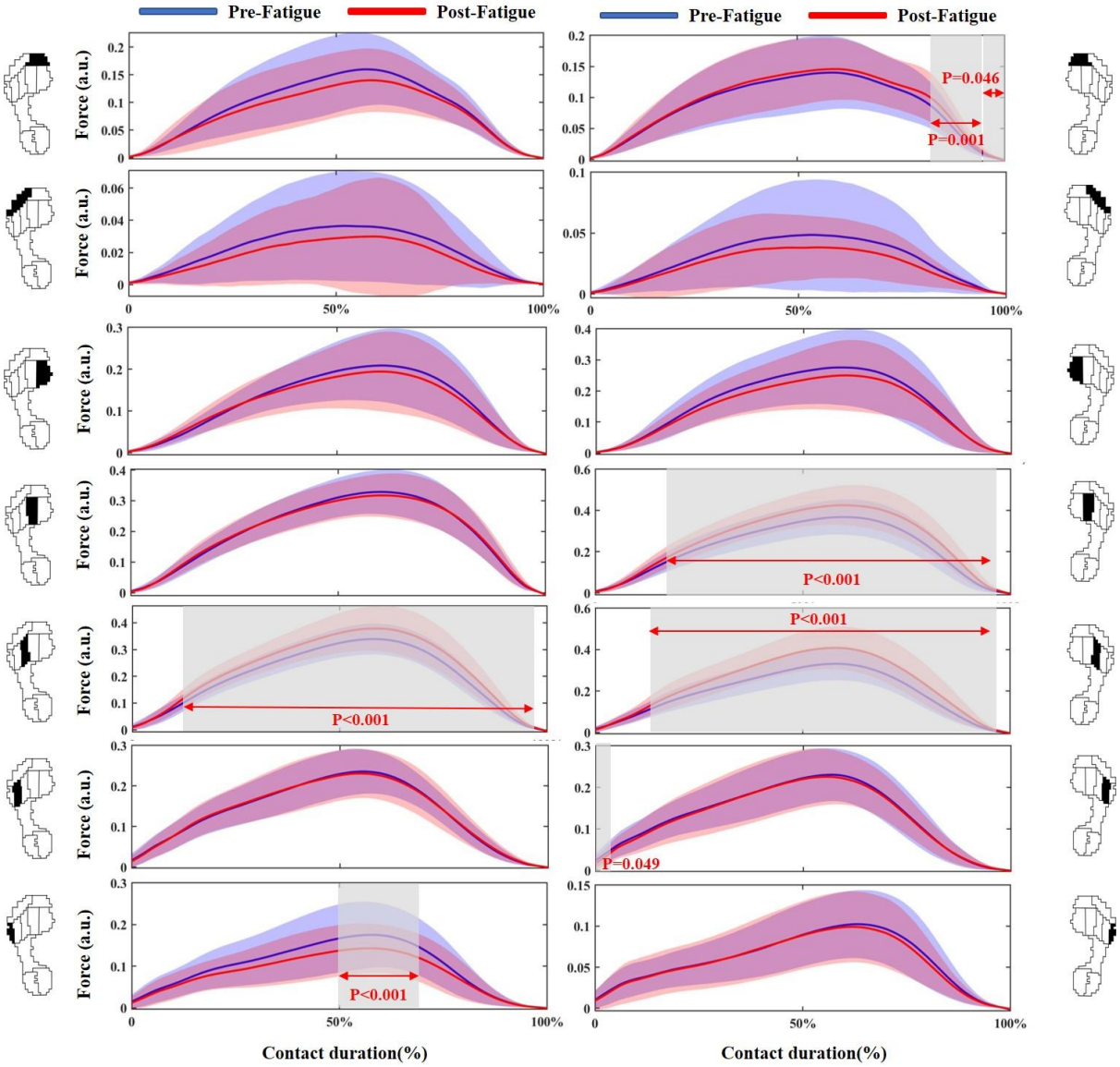

Figure 3.1.1 The time-series normalized force in the metatarsal areas in the pre-fatigue versus post-fatigue at non-dominant and dominant foot during running gait. Note: Non-dominant side: left foot; Dominant side: right foot.

As shown in Figure 3.1.1, starting from initial non-dominant foot contact, the force progression in forefoot regions differed between pre- and post-fatigue states. Specifically, the force in M3 shows a significant increase at 12-79% of contact duration after fatigue. However, the force of M5 has

decreased at 50-69% of contact duration after fatigue (p<0.001). For the dominant foot, there was a significant increase of force at OT (83-95% (p=0.001), 96-100% (p=0.046) of contact duration), M2(17-97%, p<0.001) and M3(14-97%, p<0.001) after running-induced fatigue. However, the force of M4 decreased at 0-3% of contact duration after fatigue (p=0.049).

3.1.2 Force development in the middle foot, heel, and sum areas

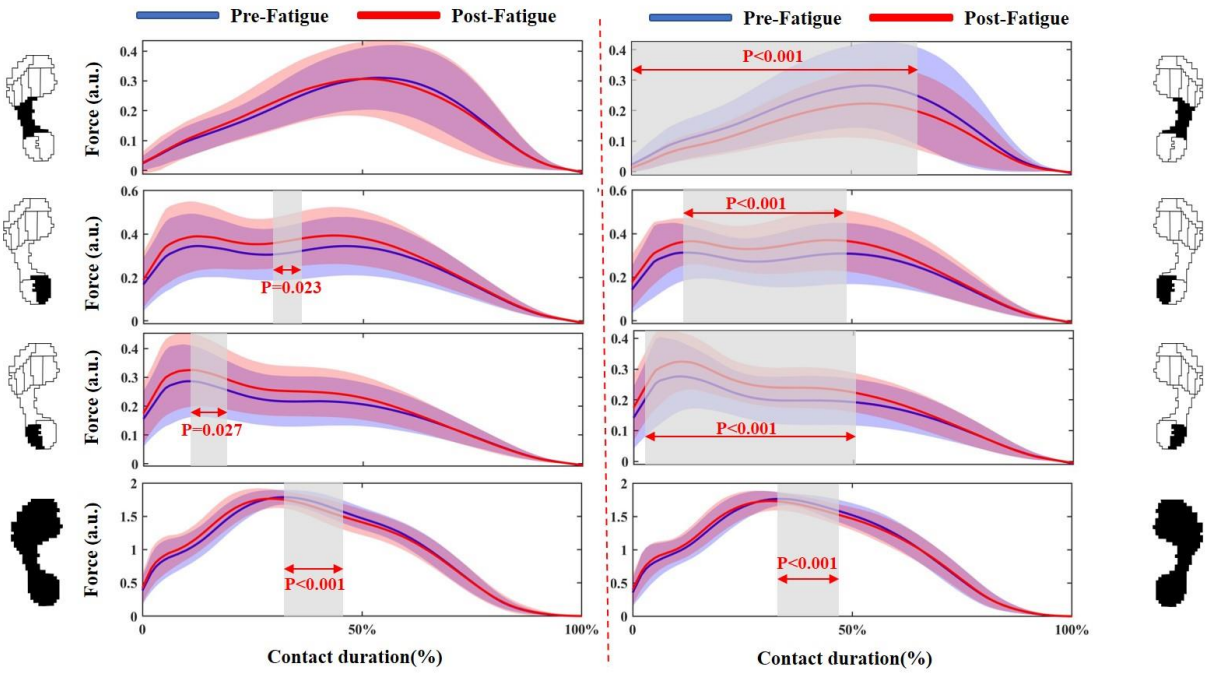

Figure 3.1.2 The time-series normalized force in the middle foot, heel and sum areas in the pre-fatigue versus post-fatigue at non-dominant and dominant foot during running gait. Note: Non-dominant side: left foot; Dominant side: right foot.

As shown in Figure 3.1.2, there was no difference in MF at the non-dominant foot. Interestingly, there was a significant decrease in plantar force at the dominant foot (0-65%, p<0.001). The heel regions were directly affected by running fatigue. For non-dominant and dominant plantar force was significantly increased at HM (non-dominant: 30-36%, p=0.023; dominant:11-49%, p<0.001) and HL regions (non-dominant: 11-19%, p=0.027; dominant:3-51%, p<0.001). However, the sum of forces from all ten regions at non-dominant (33-46%, p<0.001) and dominant (34-47%, p<0.001) significantly decreased after running-induced fatigue.

3.1.3 Relative time of peak force

Table 3.1.1 The relative of time of peak force in the 10 areas in the pre-fatigue versus post-fatigue at non-dominant and dominant foot during running gait.

Areas	Non-dominant foot			Dominant foot		
	Pre (%)	Post (%)	p-value	Pre (%)	Post (%)	p-value
H	56.99(9.07)	57.26(11.14)	0.84	55.6(12.71)	58.9(13.02)	**0.04***
O T	52.51(11.90)	55(13.46)	0.17	53.34(11.59)	52.43(12.95)	0.58
M 1	56.99(9.33)	55.8(11.58)	0.27	56.22(10.75)	56.33(10.62)	0.92
M 2	58.97(6.19)	58.7(7.09)	0.74	58.47(5.96)	58.32(6.38)	0.86
M 3	56.74(3.46)	56.87(4.62)	0.22	56.98(4.39)	56.51(5.23)	0.49
M 4	54.46(5.01)	54.00(7.09)	0.56	55.93(5.60)	55.70(6.31)	0.77
M 5	57.03(7.88)	57.38(9.23)	0.76	62.23(6.59)	59.62(11.30)	**0.05***
M F	53.26(6.40)	50.50(7.14)	**0.001***	53.87(6.75)	53.61(8.09)	0.81
H M	25.37(18.94)	25.3(17.58)	0.97	24.48(19.59)	24.57(17.30)	0.97
H L	11.02(11.54)	11.62(10.25)	0.72	14.50(15.19)	11.29(10.64)	0.07
S UM	31.61(4.76)	29.7(6.06)	**0.01***	33.47(6.32)	32.38(7.86)	0.28

Note: "*" means significant difference between pre- and post-fatigue state ($p \leq 0.05$). Non-dominant foot: left foot; Dominant foot: right foot.

As shown in Table 3.1.1, the relative time of peak force was significantly shortened at MF (p=0.001) and SUM (p=0.01) regions at non-dominant feet in a fatigued state. Similarly, there was a significant shortening in the relative time of peak force at M5 of the dominant foot after fatigue. Interestingly, for H regions, the relative time of peak force was significantly delayed.

3.1.4 Representations of deep learning models

Table 3.1.2 Classification metrics of total plantar pressure by two models

Model	Accuracy	Sensitivity	Specificity
CNN	0.800	0.874	0.718
ConvLSTM	0.867	0.874	0.859

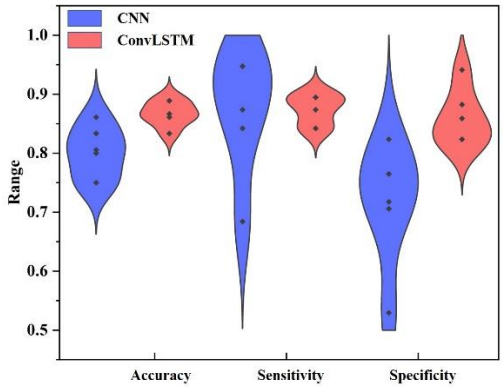

Figure 3.1.3 Violin plots of classification results of total plantar pressure at CNN and ConvLSTM model.

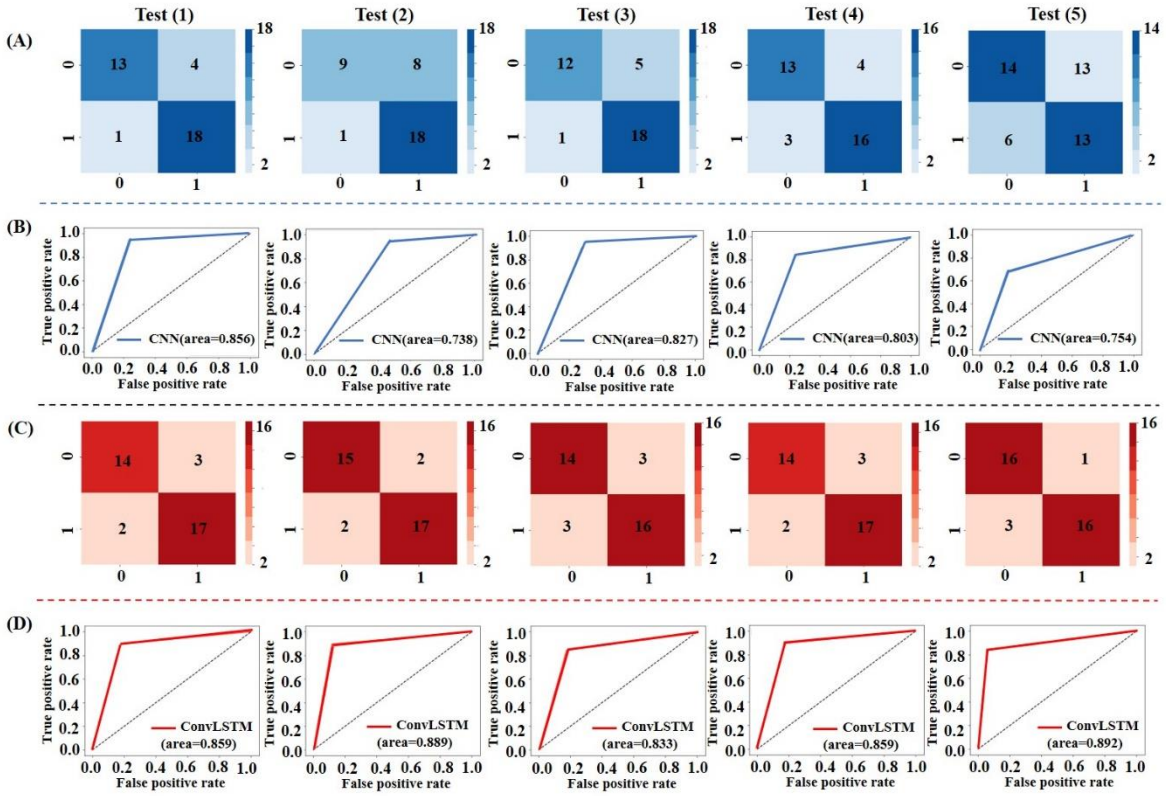

Figure 3.1.4 Confusion matrix and ROC of CNN and ConvLSTM models for 5 tests, respectively. (A) Confusion matrix of CNN model, (B) ROC of CNN model, (C) Confusion matrix of ConvLSTM model, (D) ROC of ConvLSTM model.

The classification results of total plantar pressure at CNN and ConvLSTM model shown in Figure 3.1.3 and the Confusion matrix and ROC of each model shown in Figure 3.1.4. Table 3.1.2 presents the average accuracy, specificity, and sensitivity derived from the five test sets. The ConvLSTM model outperformed the CNN with an accuracy of 86.7% versus 80%. Likewise, ConvLSTM's specificity was superior at 85.9%, compared to CNN's 71.8%. Nonetheless, both models matched with a sensitivity rate of 87.4%.

3.2 Dynamic stability

3.2.1 Maximum Lyaplov index

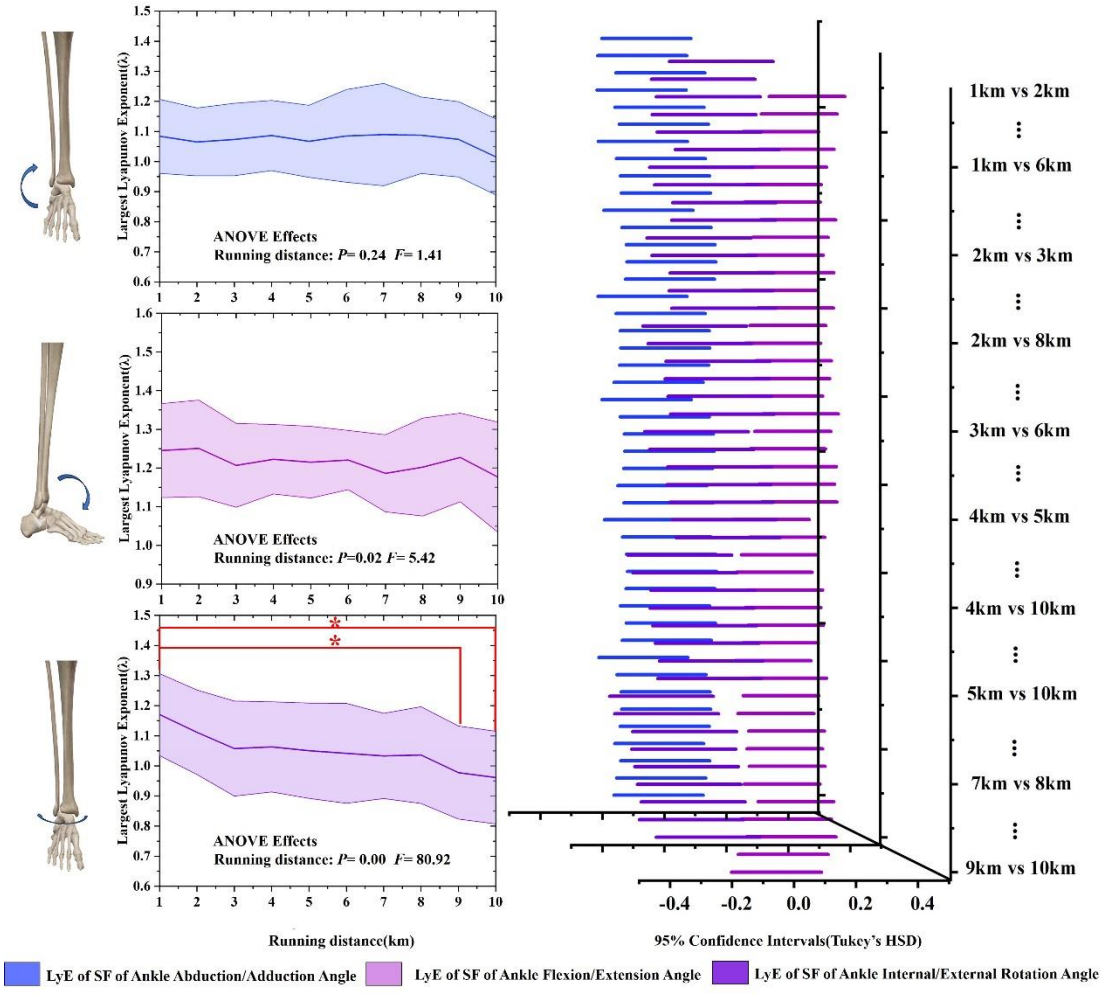

Figure 3.2.1 Post hoc analysis of groupwise comparisons for largest Lyapunov exponents of symmetry function of ankle angle during 10km running.

The participants completed the 10 km run in 46 ± 8 minutes. As shown in Figure 3.2.1, the one-way repeated measures analysis results shown that there are no statistical differences of LyE based on the SF of ankle angle data collected in Abduction/Adduction (F=1.41, P=0.24) and there are

statistical differences have found in Dorsiflexion/Plantarflexion (F=5.42, P=0.02) and Internal/External Rotation direction (F=80.92, P<0.01). Furthermore, the results of Tukey's Honest Significant Differences shown that LyE after 9 km running decreased 0.19 bit/s compared with Lye after 1km (mean difference=0.19, 95%CI: -0.36 to -0.03, p=0.01) in Internal/External Rotation direction. In addition, LyE after 10 km running decreased 0.21 bit/s compared with Lye after 1km (mean difference=0.21, 95%CI: 0.38 to -0.004, p<0.01).

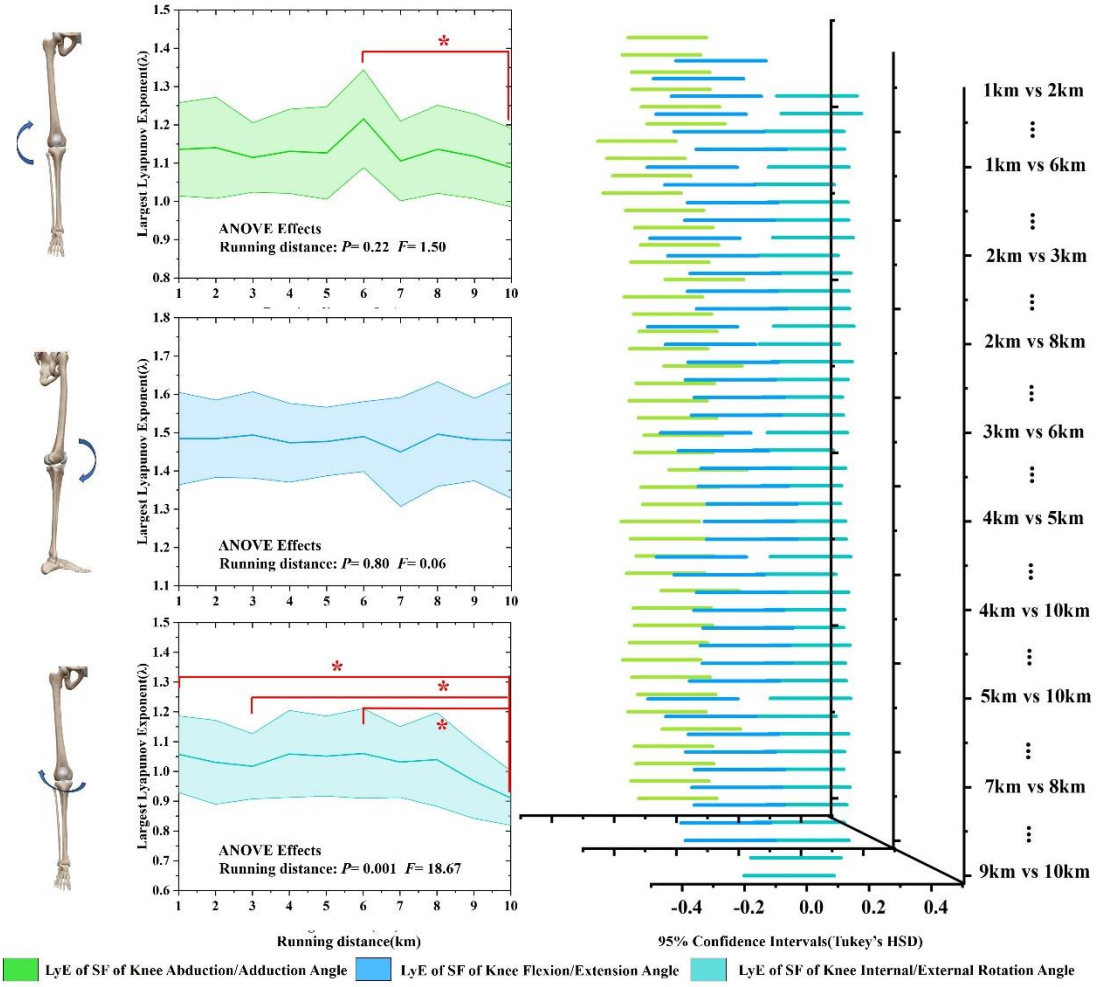

Figure 3.2.2 Post hoc analysis of groupwise comparisons for Largest Lyapunov exponents of symmetry function of knee angle during 10km running.

As shown in Figure 3.2.2, the one-way repeated measures analysis results shown that there are no statistical differences of LyE based on the SF of ankle angle data collected in Abduction/Adduction (F=1.50, P=0.22) and Dorsiflexion/Plantarflexion (F=0.06, P=0.80) direction. However, there are statistical differences have observed in Internal/External Rotation direction (F=18.67, P<0.01). Furthermore, the results of Tukey's Honest Significant Differences shown that LyE after 10 km running decreased 0.13 bit/s compared with Lye after 6km (mean difference=0.13, 95%CI: -0.25 to -0.01, p= 0.04) in Abduction/Adduction direction In addition,

LyE after 10 km running decreased 0.15 bit/s compared with Lye after 1km(mean difference=0.15, 95%CI: -0.29 to 0, p= 0.04), 3km (mean difference=0.15, 95%CI: -0.29 to 0, p= 0.04) and 6km (mean difference=0.15, 95%CI: -0.29 to 0.01, p=0.04).

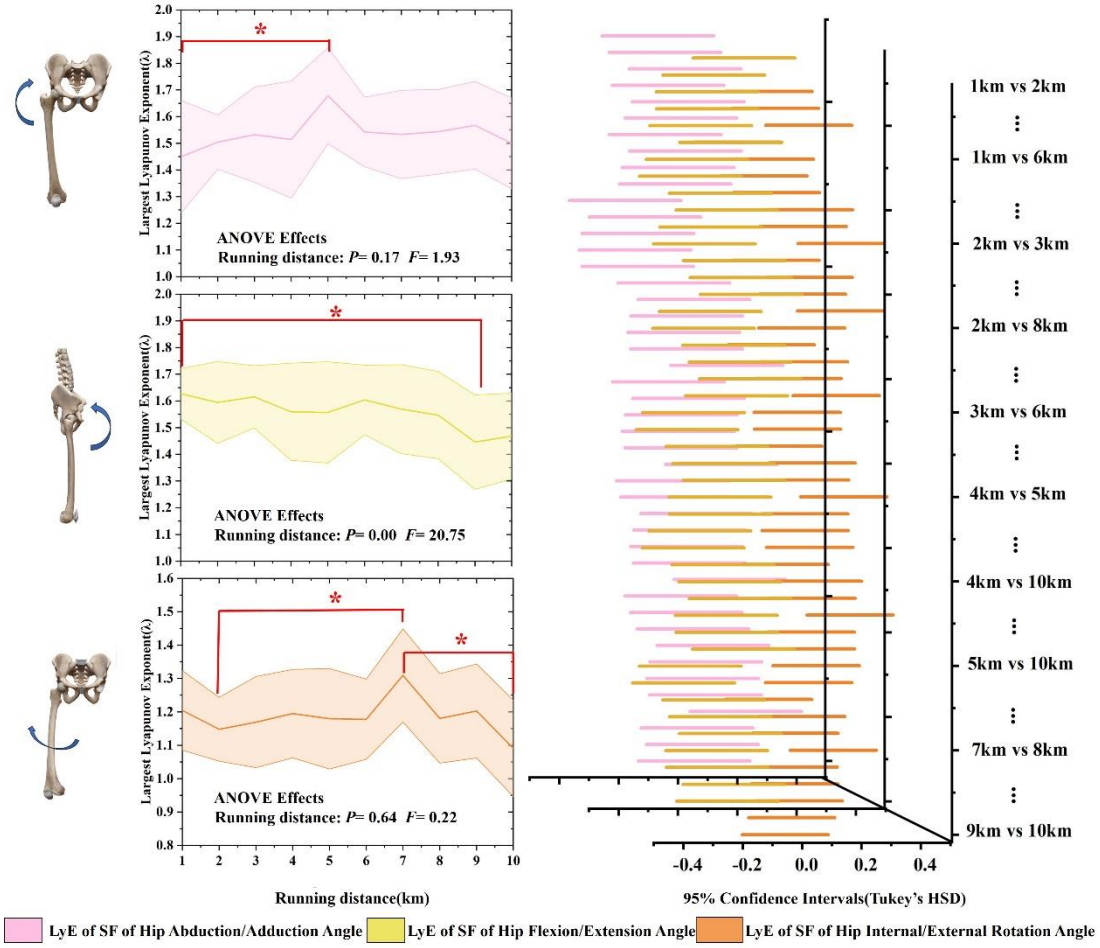

Figure 3.2.3 Post hoc analysis of groupwise comparisons for largest Lyapunov exponents of symmetry function of hip angle during 10km running.

As shown in Figure 3.2.3, the one-way repeated measures analysis results shown that there are no statistical differences of LyE based on the SF of ankle angle data collected in Abduction/Adduction (F=1.93, P=0.17) and Internal/External Rotation (F=0.22, P=0.64) direction. However, there are statistical differences have observed in Dorsiflexion/Plantarflexion direction (F=20.75, P<0.01). Furthermore, the results of Tukey's Honest Significant Differences shown that LyE after 5 km running increased 0.23 bit/s compared with Lye after 1km (mean difference=0.23, 95%CI: 0.04 to 0.42, p< 0.01) in Abduction/Adduction direction. In addition, LyE after 9 km running decreased 0.18 bit/s compared with Lye after 1km (mean difference=0.18, 95%CI: -0.35 to -0.01, p=0.03). LyE after 7 km running increased 0.16 bit/s compared with Lye after 2km (mean difference=0.16, 95%CI: 0.02 to 0.31, p=0.02). however, LyE after 10 km running have observed significant decrease (0.22 bit/s) after 7 km (mean difference=0.22, 95%CI: -0.36 to -0.07, p<0.01).

3.2.2 Embedding dimension and time Delay

Table 3.2.1 The Embedding Dimension of LyE of SF ankle, knee and hip joint angle during 10km running

Joint	Mean (±SD)									
	1 km	2 km	3 km	4 km	5 km	6 km	7 km	8 km	9 km	10km
Ankle										
Abduction/Adduction	9(1)	9(2)	9(1)	9(2)	8(2)	9(2)	9(2)	9(1)	9(2)	9(2)
Flexion/Extension	9(1)	9(1)	9(1)	9(1)	9(2)	9(1)	8(1)	8(1)	9(2)	9(1)
Internal/External Rotation	9(1)	9(1)	9(1)	9(1)	9(1)	9(1)	9(1)	9(1)	9(1)	10(1)
Knee										
Abduction/Adduction	7(1)	7(2)	7(2)	7(3)	7(1)	7(1)	7(1)	7(2)	7(1)	7(2)
Flexion/Extension	7(1)	8(1)	8(1)	7(1)	7(1)	8(1)	7(1)	8(1)	8(1)	7(1)
Internal/External Rotation	8(2)	8(2)	8(2)	8(1)	8(2)	8(1)	8(2)	8(2)	8(2)	8(2)
Hip										
Abduction/Adduction	6(1)	6(1)	6(1)	6(1)	6(1)	6(1)	6(1)	6(1)	6(1)	6(1)
Flexion/Extension	6(1)	6(1)	6(1)	6(1)	6(1)	6(1)	6(1)	6(1)	6(1)	6(1)
Internal/External Rotation	8(1)	8(2)	8(1)	8(1)	8(1)	8(2)	7(1)	8(1)	8(1)	8(1)

Table 3.2.2 The Time Delays of LyE of SF ankle, knee and hip joint angle during 10km running

Joint	Mean (±SD)									
	1 km	2 km	3 km	4 km	5 km	6 km	7 km	8 km	9 km	10km
Ankle										
Abduction/Adduction	22.06(4.94)	20.88(5.28)	20.94(6.17)	20.59(4.98)	20.47(4.96)	20.06(5.67)	20.76(6.14)	20.06(5.46)	20.65(5.06)	19.29(5.33)
Flexion/Extension	20.88(5.29)	21.47(5.60)	21.76(6.92)	19.82(5.63)	21.06(6.29)	20.65(6.24)	21.29(5.52)	21.12(5.75)	20.06(5.43)	20.06(5.72)
Internal/External Rotation	18.06(4.28)	16.47(3.97)	16.24(4.51)	17.18(4.36)	15.24(3.54)	16.76(4.07)	15.71(3.14)	15.29(3.35)	15.12(2.83)	15.35(2.78)
Knee										
Abduction/Adduction	17.18(3.15)	18.41(5.82)	18.29(4.47)	18.88(5.53)	17.18(3.97)	20.12(6.8)	19.12(5.34)	19.84(5.71)	19.24(5.76)	18.18(5.00)
Flexion/Extension	20.23(3.61)	20.71(4.06)	20.65(3.41)	21.24(4.16)	21.24(4.35)	20.06(3.21)	20.94(5.24)	20.06(3.09)	19.88(3.57)	19.76(3.21)
Internal/External Rotation	16.29(2.71)	16.06(2.93)	16.41(4.14)	17.76(4.38)	17.53(4.99)	17.35(4.78)	17.18(4.98)	17.47(4.91)	17.53(5.46)	17.71(4.51)
Hip										
Abduction/Adduction	29.24(7.51)	29.94(8.58)	27.41(4.43)	30.06(7.01)	27.53(4.96)	27.59(4.87)	28.35(7.23)	28.59(7.20)	28.53(5.78)	27.94(4.16)
Flexion/Extension	26.47(1.97)	25.76(3.75)	25.47(3.43)	26.41(3.06)	26.71(3.84)	26.35(3.32)	26.71(4.15)	27.18(4.42)	26.82(3.86)	26.59(3.68)
Internal/External Rotation	24.41(4.00)	22.82(4.59)	23.53(4.33)	25.12(6.11)	22.76(3.87)	23.24(4.93)	24(5.81)	23.47(5.09)	24.12(6.23)	21.53(3.66)

Table 3.2.1 and Table 3.2.2 describe the optimal embedding dimension and time delay calculated from the global false nearest neighbor technique and initial minimum of mutual information. All data are expressed as Mean±SD. Running distance did not affect embedding dimension or time delay of LyE in 10km running. The ankle joint had the highest embedding dimension in all three anatomical planes, and the hip joint had the lowest in the sagittal and coronal planes. In Addition, the hip had the greatest time delay in all three planes, and the knee was smaller than the ankle in the sagittal plane and larger than the ankle in the horizontal plan.

3.3 Joint stress response

3.3.1 Model validation

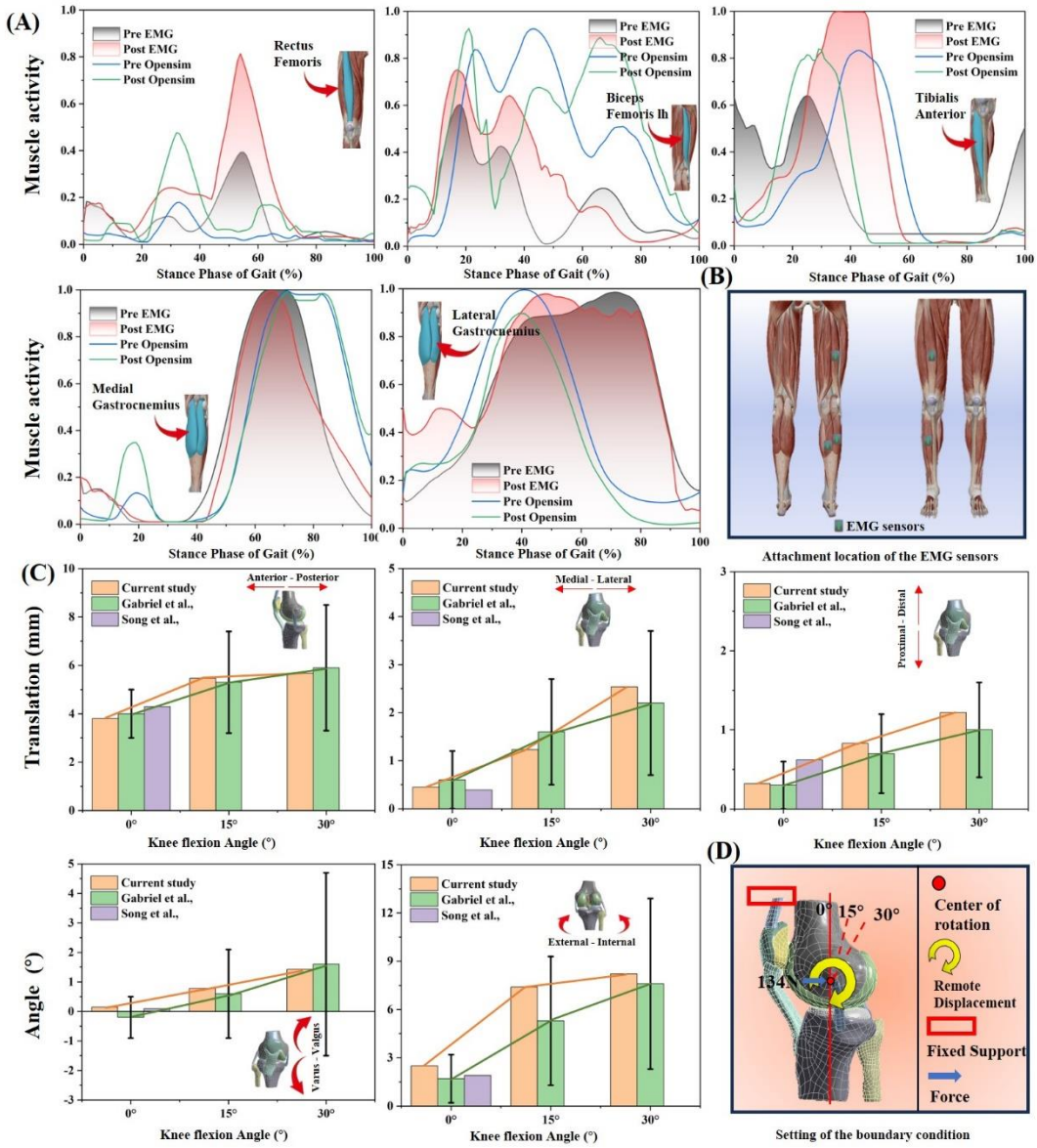

Figure 3.3.1 Validation of the musculoskeletal model and finite element model (A) Comparison of OpenSim-calculated muscle activity levels versus experimentally recorded EMG from experimental recordings. (B) Attachment position of EMG sensors. (C) Comparison of the results obtained from the finite element model of this study as the same boundary conditions with the cadaver experiments and the finite element simulation results of previous studies (D) Schematic diagram of finite element model validation.

The muscle activation levels of rectus femoris, biceps femoris, tibialis anterior, medial

gastrocnemius, and lateral gastrocnemius calculated in pre- and post-fatigue states were similar to the surface EMG signals recorded in the experiment, as shown in Figure 3.3.1 (A). In addition, under the condition of 0° knee flexion and a posterior load of 134N on the rotation center of the femur, the displacement in the anterior-posterior, proximal-distal, and medial-lateral directions in this study's knee joint model is similar to the cadaver experiments by Gabriel et al.[205] and the finite element simulations by Song et al.[204]. By applying remote displacement to the center of femoral rotation under identical boundary and loading conditions, the knee joint's displacement outcomes at 15° and 30° of flexion are congruent with the cadaveric study findings of Gabriel et al.[205], as shown in Figure 3.3.1 (B).

3.3.2 Kinematics and Kinetics

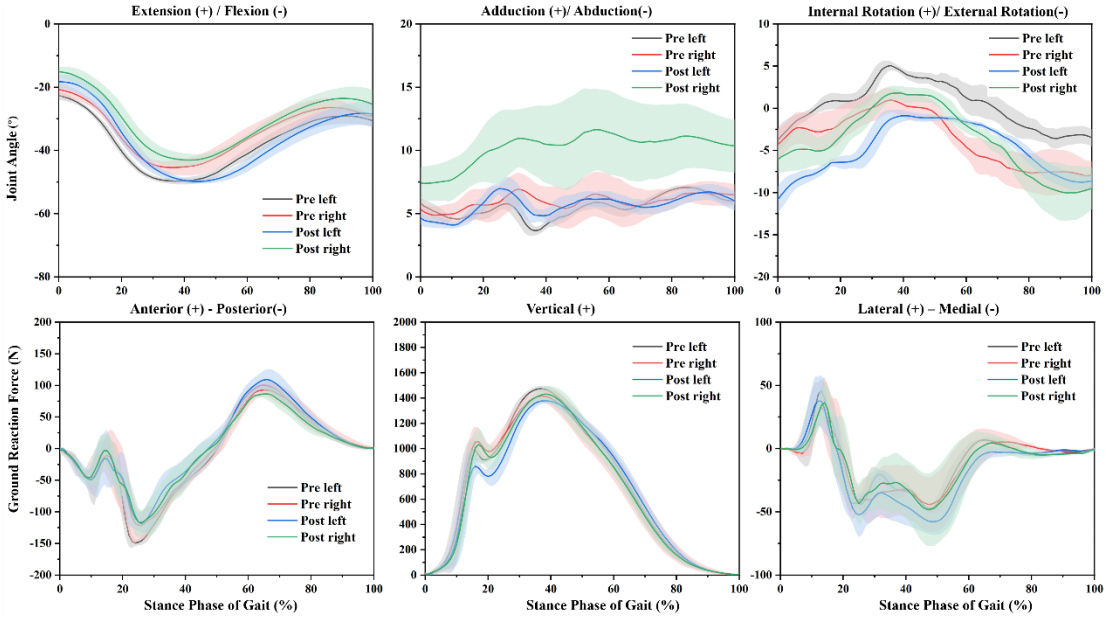

Figure 3.3.2 Knee joint angles, joint reaction forces calculated from experimental and musculoskeletal models during running gait.

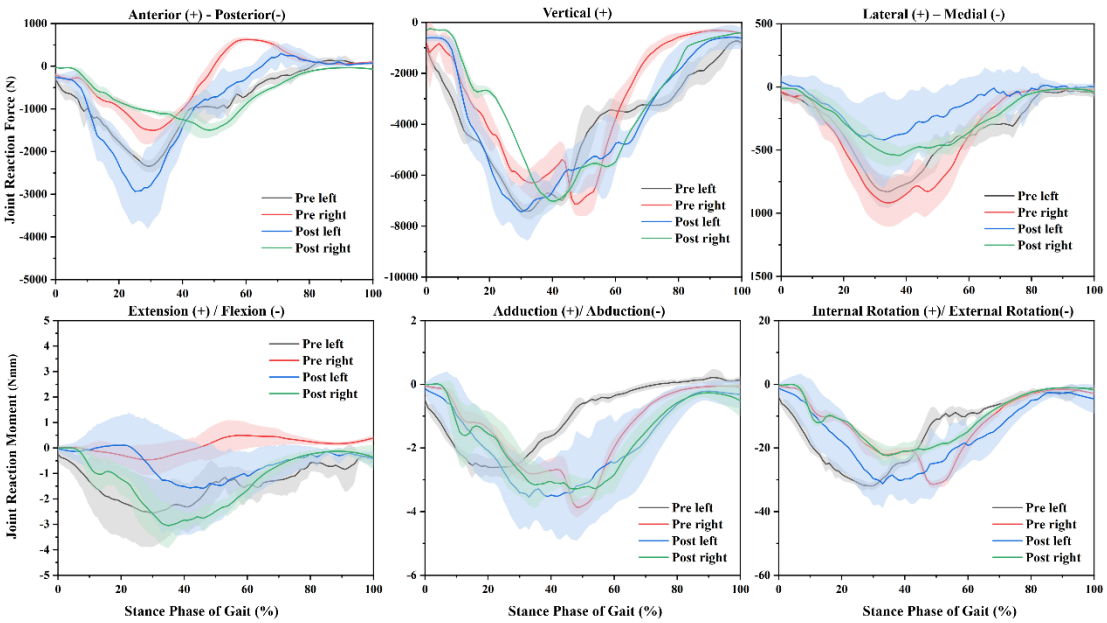

Figure 3.3.3 Knee joint reaction forces and joint reaction moments from experimental and musculoskeletal models during running gait.

As shown in Figure 3.3.2 and Figure 3.3.3, in the pre-fatigue states, a greater internal rotation angle was observed in the left knee compared to the right side, and this difference was more pronounced in the post-fatigue states during mid-stance. Additionally, a greater anterior joint reaction force was observed in the right knee. Similarly, a greater abduction joint reaction moment was noted in the left knee joint. In the post-fatigue states, the left knee exhibited a greater extension angle, and there was more pronounced adduction in the right knee. Furthermore, an increase in right knee flexion reaction moments was observed after fatigue.

Table 3.3.1 Summary of loads applied to the knee joint at five typical moments in a stance phase of gait.

Gait (%)	**angle(°)**	**Force(N)**			**Moment (Nmm)**		
		Fx	*Fy*	*Fz*	*Mx*	*My*	*Mz*
Pre left							
Initial contact	-22.63	-307.01	-1000.21	-41.05	-0.27	-0.52	-4.14
First Peak	-33.17	-1367.24	-4674.43	-228.66	-1.89	-2.55	-25.10
Mid-stance	-37.44	-1628.87	-5498.92	-315.23	-2.03	-2.58	-26.96
Second Peak	-49.71	-1673.34	-6575.96	-798.51	-2.22	-1.76	-25.23
Toe off	-30.63	94.03	-1106.56	-48.22	-0.4	0.14	-1.40
Pre right							
Initial contact	-20.71	-208.69	-814.29	-39.31	0.22	-0.05	-0.51
First Peak	-30.77	-827.09	-3424.58	-327.90	-0.18	-2.00	-10.13
Mid-stance	-36.13	-960.45	-4231.98	-490.15	-0.28	-1.40	-11.49
Second Peak	-45.41	-1233.75	-6091.67	-898.97	-0.24	-2.77	-21.64
Toe off	-29.10	100.07	-430.28	-17.98	0.39	-0.07	-2.91

Post left							
Initial contact	-18.31	-255.96	-620.13	40.21	-0.02	-0.14	-1.20
First Peak	-28.15	-1847.02	-4833.12	-161.08	0.07	-1.72	-14.63
Mid-stance	-34.26	-2317.48	-6301.40	-252.31	0.10	-2.08	-17.96
Second Peak	-49.07	-1735.97	-6916.34	-376.52	-1.47	-3.50	-30.10
Toe off	-28.50	75.88	-670.86	-0.10	-0.41	-0.32	-4.61
Post right							
Initial contact	-15.10	-20.17	-321.62	-10.93	0.01	0.01	0.19
First Peak	-25.50	-697.02	-2709.89	-205.22	-0.96	-1.32	-9.90
Mid-stance	-29.47	-833.77	-2710.82	-281.44	-1.22	-1.55	-11.20
Second Peak	-42.79	-1212.97	-6868.54	-541.09	-2.94	-3.11	-21.66
Toe off	-25.42	-68.59	-397.60	-37.15	-0.37	-0.51	-1.79

Note: Pre left: Left leg before 10km running. Pre right: Right leg before 10km running. Post left: Left leg after 10km running.

Table 3.3.1 enumerates the mechanical data applied to the finite element model for both lower limbs at five moments in pre- and post-fatigue states. Additionally, the knee joint flexion angles at each moment serve as remote displacement boundary conditions for the rotation center of the femur.

3.3.3 Finite element analysis

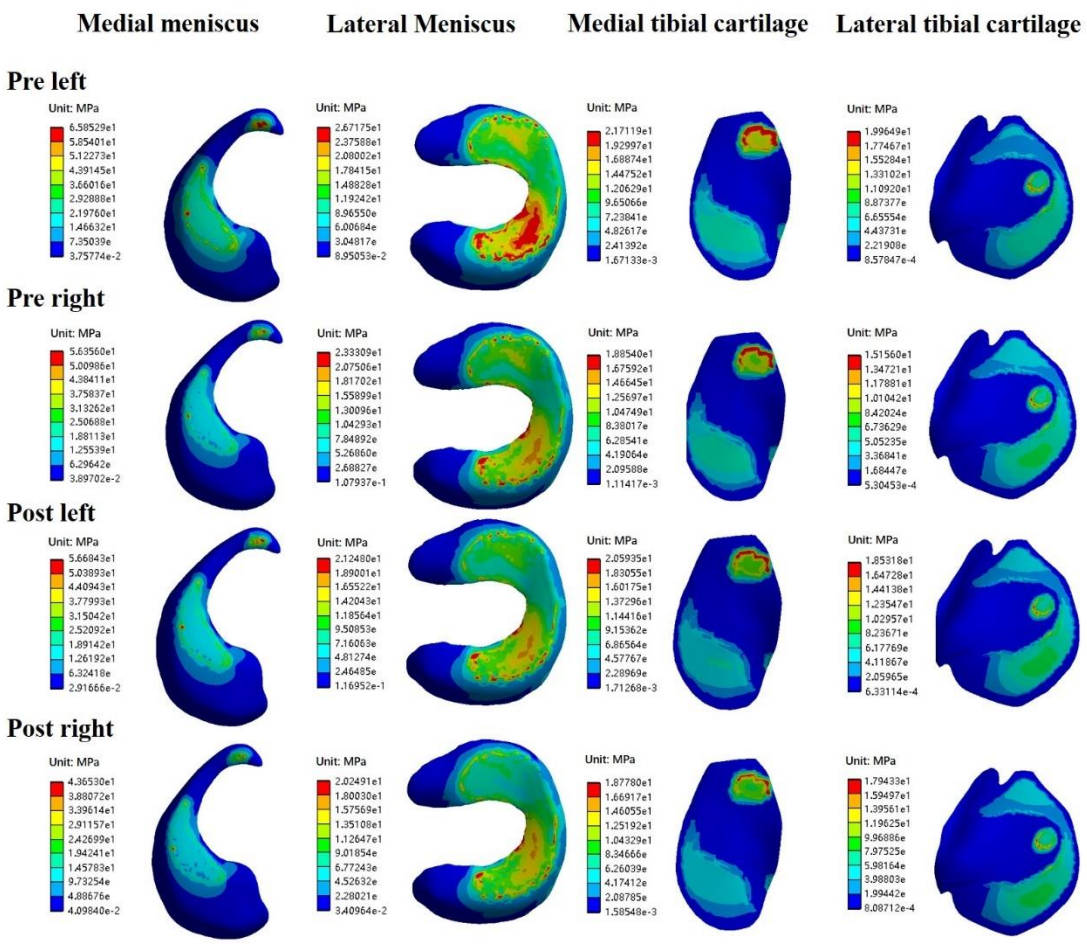

Figure 3.3.4 Von Mises stresses the bilateral knee joint in the meniscus and tibial cartilage before and after 10km of running at the moment of maximum GRF of the stance phase. The change in color scaling represents the change in stress from large (red) to small (blue) on the stress cloud. Note: Pre left: Non-dominant leg before 10km running. Pre right: Dominant leg before 10km running. Post left: Non-dominant leg after 10km running, Post right: Dominant leg after 10km running.

In Figure 3.3.4, similar stress distributions were observed on both dominant and non-dominant limb menisci in both states. Maximum stress was predominantly located at the central and anterior horn of the medial meniscus. Notably, the left knee surpassed the right knee by 9.5 MPa, and 9.12 MPa decreased after fatigue. The peak stress of the right medial meniscus decreased by 12.7 MPa after fatigue. Additionally, the anterior segment of the middle region of the lateral meniscus sustained the maximum stress, the left side by 3.39 MPa more than the right side, and 5.47 MPa decreased after fatigue.

The tibial cartilage exhibited a consistent stress distribution, with the anteromedial part of the medial tibial cartilage bearing the main load. The stress of the left tibial cartilage was higher than that of the right side by 2.86 MPa and decreased by 1.82 MPa after fatigue. For the lateral tibial

cartilage, the left side is 4.81 MPa more than the right in pre-fatigue states. The peak stress of the right lateral tibial cartilage increased by 12.7 MPa after fatigue.

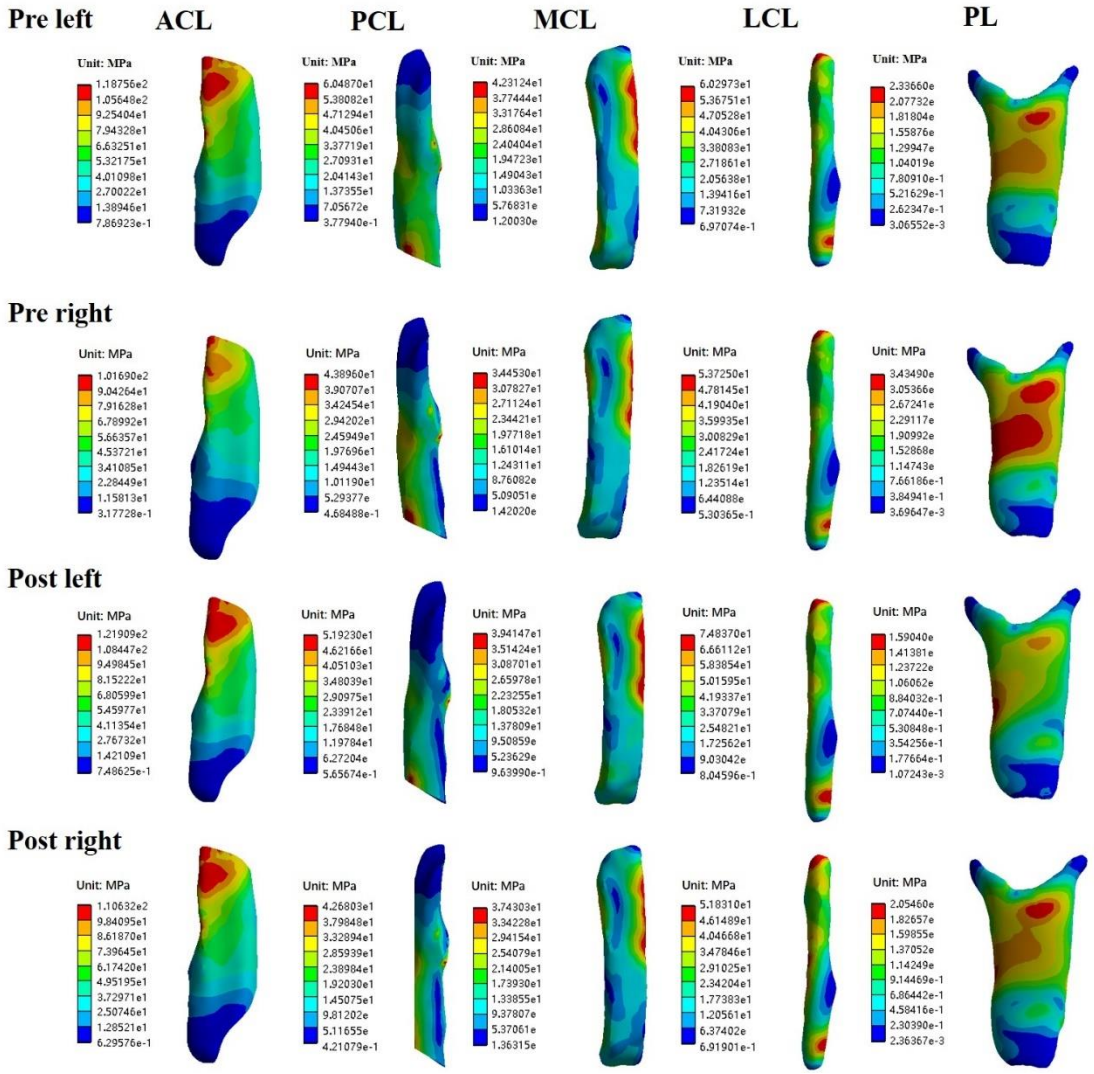

Figure 3.3.5 Von Mises stresses the bilateral knee joint in the ACL, PCL, MCL, LCL, and PTL before and after 10km running at the moment of maximum GRF of the stance phase. The change in color scaling represents the change in stress from large (red) to small (blue) on the stress cloud. Note: Pre left: Non-dominant leg before 10km running. Pre right: Dominant leg before 10km running. Post left: Non-dominant leg after 10km running, Post right: Dominant leg after 10km running. ACL: anterior cruciate ligament, PCL: posterior cruciate ligament, MCL: medial collateral ligament, LCL: lateral collateral ligament, PL: Patellar ligaments.

Similar stress distributions were observed on the ligaments in both states (Figure 3.3.5). Maximum stresses for the ACL and PCL were primarily located at the femoral contact points. The left ACL was 17.07 MPa higher than the right side, and it increased by 3.15 MPa after fatigue. In post-fatigue states, it surpasses the right side by 11.28 MPa. The left PCL was 16.59 MPa higher than

the right side and decreased by 8.56 MPa after fatigue. In post-fatigue states, it was 9.24 MPa higher than the right side.

The maximum stress for the MCL was mainly on the anterosuperior side. The left MCL was 7.86 MPa higher than the right side and decreased by 2.90 MPa after fatigue. Additionally, the stress of the left LCL was 6.56 MPa higher than the right side, and 14.54 MPa increased after fatigue. In post-fatigue states, it surpasses the right side by 23.00 MPa. The maximum stress for the PL was mainly in the middle region. Interestingly, the stress on the left side was lower than on the right side by 1.10 MPa and decreased by 1.38 MPa after fatigue. In post-fatigue states, it was 0.46 MPa higher than the left side.

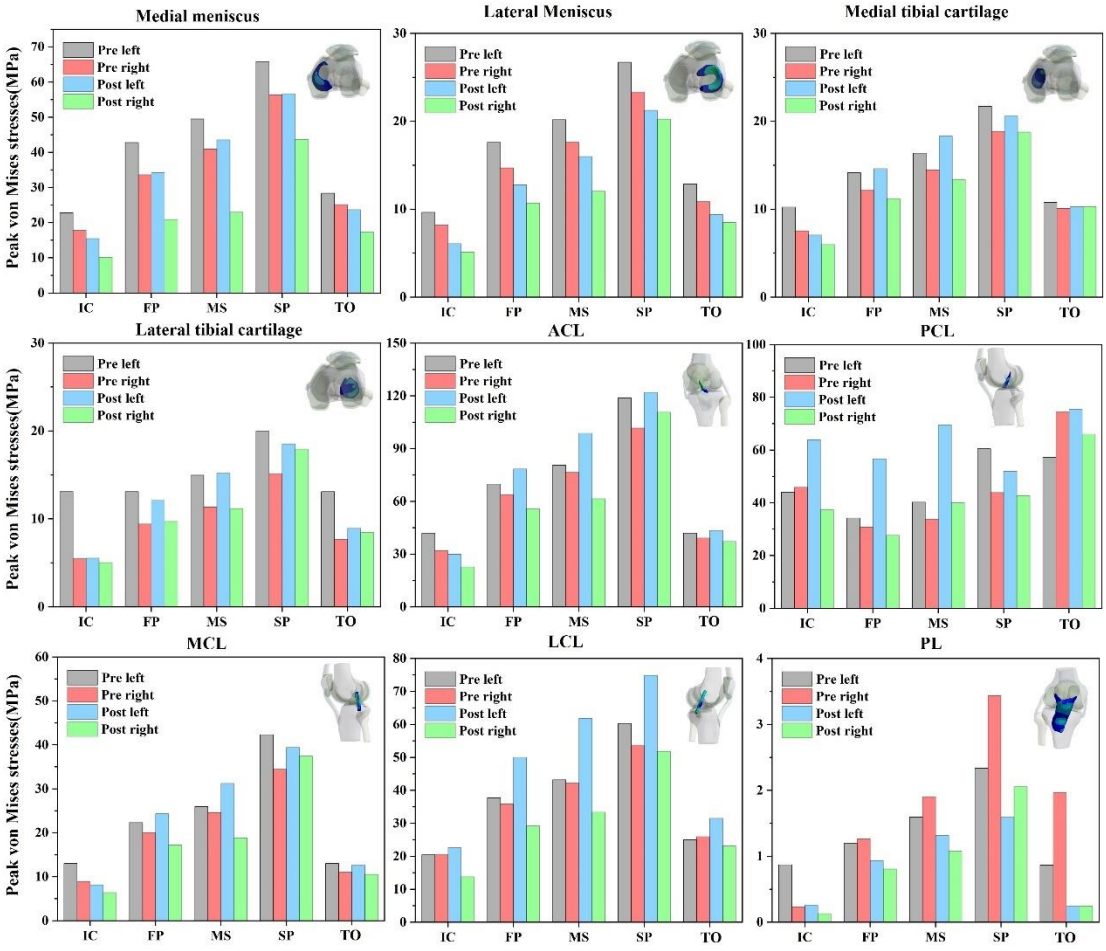

Figure 3.3.6 The peak von mises stresses changes of meniscus, cartilage and ligaments of bilateral knee joint for 5 phases of the stance phase before and after 10km running. Note: Pre left: Left leg before 10km running. Pre right: Right leg before 10km running. Post left: Left leg after 10km running. ACL: anterior cruciate ligament, PCL: posterior cruciate ligament, MCL: medial collateral ligament, LCL: lateral collateral ligament, PL: Patellar ligaments. IC: Initial contact, FP: First Peak, MS: Mid-stance, SP: Second Peak, TO: Toe off.

Figure 3.3.6 illustrates the variations in stress values for the meniscus, tibial cartilage, and ligaments of the bilateral knee during a gait stance phase in both states. Except for the PCL, the peak stress of the tissues was consistently lowest during the IC phase, gradually increased during the SP phase, reached its maximum, and decreased during the OT phase at both states. Interestingly, the maximum stress for the PCLs occurred at the TO phase, while the stress was lowest at the FP phase except on the left side in pre-fatigue and post-fatigue states, respectively. The medial and lateral menisci trend graphs reveal that peak stress in pre-fatigue states was consistently higher than in post-fatigue states, with the left side consistently exhibiting greater stress than the right. The ACLs and MCLs showed higher stress on the left side than the right of all states. The stress on the left LCL increased, while it decreased on the right side after fatigue. The peak stress for the left PL was highest at the IC phase, while the right PL was highest for all other phases in pre-fatigue states.

4 Discussion

4.1 Plantar pressure and fatigue gait recognition

The aim of current investigation was to investigate the effect of running fatigue on the bilateral plantar force distribution of the foot and the effectiveness of CNN and ConvLSTM models for fatigue gait recognition. The results of this study showed that running fatigue changed the distribution pattern of load on the plantar of the dominant and non-dominant limb. These changes are similar to previous studies[53, 55, 58]. The force distribution of the dominant plantar of runners shown major differences reflected in reduced force under the midfoot at the expense of increased force under the H, M2 and M3. This increased loading of the medial forefoot region is in agreement with previously demonstrated higher pressures under the forefoot and lower peak pressures under the midfoot, which was reported by Bisiaux et al. after fatigue induced by an intensive 30-min run[57]. These results may indicate that the load was transferred from the midfoot to the toes and metatarsals[57]. The increased loading in M2-3 may be related to reduced activity of the toe flexors and posterior tibial muscles after running fatigue[207]. In addition, Arndt et al. have also reported that higher strain rates and deformation of metatarsal bones can also occur after muscle fatigue caused by running[208]. These findings could be a risk factor for a metatarsal stress fracture[57]. Especially the M2 and M3 are vulnerable because of the difference between the applied plantar pressure and bone strength[207].

Previous studies have demonstrated that dominant feet play a propulsive role, while non-dominant feet are more likely to function as a stable gait[28]. Excessive force at the H region after fatigue appears in the dominant limb may be a compensatory effect of the functionally driven winch mechanism[52]. Willson and Kernozek [58] reported that running fatigue could cause changes in the plantar surface loading characteristics and in running technique. The current study showed that the force of M5 at non-dominant foot has decreased at metaphase(50-69%) of contact duration, while the force of M3 has increased significantly at most of the contact duration(12-79%) after fatigue, suggesting that the fatigue transferred foot loading from lateral region toward the inside of the foot, especially in the non-dominant foot [60]. This finding may be a weakening of the function of the non-dominant limb to stabilize gait after muscle fatigue[29]. Additionally, the relative time of peak force of MF at the non-dominant was significantly shortened after fatigue, suggesting that more impulse was concentrated in the MF region. This finding may be due to the damage of the active control mechanism of the MF during the contact stage leading to a reduction in the cushioning function of the non-dominant plantar, which was the potential factors for plantar fasciitis[209]. Interestingly, the relative time of the peak of H regions force at the dominant foot was significantly delayed after fatigue. This finding may be a compensatory mechanism to

maintain the propulsive function of the dominant limb, making the gravitational torque between the heel and toe region more even in the later stages of push-off [53].

Several reports have investigated the influence of the range of motion in the coronal plane of the foot on shock attenuation at heel strike [210, 211]. In addition, the ability of the musculoskeletal system to attenuate the shock magnitude generated during heel strikes also decays with the happening of fatigue[212]. In our study, the plantar forces recorded under the HM and HL region of both dominant and non-dominant revealed the changes which running fatigue during the loading stage. Without other direct measurements, we can only speculate that excessive heel loading after fatigue may be linked to weaker muscle strength which controls the movement of the ankle joint in the coronal plane after fatigue[57]. These observations were consistent with several previous studies[49, 54]. Interestingly, the sum of forces from all ten regions at non-dominant of 33-46% of contact duration significantly decreased, and the relative time of peak force was significantly shortened after running-induced fatigue, suggesting that dorsiflexor fatigue led to more vertical loading rate on the plantar. A significant interaction between loading rate and running-related calf, foot and ankle injuries was demonstrated in a study by Gerlach et al.[213]. The results of the current study could provide necessary enlightenment about the condition of different running-related injuries among runners with limbs on different sides.

Additionally, by applying the feature set of the time series bilateral plantar force data in specific deep learning predictive models for running fatigue gait, the results showed that both CNN and ConvLSTM models have good performance in predicting fatigue gait automatically. As expected, the ConvLSTM model (85.9%, 88.9%, 83.3%, 85.9% and 89.2%, respectively) has better accuracy compared to the CNN model (85.6%, 73.8%, 82.7%, 80.3% and 75.4%) in all five tests, suggesting that ConvLSTM performs better for multi-feature data with simultaneous spatiotemporal dependence[184]. Traditional time series biomechanical datasets are all characterized by high dimensionality, high variability, time dependence, and nonlinearity[214]. Therefore, with the promising findings from this study as a foundation, future research suggests applying the Convlstm model to other analyses, such as marker trajectories, ground reaction forces, myoelectric signals, and other prediction and classification needs. In addition, as shown in Table 3, the specificity of the ConvLSTM model was also higher than that of the CNN, indicating that it could detect fatigue gait better, while the performance of sensitivity was consistent in both models, indicating that both models were equally effective in predicting non-fatigue gait.

There are four limitations to the current study. Possible differences in plantar pressure distribution patterns between overground conditions and treadmill conditions were reported by Garcia-Perez et al.[215]. In this study, the running-induced fatigue protocol was carried out on a treadmill. Thus, further investigation is needed to support our findings in overground conditions. The runners were

evaluated under barefoot conditions, potentially overlooking the impact of footwear on post-fatigue running posture [40]. Additionally, we selected only two deep learning models (CNN and ConvLSTM) for data training based on data features, and more comparisons of classifiers (Such as deep neural network) for plantar pressure feature discovery should be developed in future studies. At the end, only the pedobarographic data of amateur male runners were included in this study, whether the model developed in this study applies to female or elite runners should be verified in future studies.

4.2 Dynamic stability

This was the first study to investigate the effect of long-distance running on the DS of gait symmetry. Enhancing comprehension of the methodologies employed could potentially contribute to the advancement of comprehension regarding the mediation of movement kinematic during running. The results of present study are not completely consistent with our hypothesis. Specifically, the DS of sagittal and horizontal of the hip joint decreased in the middle of the 10km run. Intristingly, the knee and ankle joints and the hip joint the coronal plane shows an increasing trend during the late period of 10km running.

The occurrence of asymmetry is commonly cited as a contributing factor to overloading of unilateral lower limb joints [119]. If gait symmetry remains in an unstable state, the lower limbs may not be able to achieve dynamic balance in terms of load distribution[136]. One factor that could potentially influence gait symmetry is an individual's level of fatigue at any given point during a task[29, 136]. In general, with prolonged activity or muscle fatigue, it is expected that symmetry would decrease[29]. Minor disturbances or incorrect recruitment of unilateral muscles can alter the movement posture, which may result in excessive local tissue loading and diminished performance[216]. Therefore, the biomechanical tolerance to unilateral lower limb overloading injuries can be partially attributed to the ability of the neuromuscular system to maintain the stability of symmetry[25].

In the event of gait analysis, linear measurements can only quantify the magnitude of variability, whereas nonlinear analytical methods can be used to investigate how this complexity changes over time [32]. Time delay state space reconstruction is essential for the computation of LyE [31]. This procedure further offers insight into the nature of the gait signal and reveals the underlying dynamics of continuous gai[217].In general, fewer state dimensions are commonly applied to describe simple dynamical systems. In contrast, complex dynamical systems need a large number of embedding dimensions to be described[218]. Therefore, the number of state variables of the system is proportional to the required dimensionality [219]. We can observe from Table 3.2.1 that the motion distance does not have a large impact on the embedding dimension. Interestingly, the limb embedding dimension increases from proximal to distal, suggesting that SF complexity appears to be lowest at the hip and highest at the ankle during running. This is inconsistent with the results of previous studies of the local DS of the lower limb joint angle, and this interesting distinction suggests that future interpretations of local stability should be cautious.

In addition, limited information is available regarding the prolonged and uninterrupted perturbations' impact on the adaptive regulation of homeostasis [220]. The present study tested the hypothesis that the biomechanics symmetry is not always stable during long distance running. The present results conld not confirm this. Existing knowledge of gait fatigue in SD of lower limb symmetry is limited. One study has assessed the vertical component of back-waist acceleration and observed increases LyE values as fatigue happend in walking gait [221]. However, there are no existing direct empirical measurements of stability to test whether fatigue influences gait asymmetry stability during long-distance running [29]. To provide a better understanding of the role of symmetry in running, the assessment of DS may be useful. The study by Granata et al. reported that the trunk was more unstable after a fatigue protocol than the non-fatigue states[219]. Some previous studies have suggested that fatigue has a negative impact on DS [221, 222]. However, the biomechanics background of an running induced decrease in DS is not well

understood [34]. Changes in muscle recruitment and gait asymmetry degree have been mentioned as possible explanations[36, 219]. These findings suggest mixed results regarding the impact of running fatigue nonlinear dynamic variables[35, 39, 220, 222, 223]. Future studies should unify the setting of fatigue mechanisms and evaluation parameters. Only LyE of coronal of the hip increased during running was observed in present study. This effect may be attributed to altered symmetry induced by previously reported fatigue-related changes in muscle recruitment and changes in feedback neural control[29], suggesting that ability of neuromuscular control of hip joint becomes unstable with running fatigue.

Interstingly, the runners showed three overall trends in the DS of SF in the 10km run, which differed from the hyoithesis of the current study. First of all, the measured DS of ankle in sagittal and coronal plane and knee in sagittal plane remains unafeected in the function of running distance, the stability of these variables did not change significantly with the occurrence of fatigue.Previous study reported that the joint angle of these parts are symmetryic were obvered during running gait [29], therefore we can assume that this state cam be maintained steadily until the end of 10km running. However, the joint abduction angle of knee became more symmetrical after a fatigue-induce protocol [29]. This interesting difference my be not acute, so caution should be exercised when interpreting linear analysis results.In addition, the LyE of SF of knee and ankle in the horizontal plane and hip in the sagittal plane was continuously downward trend until last 1km (9-10 km), suggesting that the ability to withstand local perturbations increased of these variates after fatigue [34]. This positive change is likely to be slow an steady. This result is positive, and future studies should explore the mechanism by which it increases and whether it continues to increase during longer running tasks. However, the measured DS of knee in coronal plane and hip in coronal and horizontal plane is decreased in the first part of the running distance. Approximately at the half of the distance a sudden peak can be observed, which is followed by a continuous improvement in stability. We can deduce that in the later stages of middle-distance running (about 5-7 km), the symmetry of the hip and knee joints is less resistant to interference and, therefore, the load distribution in the joints does not reach a stable dynamic balance. Runner and coaches should focus on the possibility of risk when running middle distances when developing training programmers.

In addition, there are three limitations of this study. Firstly, previous study report that low variability is considered a healthy running gait pattern[224], the nonlinear study of gait symmetry of professional runners should be considered in our future research. Furthermore, this study is based on some assumptions, described by research on DS in human walking. We suggest to further evaluate similarities and differences of walking and running regarding DS. At the end, the execution of this study was done on a treadmill, therefore, whether the results of this study apply to ground running needs further research because of the differences between treadmill and ground running as reported in previous studies[225]

4.3 Joint stress response

To find out what changes in the dominant and non-dominant knee joints during different running phases and how a 10 km submaximal intensity run affects these variables, this study coupled variables from musculoskeletal models (GRF, knee joint angles, reaction forces, and moments) to drive finite element simulations (menisci, tibial cartilage, ACL, PCL, MCL, LCL, and PL). Specifically, the distribution of loads on the tissues was similar in both knees and all states. Moreover, the load on the meniscus and tibial cartilage were greater on the non-dominant side and greater in the pre-fatigue state. The load on the ACL, PCL, and LCL of non-dominant limb were increased after fatigue. However, they were decreased in the dominant side. Interestingly, the load on the PL of the dominant side was greater in pre- fatigue state. Therefore, the results of the current study are consistent with hypotheses (2) but present some contradictory findings with hypotheses (1) and (3).

In this study, the stance phase of gait was divided into five distinct postural stages based on the pattern of vertical GRFs. The goal was to explore the disparities in internal loading of the bilateral knee joints across different ground contact stages and the influence of fatigue thereon. Previous research reported no differences in both knee joint angles at the pre-fatigue states[29]. A greater internal rotation angle in the non-dominant knee joint during the MS period could explain the excessive load on its ACL and LCL. Additionally, the study found a greater anterior joint reaction force peak in the dominant knee, potentially indicating a higher load on the patellofemoral joint of the dominant knee[226]. This is corroborated by the noted excess load on the PL of dominant knee. Hence, patellofemoral joint pain in the dominant limb should be a consideration for amateur runners [52, 152, 227].

The findings of this study show that fatigue heightened the flexion reaction moment in the dominant knee, hinting at diminished quadricep control, which might lead to an increased load on the PCL of the dominant knee post-fatigue[228]. The larger loading of the dominant knee's PCL during the MS period after fatigue is observed in the current FEM simulations, which can also support this conclusion. Additionally, a greater abduction joint reaction moment of the non-dominant knee joint in the pre-fatigue states occurred during the mid-stance phase, indicating a greater load on the medial tibial plateau[30]. This finding is consistent with the observation of a greater load on the medial meniscus and tibial cartilage of the non-dominant knee joint.

The meniscus functions to transmit and evenly distribute forces from the femur to the tibial plateau. However, this load-transferring mechanism can become compromised due to recurrent overloading, resulting in localized stress peaks and subsequent damage to the knee joint[229]. The current study observed that the load on the medial meniscus was primarily concentrated at the anterior horn, and the load on the lateral meniscus was concentrated on the posteromedial side,

consistent with previous studies[230, 231]. Greater loads may cause tears at the anterior horn of the medial meniscus and the middle of the lateral meniscus. Interestingly, we found a similar load distribution in both the non-dominant and dominant knee joints before and after fatigue. It can be hypothesized that fatigue and limb preference do not affect the location of the meniscus, tibial cartilage, and ligaments where injuries can develop during the running event and that injuries are generally only related to the magnitude of the load. In addition, the load on the ACL and PCL was mainly concentrated at the contact points with the femur. This is consistent with the findings of the previous study [232].

By observing the load distribution of the LCL, we found that most of it was concentrated near the points where the ligaments attached to the bones which could be the most vulnerable area to strains. Additionally, larger loads were found in the non-dominant LCL after fatigue, which may be induced by foot pronation after fatigue[233]. The correlation between CLC loading and the degree of foot pronation should be further addressed in future studies. However, most of the MCL's load was concentrated in the anterosuperior direction and was more pronounced on the non-dominant side. This is a key area where too much MCL load is caused by the femur rotating during knee flexion[203]. Furthermore, the reduced PL load after fatigue suggests that running fatigue is not the leading cause of patellar pain, which has had mixed results in previous studies[234-237].

The findings of the current study demonstrated that the load on the bilateral menisci, tibial cartilage, and ligaments during the gait support phase shows a consistent trend of change both pre- and post-fatigue, being almost at its lowest during the IC phase, then gradually increasing, peaking during the SP phase, and subsequently decreasing during the TO phase. This presents a divergent trend from the findings of a previous study, where the greatest load occurred during the FP phase[172]. The cause of this discrepancy may be attributed to the different postures associated with walking and running gaits. Previous studies have indicated an increased injury risk in the non-dominant limb within the running gait[29, 238]. This study indicates that the non-dominant limb typically bears a greater load, particularly in the meniscus, tibial cartilage, ACL, MCL, and LCL. It could potentially account for the overload in a single knee joint. Furthermore, the study observed that the effect of fatigue on the ACL, PCL, and LCL of the non-dominant limb during the gait support phase is often negative. Interestingly, this is manifested as the opposite effect on the dominant limb. This may be due to the dominant limb's weaker fatigue tolerance, and the increased load on the knee joint tissues of the non-dominant limb caused by fatigue should be given attention by runners and coaches[28].

When interpreting the significant findings of this study, certain limitations should be considered. First, the study did not incorporate bilateral knee MRI data for the finite element model. Instead, it

applied boundary conditions collected from both knees during the experiment to a single model, which did not account for morphological variances between the two knees. The study's participant was an amateur male runner, so the results might not be generalizable to female runners. Additionally, future research should involve more participants to enable a more robust statistical analysis of the observed differences.

5 Conclusions and future works

5.1 Plantar pressure and fatigue gait recognition

A running-induced fatigue protocol caused different changes in the distribution of plantar force on the dominant and non-dominant limb. These changes may be part of the underlying mechanism of unilateral limb overuse injury. Future discussions of lower limb lesions or running-related injuries should take this into account. Furthermore, the ConvLSTM model showed high performance (acc= 0.867) in detecting fatigue gait, and it outperformed the CNN model (0.800). This will broaden the possibilities for future research on running-related gait biomechanical features recognition and enhance the development of fatigue monitoring tools.

5.2 Dynamic stability

This research investigates how DS of gait symmetry varies across 10km running. Investigating the kinematic symmetry of runners as assessed at lower limbs, revealed noteworthy variations during the progression of a 10-km run. Specifically, With the exception of the hip, all lower extremity joints experienced either elevated or no significant change in DS of symmetry. Future research should consider the reasons why hip control deteriorates at 5-7km. The findings of the current investigation underscore the significance of nonlinear assessing gait symmetry in the context of long-distance running. Such assessments can potentially contribute to a more comprehensive comprehension of gait biomechanics, particularly within clinical or research contexts involving athletes. As discussed in this study, the degree of symmetry of kinetics and muscle activity information can be studied nonlinear in the future.

5.3 Joint stress response

The research examines the differences in load distribution and magnitude within the bilateral knee joint's internal tissues and the effects of running-induced fatigue on these aspects. Although the load distribution areas of the menisci, cartilage, and ligaments in both knee joints are similar, the differences in their magnitude should also be considered as potential causes of excessive loading. This study found that the internal tissue load in the non-dominant limb during the stance phase of gait is greater than that in the dominant limb, and fatigue has a negative effect on the internal tissue load of the non-dominant limb, whereas the effect is reversed in the dominant limb. Compared to previous studies, the current research results are more comprehensive. The methodologies employed herein can be additionally utilized to delve into the etiologies of knee injuries associated with running.

Thesis points

1st Thesis point:

Based on experimental data, I divided the left and right plantar into 22 anatomic regions, where I have quantitatively allocated those time-intervals (contact durations) which can inflict overload on the feet (see Figure 3.1.2). These findings, to my knowledge, have not yet published before. Furthermore, these results offer empirical data for evaluating risk factors associated with overuse injuries and assist in the early detection of fatigued gait.

In addition, I created an augmented ConvLSTM model to recognize fatigue on running gait, from the perspective of deep learning, by the use of time-series planter pressure data. This data was based on high number of samples (thirty amateur runners). With this model, compared to the traditional CNN model, fatigue can be detected with higher accuracy (7%) and specificity (17%) as it is seen in the Table.

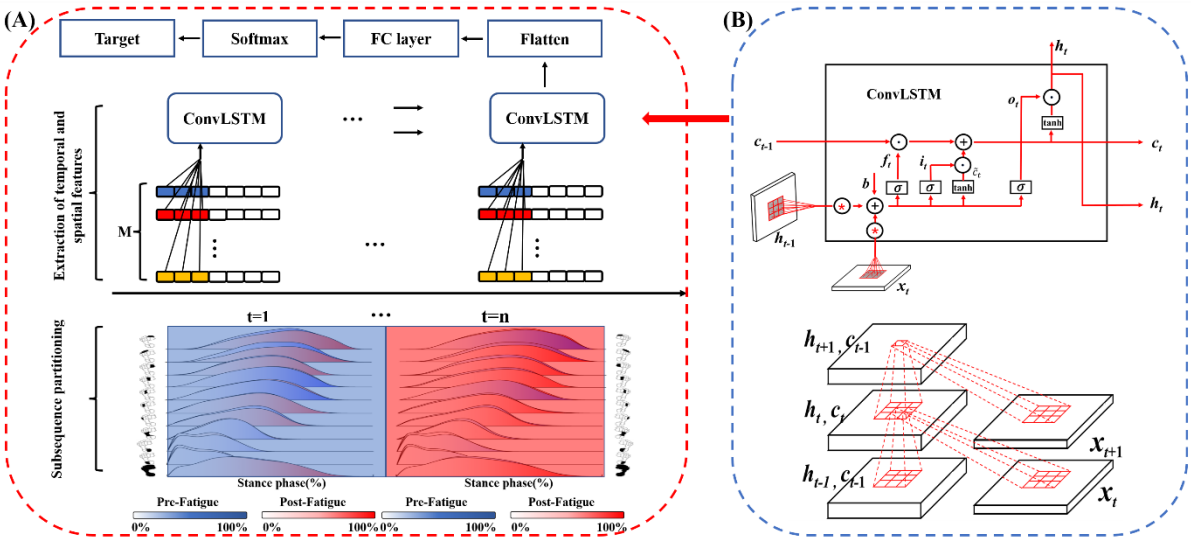

Model	Accuracy	Percentage difference	Sensitivity	Percentage difference	Specificity	Percentage difference
CNN	0.800	7%	0.874	0%	0.718	17%
aug. ConvLSTM	0.867		0.874		0.859	

Related articles to the 1st thesis point:

1. **Gao, Z.,** Xiang, L., Fekete, G., Baker, J. S., Mao, Z., & Gu, Y. (2023). A Data-Driven Approach for Fatigue Detection during Running Using Pedobarographic Measurements. Applied Bionics and Biomechanics, 2023, 1-11. **IF: 2.2, Q3**
2. **Gao, Z.,** Zhu, Y., Fang, Y., Fekete, G., Kovács, A., Baker, J. S., ... & Gu, Y. (2023).

Automated recognition of asymmetric gait and fatigue gait using ground reaction force data. Frontiers in Physiology, 14: 369-382. **IF:4.000, Q2**

2nd Thesis point:

I described the dynamic stability behaviour of nine major biomechanical parameters, namely abduction-adduction, flexion-extension and internal-external rotational angle of the hip-, knee-, and ankle joint by means of the Largest Lyapunov exponent (LLE) as a function of running distance.

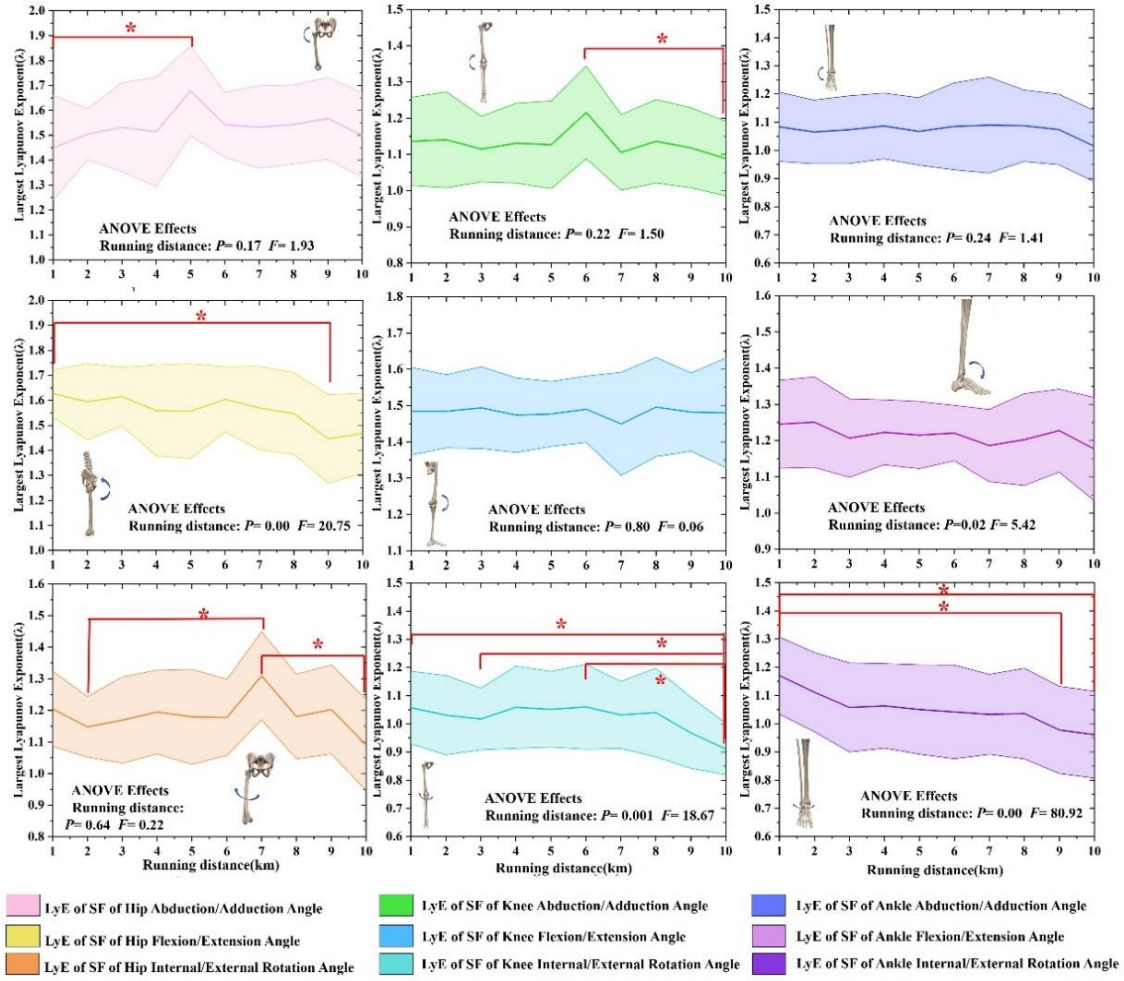

Based on my experiments (carried out on 17 male amateur runners) and calculations I could differentiate three groups for the biomechanical parameters such as *stable*, *continuously improving* and *fluctuating* and I could drew general conclusions. All angles were transformed into symmetry functions (SF).

	Ankle	**Knee**	**Hip**	**Dynamic stability**
Stable parameters	ad/abduction, flexion-extension	flexion-extension	-	The stability of these parameters remain unaffected in the function of running distance.
Continuously improving parameters	internal-external rotation	internal-external rotation	flexion-extension	The stability of these parameters improve in the function of running distance.
Fluctuating parameters	-	ad/abduction	ad/abduction, internal-external	The stability of these parameters is decreased in the first part of the running distance. Approximately at the half of the distance a sudden peak can be

	rotation	observed, which is followed by a continuous improvement in stability.

Related articles to the 2nd thesis point:

1. **Gao, Z.,** Fekete, G., Baker, J. S., Liang, M., Xuan, R., & Gu, Y. (2022). Effects of running fatigue on lower extremity symmetry among amateur runners: From a biomechanical perspective. Frontiers in Physiology, 13: 899818-899830. **IF: 4.000, Q2**
2. Xiang, L., Gu, Y., Wang, A., Shim, V., **Gao, Z.,** & Fernandez, J. (2023). Foot Pronation Prediction with Inertial Sensors during Running: A Preliminary Application of Data-Driven Approaches. Journal of Human Kinetics, 87: 29-40. **IF: 2.300, Q3**
3. Xiang, L., Gu, Y., **Gao, Z.,** Yu, P., Shim, V., Wang, A., & Fernandez, J. (2024). Integrating an LSTM framework for predicting ankle joint biomechanics during gait using inertial sensors. Computers in Biology and Medicine, 170, 1-12. **IF: 7.700, Q2**
4. Xiang, L#., **Gao, Z#.,** Wang, A., Shim, V., Fekete, G., Gu, Y., & Fernandez, J. (2024). Rethinking running biomechanics: a critical review of ground reaction forces, tibial bone loading, and the role of wearable sensors. Frontiers in Bioengineering and Biotechnology, 12, 1-13. **IF: 5.700, Q2**

3rd Thesis point:

I created a high accurate 3D Knee FE model. The joint reaction forces and joint reaction moments calculated from the musculoskeletal model simulation were used as boundary conditions to investigate the distribution and magnitude of loads on the meniscus, articular cartilage, and ligaments of the bilateral knee joints before and after a 10-kilometer run at this maximum intensity. I found similar load distribution in both knee joints regardless of the state. The left ACL was 17.07 MPa higher than the right side, and it increased by 3.15 MPa after fatigue. In post-fatigue states, it surpasses the right side by 11.28 MPa.

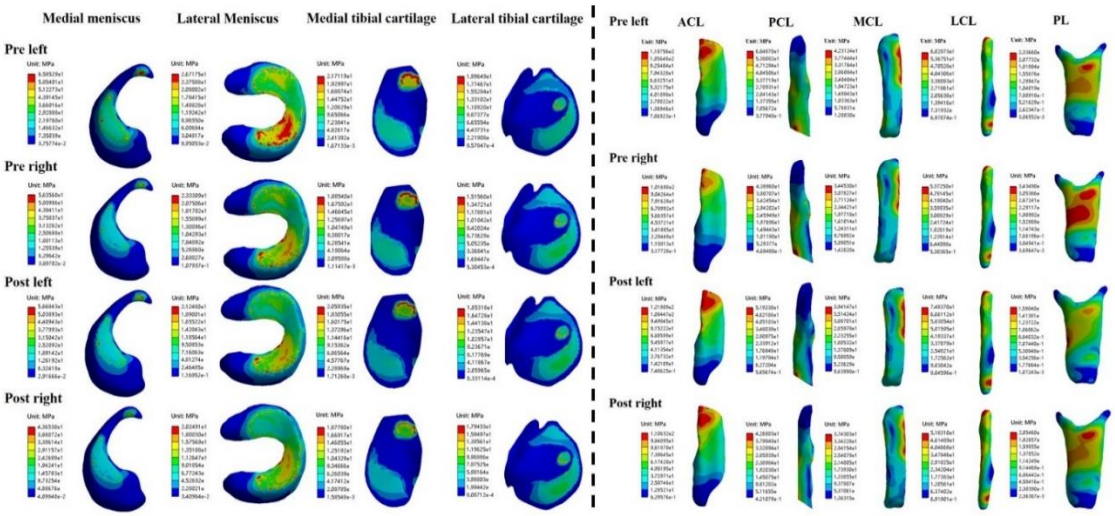

I propose a more comprehensive approach to load analysis by dividing the gait support period into five typical phases based on vGRF for comparison of organizational loads at the maximum moment. The results showed that the load on the meniscus and tibial cartilage were greater on the non-dominant side and greater in the pre-fatigue state. The load on the ACL, PCL, and LCL of non-dominant limb were increased after fatigue. However, they were decreased in the dominant side.

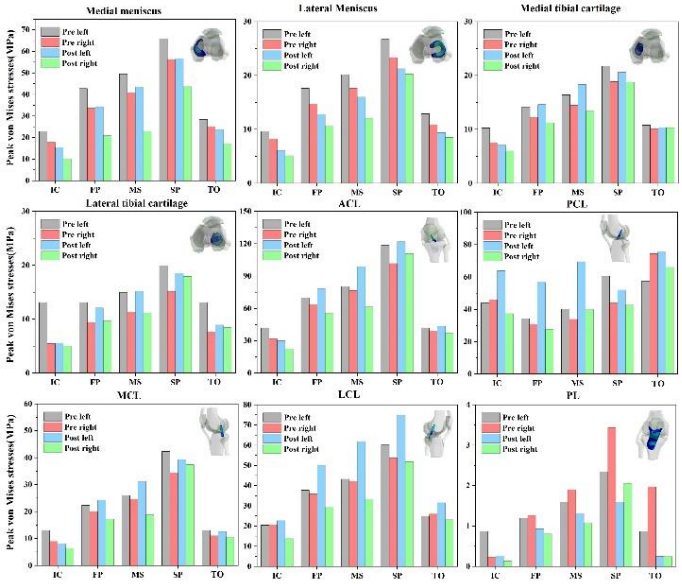

Related articles to the 3rd thesis point:

1. **Gao, Z.,** Zhao, L., Fekete, G., Katona, G., Baker, J. S., & Gu, Y. (2022). Continuous time series analysis on the effects of induced running fatigue on leg symmetry using kinematics and kinetic variables: Implications for knee joint injury during a countermovement jump. Frontiers in Physiology, 13: 877394. **IF: 4.000, Q2**
2. **Gao, Z.,** Fekete, G., Baker, J. S., Liang, M., Xuan, R., & Gu, Y. (2022). Effects of running fatigue on lower extremity symmetry among amateur runners: From a biomechanical perspective. Frontiers in Physiology, 13: 899818-899830. **IF: 4.000, Q2**

List of publications

Referred articles related to this thesis:

1. **Gao, Z.,** Xiang, L., Fekete, G., Baker, J. S., Mao, Z., & Gu, Y. (2023). A Data-Driven Approach for Fatigue Detection during Running Using Pedobarographic Measurements. Applied Bionics and Biomechanics, 2023, 1-11. **IF: 2.2, Q3**
2. **Gao, Z.,** Zhu, Y., Fang, Y., Fekete, G., Kovács, A., Baker, J. S., ... & Gu, Y. (2023). Automated recognition of asymmetric gait and fatigue gait using ground reaction force data. Frontiers in Physiology, 14: 369-382. **IF:4.000, Q2**
3. **Gao, Z.,** Fekete, G., Baker, J. S., Liang, M., Xuan, R., & Gu, Y. (2022). Effects of running fatigue on lower extremity symmetry among amateur runners: From a biomechanical perspective. Frontiers in Physiology, 13: 899818-899830. **IF: 4.000, Q2**
4. **Gao, Z.,** Zhao, L., Fekete, G., Katona, G., Baker, J. S., & Gu, Y. (2022). Continuous time series analysis on the effects of induced running fatigue on leg symmetry using kinematics and kinetic variables: Implications for knee joint injury during a countermovement jump. Frontiers in Physiology, 13: 877394. **IF: 4.000, Q2**
5. Xiang, L., Gu, Y., Wang, A., Shim, V., **Gao, Z.,** & Fernandez, J. (2023). Foot Pronation Prediction with Inertial Sensors during Running: A Preliminary Application of Data-Driven Approaches. Journal of Human Kinetics, 87: 29-40. **IF: 2.300, Q3**
6. Xiang, L., Gu, Y., Rong, M., **Gao, Z.,** Yang, T., Wang, A., ... & Fernandez, J. (2022). Shock acceleration and attenuation during running with minimalist and maximalist shoes: a time-and frequency-domain analysis of tibial acceleration. Bioengineering, 9(7), 2-9. **IF:5.046, Q2**
7. Xiang, L., Gu, Y., **Gao, Z.,** Yu, P., Shim, V., Wang, A., & Fernandez, J. (2024). Integrating an LSTM framework for predicting ankle joint biomechanics during gait using inertial sensors. Computers in Biology and Medicine, 170, 1-12. **IF: 7.700, Q2**
8. Xiang, L#., **Gao, Z#.,** Wang, A., Shim, V., Fekete, G., Gu, Y., & Fernandez, J. (2024). Rethinking running biomechanics: a critical review of ground reaction forces, tibial bone loading, and the role of wearable sensors. Frontiers in Bioengineering and Biotechnology, 12, 1-13. **IF: 5.700, Q2**

International conference abstracts related to this thesis:

1. **Zixiang Gao,** Yuqi He, Gusztav Fekete and Yaodong Gu. The Effect of The of Running-Induced Fatigue on The Symmetry of Kinematics and Kinetic Variables of Knee Joints in

a Countermovement Jump. 27th Congress of the European Society of Biomechanics, Portugal.2022

2. **Zixiang Gao,** Yuqi He, Gusztav Fekete and Yaodong Gu. Effects of Running Fatigue on Knee Joint Symmetry Among Amateur Runners. International Society of Biomechanics in Sports. Britain.2022

3. **Zixiang Gao,** Yuqi He, Liangliang Xiang, Gusztav Fekete, András Kovács and Yaodong Gu. Automatically Detecting Fatigue Gait Based on Time Series Bilateral Plantar Force Distribution Using Deep Learning Algorithms, 28th Congress of the European Society of Biomechanics, Netherlands, 2023

Other publications:

1. **Gao, Z.** (2022). The Effect of Application of Asymmetry Evaluation in Competitive Sports: A Systematic Review. Physical Activity and Health, 6(1).**CS: 3.9**(Scopus), **Q1**
2. **Gao, Z.,** Mei, Q., Fekete, G., Baker, J.S. and Gu, Y., (2020). The Effect of Prolonged Running on the Symmetry of Biomechanical Variables of the Lower Limb Joints. Symmetry, 12(5),1-11. **IF: 2.713, Q2**
3. **Gao, Z.,** Mei, Q., Xiang, L., Gu, Y., (2020). Difference of walking plantar loadings in experienced and novice long-distance runners. Acta of bioengineering and biomechanics, 22(3), 127-147. **IF: 1.281, Q4**
4. **Gao, Z.,** Mei, Q., Xiang, L., Baker, J.S., Fernandez, J., & Gu, Y. (2020). Effects of limb dominance on the symmetrical distribution of plantar loading during walking and running. Proceedings of the Institution of Mechanical Engineers Part P-Journal of Sports Engineering and Technology, 1-7. **IF: 1.238, Q4**
5. **Gao, Z.,** Song, Y., Yu, P. M., Zhang, Y., & Li, S. D. (2019). Acute Effects of Different Stretching Techniques on Lower Limb Kinematics, Kinetics and Muscle Activities during Vertical Jump. In Journal of Biomimetics, Biomaterials and Biomedical Engineering 40, 1-15. EI (Scopus)**, EI (Scopus) IF: 0.70, Q3**
6. Zhou, Z., Li, S., Yang, L., **Gao, Z.,** Lin, Y., Radak, Z., & Gu, Y. (2023). Inter-Segmental Coordination of the Swimming Start among Paralympic Swimmers: A Comparative Study between S9, S10, and S12 Swimmers. Applied Sciences, 13(16), 1-12, 9097. **IF: 2.700, Q1**
7. Wang, Y., Jiang, H., Yu, L., **Gao, Z.,** Liu, W., Mei, Q., & Gu, Y. (202). Understanding the Role of Children's Footwear on Children's Feet and Gait Development: A Systematic

Scoping Review. Healthcare, 11 (10), 1-14. **IF: 2.800, Q2**

8. Mei, Q., Gu, Y., Xiang, L., Yu, P., **Gao, Z.,** Shim, V. and Fernandez, J., (2019). Foot shape and plantar pressure relationships in shod and barefoot populations. Biomechanics and Modeling in Mechanobiology, pp.1-14. **IF:2.527, Q3**
9. Liu W, Mei Q, Yu P, **Gao, Z.,** Biomechanical Characteristics of the Typically Developing Toddler Gait: A Narrative Review (2022). Children, 9(3): 2-16. **IF:2.400, Q3**
10. Yu, L., Yu, P., Liu, W., **Gao, Z.,** Sun, D., Mei, Q., Gu, Y. (2022). Understanding Foot Loading and Balance Behavior of Children with Motor Sensory Processing Disorder. Children, 9(3): 1-19. **IF:2.863, Q2**
11. Xiang, L., Deng, K., Mei, Q., **Gao, Z.,** Yang, T., Wang, A., ... & Gu, Y. (2021). Population and Age-Based Cardiorespiratory Fitness Level Investigation and Automatic Prediction. Frontiers in Cardiovascular Medicine, 8: 1-9. **IF:6.050, Q1**
12. Zhang, Y., Xu, Y., **Gao, Z.,** Yan, H., Li, J., & Lu, Y. (2022). The Effect of Standing Mats on Biomechanical Characteristics of Lower Limbs and Perceived Exertion for Healthy Individuals during Prolonged Standing. Applied Bionics and Biomechanics, 2022: 1-11. **IF: 2.2, Q3**
13. Mei, Q., Fernandez, J., Xiang, L., **Gao, Z.,** Yu, P., Baker, J. S., & Gu, Y. (2022). Dataset of lower extremity joint angles, moments and forces in distance running. Heliyon, 8(11), e11517. **IF:4.000, Q3**
14. Cen, X., Liang, Z., **Gao, Z.,** Lian, W., & Wang, Z. (2019). The Influence of the Improvement of Calf Strength on Barefoot Loading. In Journal of Biomimetics, Biomaterials and Biomedical Engineering, 40, 16-25. EI (Scopus)**, EI (Scopus) IF: 0.70, Q3.**
15. Mei, Q., **Gao, Z.,** Fernandez, J., & Gu, Y. (2019). 3D Foot Shape Modelling Based on Statistical Shape Model.Journal of Medical Biomechanics. CSSCI, **IF: 0.964**
16. Mei, Q., Gu, Y., Xiang, L., Yu, P., **Gao, Z.,** Shim, V. and Fernandez, J., (2019). Foot shape and plantar pressure relationships in shod and barefoot populations. Biomechanics and Modeling in Mechanobiology, 19: 1211-1224. **IF: 2.527, Q3**

Reviewer for international journal articles:

1. Plos One
2. Frontiers in Physiology
3. Frontiers in Bioengineering and Biotechnology

4. BMC Musculoskeletal Disorders
5. Int. J. of Biomedical Engineering and Technology
6. Ergonomics
7. Frontiers in Sports and Active Living
8. BMC Sports Science, Medicine and Rehabilitation
9. Journal of Orthopaedic Surgery and Research
10. Physical Activity and Health Journal
11. Scientific Report

ORCID: 0000-0002-4345-8201

Total independent citations:

Scopus Database: 24 (https://www.scopus.com/authid/detail.uri?authorId=57207686220)

Independent citations: 133

Total Impact Factor: 67.379 (Web of Science)

ACKNOWLEDGEMENTS

As I bring to close this significant chapter of my PhD academic journey, I am filled with immense gratitude towards numerous individuals and institutions whose support and guidance have been invaluable. Foremost, I extend my deepest appreciation to my supervisor, Dr. habil. Gusztáv Fekete, Dr. András Kovács and Prof. Dr. Yaodong Gu for them unwavering guidance, insightful feedback, and relentless support throughout this research. Them expertise and wisdom have been pivotal in shaping this thesis.

I would like to acknowledge the Faculty of Engineering at the University of Pannonia (PE), Savaria Institute of Technology at Eötvös Loránd University (ELTE), and the Faculty of Sports Science at the Research Academy of Grand Health, Ningbo University (NBU). The facilities, resources, and support provided by these esteemed institutions have been fundamental to the success of my research. Special thanks are due to my esteemed professors and colleagues - Prof. Dr. István BÍRÓ, Dr. Ildikó Molnár, Dr. Endre Jánosi, Dr. Tej Singh, Dr. Qichang Mei, Dr. Dong Sun, Dr. Liangliang Xiang, Dr. Meizi wang, Dr. Siqin Shen, Dr. Wenjing Quan, Dr. Yuqi He and all the PhD and master students. Their assistance, whether academic or life, has been of great help and is sincerely appreciated. My heartfelt thanks to all participants who took part in the studies of this dissertation. Your involvement and time were essential to the success of this research and are greatly appreciated.

On a personal note, I extend my profound gratitude to my family. To my father, Mr. Feng Gao, and my mother, Mrs. Qinyang Li, for their unwavering support and belief in me. To my beloved girlfriend, Ms. Wenjing Pi, thank you for your endless motivation, unconditional love, and for being my pillar of strength.

Finally, I am deeply thankful for the financial support provided by the Stipendium Hungaricum Programme, Tempus Public Foundation, and the China Scholarship Council (CSC). This support has been crucial in facilitating my research and academic endeavors.

References

[1] Kapandji IA. The physiology of the joints: annotated diagrams of the mechanics of the human joints. (No Title). 1984.

[2]Magee DJ, Zachazewski JE, Quillen WS. Scientific foundations and principles of practice in musculoskeletal rehabilitation. Elsevier Health Sciences. 2007.

[3] Srivastava P, Singh VP. Tribological and mechanical testing of artificial bio-bearing materials followed by design and analysis of patient-specific artificial hip joint. International Journal on Interactive Design and Manufacturing (IJIDeM). 2024; : 1-16.

[4] https://teachmeanatomy.info/lower-limb/joints/hip-joint/

[5] Aresti N, Kassam J, Nicholas N, Achan P. Hip osteoarthritis. BMj. 2016; 354: 1-10.

[6] Miyoshi H, Mikami H, Oba K, Amari R. Anteversion of the acetabular component aligned with the transverse acetabular ligament in total hip arthroplasty. The Journal of Arthroplasty. 2012; 27: 916-922.

[7] Carr AJ, Robertsson O, Graves S, Price AJ, Arden NK, Judge A, *et al.* Knee replacement. The Lancet. 2012; 379: 1331-1340.

[8] Hirschmann MT, Müller W. Complex function of the knee joint: the current understanding of the knee. Knee Surgery, Sports Traumatology, Arthroscopy. 2015; 23: 2780-2788.

[9] BAWUAH P. Dissertations in Forestry and Natural Sciences.

[10] McNulty AL, Guilak F. Mechanobiology of the meniscus. Journal of biomechanics. 2015; 48: 1469-1478.

[11] Rath E, Richmond JC. The menisci: basic science and advances in treatment. British journal of sports medicine. 2000; 34: 252-257.

[12] Mow VC, Gu WY, Chen FH. Structure and function of articular cartilage and meniscus. Basic orthopaedic biomechanics and mechano-biology. 2005; 3: 181-258.

[13] Sakane M, Fox RJ, Glen SLYW, Livesay A, Li G, Fu FH. In situ forces in the anterior cruciate ligament and its bundles in response to anterior tibial loads. Journal of Orthopaedic Research. 1997; 15: 285-293.

[14] Woo SL, Fox RJ, Sakane M, Livesay GA, Rudy TW, Fu FH. Biomechanics of the ACL: measurements of in situ force in the ACL and knee kinematics. The Knee. 1998; 5: 267-288.

[15] Markolf KL, Burchfield DM, Shapiro MM, Shepard MF, Finerman GA, Slauterbeck JL. Combined knee loading states that generate high anterior cruciate ligament forces. Journal of Orthopaedic Research. 1995; 13: 930-935.

[16] Markolf KL, Willems MJ, Jackson SR, Finerman GA. In situ calibration of miniature sensors implanted into the anterior cruciate ligament. Part I: Strain measurements. Journal of Orthopaedic Research. 1998; 16: 455-463.

[17] Hertel J. Functional anatomy, pathomechanics, and pathophysiology of lateral ankle instability. Journal of Athletic Training. 2002; 37: 364-375.

[18] Doral MN, Alam M, Bozkurt M, Turhan E, Atay OA, Dönmez G, *et al.* Functional anatomy of the Achilles tendon. Knee Surgery, Sports Traumatology, Arthroscopy. 2010; 18: 638-643.

[19]Angin S, Simsek I. Comparative kinesiology of the human body: normal and pathological conditions. Academic Press. 2020.

[20] Jain R, Semwal VB, Kaushik P. Stride segmentation of inertial sensor data using statistical methods for different walking activities. Robotica. 2022; 40: 2567-2580.

[21] Furlong L, Egginton NL. Kinetic Asymmetry during Running at Preferred and Nonpreferred

Speeds. Medicine & Science in Sports & Exercise. 2018; 50: 1241-1248.
[22] Gao Z. The Effect of Application of Asymmetry Evaluation in Competitive Sports: A Systematic Review. Physical Activity and Health. 2022; 251-272.
[23] Meardon SA, Hamill J, Derrick TR. Running injury and stride time variability over a prolonged run. Gait & posture. 2011; 33: 36-40.
[24] Gandevia SC. Spinal and supraspinal factors in human muscle fatigue. Physiological reviews. 2001; 81:1725-1788.
[25] Sadeghi H, Allard P, Prince F, Labelle H. Symmetry and limb dominance in able-bodied gait: a review. Gait & posture. 2000; 12: 34-45.
[26] Winter DA. Kinematic and kinetic patterns in human gait: variability and compensating effects. Human movement science. 1984; 3: 51-76.
[27] Bajelani K, Arshi AR, Akhavan AN. Influence of compression garments on fatigue behaviour during running based on nonlinear dynamical analysis. Sports Biomechanics. 2022: 1-14.
[28] Gao Z, Zhao L, Fekete G, Katona G, Baker JS, Gu Y. Continuous time series analysis on the effects of induced running fatigue on leg symmetry using kinematics and kinetic variables: Implications for knee joint injury during a countermovement jump. Frontiers in Physiology. 2022; 13: 877394.
[29] Gao Z, Fekete G, Baker JS, Liang M, Xuan R, Gu Y. Effects of running fatigue on lower extremity symmetry among amateur runners: From a biomechanical perspective. Frontiers in Physiology. 2022; 13: 899818-899830.
[30] Mei Q, Fernandez J, Xiang L, Gao Z, Yu P, Baker JS, *et al*. Dataset of lower extremity joint angles, moments and forces in distance running. Heliyon. 2022; 8: 1-11.
[31] Rosenstein MT, Collins JJ, De Luca CJ. A practical method for calculating largest Lyapunov exponents from small data sets. Physica D: Nonlinear Phenomena. 1993; 65: 117-134.
[32] Dingwell J, Cusumano JP, Cavanagh P, Sternad D. Local dynamic stability versus kinematic variability of continuous overground and treadmill walking. J. Biomech. Eng. 2001; 123: 27-32.
[33] Matcuk GR, Mahanty SR, Skalski MR, Patel DB, White EA, Gottsegen CJ. Stress fractures: pathophysiology, clinical presentation, imaging features, and treatment options. Emergency radiology. 2016; 23: 365-375.
[34] Hoenig T, Hamacher D, Braumann K-M, Zech A, Hollander K. Analysis of running stability during 5000 m running. European Journal of Sport Science. 2019; 19: 413-421.
[35] Buzzi UH, Stergiou N, Kurz MJ, Hageman PA, Heidel J. Nonlinear dynamics indicates aging affects variability during gait. Clinical biomechanics. 2003; 18: 435-443.
[36] Bailey CA, Hill A, Graham RB, Nantel J. Effects of arm swing amplitude and lower limb asymmetry on motor variability patterns during treadmill gait. Journal of biomechanics. 2022; 130: 110855.
[37] Hunter B, Karsten B, Greenhalgh A, Burnley M, Muniz-Pumares D. The Application of non-linear methods to quantify changes to movement dynamics during running: A scoping review. Journal of Sports Sciences. 2023; : 1-14.
[38] Hollander K, Hamacher D, Zech A. Running barefoot leads to lower running stability compared to shod running-results from a randomized controlled study. Scientific Reports. 2021; 11: 4376-4385.
[39] Schütte KH, Maas EA, Exadaktylos V, Berckmans D, Venter RE, Vanwanseele B. Wireless tri-axial trunk accelerometry detects deviations in dynamic center of mass motion due to running-induced fatigue. PloS one. 2015; 10: 1-12.

[40] Schütte KH, Seerden S, Venter R, Vanwanseele B. Influence of outdoor running fatigue and medial tibial stress syndrome on accelerometer-based loading and stability. Gait & posture. 2018; 59: 222-228.
[41] Wouters I, Almonroeder T, DeJarlais B, Laack A, Willson JD, Kernozek TW. Effects of a movement training program on hip and knee joint frontal plane running mechanics. International journal of sports physical therapy. 2012; 7: 637-646.
[42] Lee D-c, Pate RR, Lavie CJ, Sui X, Church TS, Blair SN. Leisure-time running reduces all-cause and cardiovascular mortality risk. Journal of the American College of Cardiology. 2014; 64: 472-481.
[43] Chakravarty EF, Hubert HB, Lingala VB, Fries JF. Reduced disability and mortality among aging runners: a 21-year longitudinal study. Archives of internal medicine. 2008; 168: 1638-1646.
[44] Van Gent R, Siem D, van Middelkoop M, Van Os A, Bierma-Zeinstra S, Koes B. Incidence and determinants of lower extremity running injuries in long distance runners: a systematic review. British journal of sports medicine. 2007; 41: 469-480.
[45] Hulme A, Nielsen RO, Timpka T, Verhagen E, Finch C. Risk and protective factors for middle-and long-distance running-related injury. Sports Medicine. 2017; 47: 869-886.
[46] Abd-Elfattah HM, Abdelazeim FH, Elshennawy S. Physical and cognitive consequences of fatigue: A review. Journal of advanced research. 2015; 6: 351-358.
[47] Dierks TA, Davis IS, Hamill J. The effects of running in an exerted state on lower extremity kinematics and joint timing. Journal of biomechanics. 2010; 43: 2993-2998.
[48] Buist I, Bredeweg SW, Lemmink KA, Van Mechelen W, Diercks RL. Predictors of running-related injuries in novice runners enrolled in a systematic training program: a prospective cohort study. The American journal of sports medicine. 2010; 38: 273-280.
[49] Willems TM, De Ridder R, Roosen P. The effect of a long-distance run on plantar pressure distribution during running. Gait & posture. 2012; 35: 405-409.
[50] Meeuwisse WH. Assessing causation in sport injury: a multifactorial model. Clinical Journal of Sport medicine.1994; 4: 166-170.
[51] Fourchet F, Kelly L, Horobeanu C, Loepelt H, Taiar R, Millet G. High-intensity running and plantar-flexor fatigability and plantar-pressure distribution in adolescent runners. Journal of Athletic Training. 2015; 50: 117-125.
[52] Gao Z, Mei Q, Xiang L, Gu Y. Difference of walking plantar loadings in experienced and novice long-distance runners. Acta Bioeng. Biomech. 2020; 22: 127-147.
[53] Zhang X, Wang W, Chen G, Ji A, Song Y. Effects of standing and walking on plantar pressure distribution in recreational runners before and after long-distance running. Journal of biomechanics. 2021; 129: 110779-110786.
[54] Willems TM, De Clercq D, Delbaere K, Vanderstraeten G, De Cock A, Witvrouw E. A prospective study of gait related risk factors for exercise-related lower leg pain. Gait & posture. 2006; 23: 91-98.
[55] Nagel A, Fernholz F, Kibele C, Rosenbaum D. Long distance running increases plantar pressures beneath the metatarsal heads: a barefoot walking investigation of 200 marathon runners. Gait & posture. 2008; 27: 152-155.
[56] Weist R, Eils E, Rosenbaum D. The influence of muscle fatigue on electromyogram and plantar pressure patterns as an explanation for the incidence of metatarsal stress fractures. The American journal of sports medicine. 2004; 32: 1893-1898.
[57] Bisiaux M, Moretto P. The effects of fatigue on plantar pressure distribution in walking. Gait & posture. 2008; 28: 693-698.

[58] Willson JD, Kernozek TW. Plantar loading and cadence alterations with fatigue. Medicine and science in sports and exercise. 1999; 31: 1828-1833.
[59] Hesar NGZ, Van Ginckel A, Cools A, Peersman W, Roosen P, De Clercq D, *et al.* A prospective study on gait-related intrinsic risk factors for lower leg overuse injuries. British journal of sports medicine. 2009; 43: 1057-1061.
[60] Anbarian M, Esmaeili H. Effects of running-induced fatigue on plantar pressure distribution in novice runners with different foot types. Gait & posture. 2016; 48: 52-56.
[61] Hasler E, Herzog W, Leonard T, Stano A, Nguyen H. In vivo knee joint loading and kinematics before and after ACL transection in an animal model. Journal of biomechanics. 1997; 31: 253-262.
[62] Van Mechelen W. Running injuries: a review of the epidemiological literature. Sports Medicine. 1992; 14: 320-335.
[63] Fredericson M, Misra AK. Epidemiology and aetiology of marathon running injuries. Sports Medicine. 2007; 37: 437-439.
[64] Horisberger M, Fortuna R, Valderrabano V, Herzog W. Long-term repetitive mechanical loading of the knee joint by in vivo muscle stimulation accelerates cartilage degeneration and increases chondrocyte death in a rabbit model. Clinical biomechanics. 2013; 28: 536-543.
[65] Egloff C, Hügle T, Valderrabano V. Biomechanics and pathomechanisms of osteoarthritis. Swiss medical weekly. 2012; 142: w13583-w13583.
[66] Yang NH, Nayeb-Hashemi H, Canavan PK, Vaziri A. Effect of frontal plane tibiofemoral angle on the stress and strain at the knee cartilage during the stance phase of gait. Journal of Orthopaedic Research. 2010; 28: 1539-1547.
[67] Amoako AO, Pujalte GGA. Osteoarthritis in young, active, and athletic individuals. Clinical Medicine Insights: Arthritis and Musculoskeletal Disorders. 2014; 7: 27-32.
[68] Lohmander LS, Englund PM, Dahl LL, Roos EM. The long-term consequence of anterior cruciate ligament and meniscus injuries: osteoarthritis. The American journal of sports medicine. 2007; 35: 1756-1769.
[69] Miller RH, Edwards WB, Brandon S, Morton AM, Deluzio KJ. Why don't most runners get knee osteoarthritis? A case for per-unit-distance loads. Medicine and science in sports and exercise. 2014; 46: 572-579.
[70] Ceyssens L, Vanelderen R, Barton C, Malliaras P, Dingenen B. Biomechanical risk factors associated with running-related injuries: a systematic review. Sports Medicine. 2019; 49: 1095-1115.
[71] Furlong L-A, Egginton NL. Kinetic asymmetry during running at preferred and non-preferred speeds.2018; 50:1241–1248.
[72] Brown SR, Feldman ER, Cross MR, Helms ER, Marrier B, Samozino P, *et al.* The Potential for a Targeted Strength-Training Program to Decrease Asymmetry and Increase Performance: A Proof of Concept in Sprinting. Int J Sports Physiol Perform. 2017; 12: 1392-1395.
[73] Botelho MB, Alvarenga BA, Molina N, Ribas M, Baptista AF. Spinal manipulative therapy and sports performance enhancement: a systematic review. Journal of manipulative and physiological therapeutics. 2017; 40: 535-543.
[74] Parrington L, Ball K. Biomechanical Considerations of Laterality in Sport. *In* Laterality in Sports .2016. 279-308.
[75] Tomkinson GR, Olds T. Physiological correlates of bilateral symmetry in humans. International journal of sports medicine. 2000; 21: 545-550.
[76] Maloney SJ. The relationship between asymmetry and athletic performance: A critical review. The

Journal of Strength & Conditioning Research. 2019; 33: 2579-2593.
[77] Haugen T, Danielsen J, McGhie D, Sandbakk O, Ettema G. Kinematic stride cycle asymmetry is not associated with sprint performance and injury prevalence in athletic sprinters. Scand J Med Sci Sports. 2018; 28: 1001-1008.
[78] Tucker CB, Hanley B. Gait variability and symmetry in world-class senior and junior race walkers. J Sports Sci. 2017; 35: 1739-1744.
[79] Brown SR, Cross MR, Girard O, Brocherie F, Samozino P, Morin JB. Kinetic Sprint Asymmetries on a non-motorised Treadmill in Rugby Union Athletes. Int J Sports Med. 2017; 38: 1017-1022.
[80] Bishop C, Turner A, Read P. Effects of inter-limb asymmetries on physical and sports performance: A systematic review. Journal of Sports Sciences. 2018; 36: 1135-1144.
[81]Afonso J, Bessa C, Pinto F, Ribeiro D, Moura B, Rocha T, *et al.* Asymmetry as a Foundational and Functional Requirement in Human Movement: From Daily Activities to Sports Performance. Springer Nature. 2020.
[82] BARBER SD, NOYES FR, MANGINE RE, HARTMAN W. Quantitative assessment of functional limitations in normal and anterior cruciate ligament-deficient knees. Clinical Orthopaedics and Related Research (1976-2007). 1990; 255: 204-214.
[83] Grindem H, Logerstedt D, Eitzen I, Moksnes H, Axe MJ, Snyder-Mackler L, *et al.* Single-legged hop tests as predictors of self-reported knee function in nonoperatively treated individuals with anterior cruciate ligament injury. The American journal of sports medicine. 2011; 39: 2347-2354.
[84] Kyritsis P, Bahr R, Landreau P, Miladi R, Witvrouw E. Likelihood of ACL graft rupture: not meeting six clinical discharge criteria before return to sport is associated with a four times greater risk of rupture. British journal of sports medicine. 2016; 50: 946-951.
[85] Rohman E, Steubs JT, Tompkins M. Changes in involved and uninvolved limb function during rehabilitation after anterior cruciate ligament reconstruction: implications for Limb Symmetry Index measures. The American journal of sports medicine. 2015; 43: 1391-1398.
[86] Trivers R, Palestis BG, Manning JT. The symmetry of children's knees is linked to their adult sprinting speed and their willingness to sprint in a long-term Jamaican study. PloS one. 2013; 8: e72244.
[87] Preatoni E, Hamill J, Harrison AJ, Hayes K, Van Emmerik RE, Wilson C, *et al.* Movement variability and skills monitoring in sports. Sports Biomechanics. 2013; 12: 69-92.
[88] Warmenhoven J, Smith R, Draper, C., , Harrison AJ, Bargary N, Cobley S. Force coordination strategies in on- water single sculling: Are asymmetries related to better rowing performance? Scandinavian Journal of Medicine & Science in Sports. 2018; 28: 1379-1388.
[89] Vincent HK, Vincent KR. Rehabilitation and Prehabilitation for Upper Extremity in Throwing Sports: Emphasis on Lacrosse. Current sports medicine reports. 2019; 18: 229-238.
[90] Hoffman JR, Ratamess NA, Klatt M, Faigenbaum AD, Kang J. Do bilateral power deficits influence direction-specific movement patterns? Research in Sports Medicine. 2007; 15: 125-132.
[91] Bell DR, Sanfilippo JL, Binkley N, Heiderscheit BC. Lean mass asymmetry influences force and power asymmetry during jumping in collegiate athletes. Journal of strength and conditioning research/National Strength & Conditioning Association. 2014; 28: 884-891.
[92] Tomkinson GR, Popović N, Martin M. Bilateral symmetry and the competitive standard attained in elite and sub-elite sport. Journal of Sports Sciences. 2003; 21: 201-211.
[93] Loturco I, Pereira LA, Kobal R, Abad CC, Rosseti M, Carpes FP, *et al.* Do asymmetry scores influence speed and power performance in elite female soccer players? Biology of sport. 2019; 36:

209-216.
[94]Nigg BM. Biomechanics of the musculo-skeletal system. John Wiley & Sons Incorporated. 2007.
[95] Jordan MJ, Aagaard P, Herzog W. Lower limb asymmetry in mechanical muscle function: a comparison between ski racers with and without ACL reconstruction. Scandinavian Journal of Medicine & Science in Sports. 2015; 25: e301-e309.
[96] Hewett TE, Di Stasi SL, Myer GD. Current concepts for injury prevention in athletes after anterior cruciate ligament reconstruction. The American journal of sports medicine. 2013; 41: 216-224.
[97] Mokhtarzadeh H, Ewing K, Janssen I, Yeow C-H, Brown N, Lee PVS. The effect of leg dominance and landing height on ACL loading among female athletes. Journal of biomechanics. 2017; 60: 181-187.
[98] Montalvo AM, Schneider DK, Webster KE, Yut L, Galloway MT, Heidt Jr RS, *et al.* Anterior cruciate ligament injury risk in sport: a systematic review and meta-analysis of injury incidence by sex and sport classification. Journal of Athletic Training. 2019; 54: 472-482.
[99] Brown SR, Brughelli M. Determining return-to-sport status with a multi-component assessment strategy: a case study in rugby. Phys Ther Sport. 2014; 15: 211-215.
[100] Schache A, Wrigley T, Baker R, Pandy M. Biomechanical response to hamstring muscle strain injury: A single case study. Journal of Science and Medicine in Sport. 2009; 12: S47-S50.
[101] Auerbach BM, Raxter MH. Patterns of clavicular bilateral asymmetry in relation to the humerus: variation among humans. Journal of human evolution. 2008; 54: 663-674.
[102] Oyama S, Myers JB, Wassinger CA, Daniel Ricci R, Lephart SM. Asymmetric resting scapular posture in healthy overhead athletes. Journal of Athletic Training. 2008; 43: 565–570.
[103] Ramos Dalla Bernardina G, Danillo Matos Dos Santos M, Alves Resende R, Tulio de Mello M, Rodrigues Albuquerque M, Augusto Paolucci L, *et al.* Asymmetric velocity profiles in Paralympic powerlifters performing at different exercise intensities are detected by functional data analysis. J Biomech. 2021; 123: 110523-110528.
[104] Goosey V. Symmetry of the elbow kinematics during racing wheelchair propulsion. Ergonomics. 1998; 41: 1810-1820.
[105] Gray J, Aginsky KD, Derman W, Vaughan CL, Hodges PW. Symmetry, not asymmetry, of abdominal muscle morphology is associated with low back pain in cricket fast bowlers. J Sci Med Sport. 2016; 19: 222-226.
[106] Paterno MV, Schmitt LC, Ford KR, Rauh MJ, Myer GD, Huang B, *et al.* Biomechanical measures during landing and postural stability predict second anterior cruciate ligament injury after anterior cruciate ligament reconstruction and return to sport. Am J Sports Med. 2010; 38: 1968-1978.
[107] Kotsifaki A, Van Rossom S, Whiteley R, Korakakis V, Bahr R, Sideris V, *et al.* Symmetry in Triple Hop Distance Hides Asymmetries in Knee Function After ACL Reconstruction in Athletes at Return to Sports. Am J Sports Med. 2022; 50: 441-450.
[108] Alvarenga B, Botelho M, Lara J, Joao F, Veloso A. Preliminary Feasibility Study to Measure the Immediate Changes of Bilateral Asymmetry After Lumbar Spinal Manipulative Therapy in Asymptomatic Athletes. J Chiropr Med. 2019; 18: 205-212.
[109]Levine D, Richards J, Whittle MW. Whittle's gait analysis. Elsevier health sciences. 2012.
[110] Exell TA, Gittoes MJ, Irwin G, Kerwin DG. Gait asymmetry: composite scores for mechanical analyses of sprint running. J Biomech. 2012; 45: 1108-1111.
[111] Girard O, Morin JB, Ryu J, Read P, Townsend N. Running Velocity Does Not Influence Lower Limb Mechanical Asymmetry. Front Sports Act Living. 2019; 1: 36-48.

[112] Exell TA, Irwin G, Gittoes MJ, Kerwin DG. Implications of intra-limb variability on asymmetry analyses. J Sports Sci. 2012; 30: 403-409.
[113] Girard O, Brocherie F, Morin JB, Millet GP. Lower limb mechanical asymmetry during repeated treadmill sprints. Hum Mov Sci. 2017; 52: 203-214.
[114] Grabowski AM, Kram R. Effects of velocity and weight support on ground reaction forces and metabolic power during running. Journal of Applied Biomechanics. 2008; 24: 288-297.
[115] Kyröläinen H, Avela J, Komi PV. Changes in muscle activity with increasing running speed. J Sports. 2005; 23: 1101-1109.
[116] Beck ON, Azua EN, Grabowski AM. Step time asymmetry increases metabolic energy expenditure during running. European journal of applied physiology. 2018; 118: 2147-2154.
[117] Radzak KN, Putnam AM, Tamura K, Hetzler RK, Stickley CD. Asymmetry between lower limbs during rested and fatigued state running gait in healthy individuals. Gait & posture. 2017; 51: 268-274.
[118] Mastalerz A. The Symmetry of Fatigue of Lower Limb Muscles in 400 m Run Based on Electromyography Signals. Symmetry. 2021; 13: 1-10.
[119] Gao Z, Mei Q, Xiang L, Baker JS, Fernandez J, Gu Y. Effects of limb dominance on the symmetrical distribution of plantar loading during walking and running. Proceedings of the Institution of Mechanical Engineers, Part P: Journal of Sports Engineering and Technology. 2022; 236: 17-23.
[120] Nakayama Y, Kudo K, Ohtsuki T. Variability and fluctuation in running gait cycle of trained runners and non-runners. Gait & posture. 2010; 31: 331-335.
[121] García-Pinillos F, Cartón-Llorente A, Jaén-Carrillo D, Delgado-Floody P, Carrasco-Alarcón V, Martínez C, *et al*. Does fatigue alter step characteristics and stiffness during running? Gait & posture. 2020; 76: 259-263.
[122] Simoni L, Scarton A, Macchi C, Gori F, Pasquini G, Pogliaghi S. Quantitative and Qualitative Running Gait Analysis through an Innovative Video-Based Approach. Sensors. 2021; 21: 2977-2989.
[123] Zifchock RA, Davis I, Hamill J. Kinetic asymmetry in female runners with and without retrospective tibial stress fractures. Journal of biomechanics. 2006; 39: 2792-2797.
[124] Williams K, Cavanagh P, Ziff J. Biomechanical studies of elite female distance runners. International journal of sports medicine. 1987; 8: S107-S118.
[125] Seeley MK, Umberger BR, Shapiro R. A test of the functional asymmetry hypothesis in walking. Gait & posture. 2008; 28: 24-28.
[126] Cen X, Lu Z, Baker JS, István B, Gu Y. A Comparative Biomechanical Analysis during Planned and Unplanned Gait Termination in Individuals with Different Arch Stiffnesses. Applied Sciences. 2021; 11: 1871: 1-10.
[127] Ceyssens L, Vanelderen R, Barton C, Malliaras P, Dingenen B. Biomechanical risk factors associated with running-related injuries: a systematic review. Sports medicine. 2019; 49: 1095-1115.
[128] Enoka RM, Stuart DG. Neurobiology of muscle fatigue. Journal of applied physiology. 1992; 72: 1631-1648.
[129] Makris EA, Hadidi P, Athanasiou KA. The knee meniscus: structure–function, pathophysiology, current repair techniques, and prospects for regeneration. Biomaterials. 2011; 32: 7411-7431.
[130] Walker PS, Erkiuan MJ. The role of the menisci in force transmission across the knee. Clinical Orthopaedics and Related Research®. 1975; 109: 184-192.
[131] Taunton JE, Ryan MB, Clement D, McKenzie DC, Lloyd-Smith D, Zumbo B. A retrospective case-control analysis of 2002 running injuries. British journal of sports medicine. 2002; 36: 95-101.
[132] Adams J, McAlindon T, Dimasi M, Carey J, Eustace S. Contribution of meniscal extrusion and

cartilage loss to joint space narrowing in osteoarthritis. Clinical radiology. 1999; 54: 502-506.
[133] Khassetarash A, Haider I, Baggaley M, Edwards WB. Tibial Strains During Prolonged Downhill Running: A Finite Element Analysis. Journal of Biomechanical Engineering. 2023; 145: 041007.
[134] Cho J-R, Park S-B, Ryu S-H, Kim S-H, Lee S-B. Landing impact analysis of sports shoes using 3-D coupled foot-shoe finite element model. Journal of mechanical science and technology. 2009; 23: 2583-2591.
[135] Gilbert S, Chen T, Hutchinson ID, Choi D, Voigt C, Warren RF, *et al.* Dynamic contact mechanics on the tibial plateau of the human knee during activities of daily living. Journal of biomechanics. 2014; 47: 2006-2012.
[136] Hanley B, Tucker CB. Gait variability and symmetry remain consistent during high-intensity 10,000 m treadmill running. Journal of biomechanics. 2018; 79: 129-134.
[137] Zifchock RA, Davis I, Higginson J, McCaw S, Royer T. Side-to-side differences in overuse running injury susceptibility: a retrospective study. Human movement science. 2008; 27: 888-902.
[138] Walter SD, Hart L, McIntosh JM, Sutton JR. The Ontario cohort study of running-related injuries. Archives of internal medicine. 1989; 149: 2561-2564.
[139] Ferber R, Davis IM, Hamill J, Pollard CD. Prospective biomechanical investigation of iliotibial band syndrome in competitive female runners. Medicine & Science in Sports & Exercise. 2003; 35: S91.
[140] Milner CE, Ferber R, Pollard CD, Hamill J, Davis IS. Biomechanical factors associated with tibial stress fracture in female runners. Medicine & Science in Sports & Exercise. 2006; 38: 323-328.
[141] Xiang L, Gu Y, Mei Q, Wang A, Shim V, Fernandez J. Automatic classification of barefoot and shod populations based on the foot metrics and plantar pressure patterns. Frontiers in Bioengineering and Biotechnology. 2022; 10: 843204.
[142] Gao Z, Zhu Y, Fang Y, Fekete G, Kovács A, Baker JS, *et al.* Automated recognition of asymmetric gait and fatigue gait using ground reaction force data. Frontiers in Physiology. 2023; 14: 369-382.
[143] Uhlrich SD, Uchida TK, Lee MR, Delp SL. Ten steps to becoming a musculoskeletal simulation expert: A half-century of progress and outlook for the future. Journal of biomechanics. 2023; 154: 111623-111634.
[144] Jiang Y, Ye Y, Gopinath D, Won J, Winkler AW, Liu CK. Transformer Inertial Poser: Real-time human motion reconstruction from sparse IMUs with simultaneous terrain generation. *In* SIGGRAPH Asia 2022 Conference Papers.2022. 1-9.
[145] Sharifi Renani M, Eustace AM, Myers CA, Clary CW. The use of synthetic imu signals in the training of deep learning models significantly improves the accuracy of joint kinematic predictions. Sensors. 2021; 21: 5876-5895.
[146] Shimada S, Golyanik V, Xu W, Theobalt C. Physcap: Physically plausible monocular 3d motion capture in real time. ACM Transactions on Graphics (ToG). 2020; 39: 1-16.
[147] Yuan Y, Wei S-E, Simon T, Kitani K, Saragih J. Simpoe: Simulated character control for 3d human pose estimation. *In* Proceedings of the IEEE/CVF conference on computer vision and pattern recognition. 2021.7159-7169.
[148] Zhang J, Zhao Y, Shone F, Li Z, Frangi AF, Xie SQ, *et al.* Physics-informed deep learning for musculoskeletal modeling: Predicting muscle forces and joint kinematics from surface EMG. IEEE Transactions on Neural Systems and Rehabilitation Engineering. 2022; 31: 484-493.
[149] Kidziński Ł, Mohanty SP, Ong CF, Hicks JL, Carroll SF, Levine S, *et al.* Learning to run

challenge: Synthesizing physiologically accurate motion using deep reinforcement learning. *In* The NIPS'17 Competition: Building Intelligent Systems. Springer.2018. 101-120.
[150] Dong H, Ugalde I, Figueroa N, Saddik AE. Towards whole body fatigue assessment of human movement: A fatigue-tracking system based on combined semg and accelerometer signals. Sensors. 2014; 14: 2052-2070.
[151] Jiang Y, Hernandez V, Venture G, Kulić D, K. Chen B. A data-driven approach to predict fatigue in exercise based on motion data from wearable sensors or force plate. Sensors. 2021; 21: 1499-1515.
[152] Mei Q, Gu Y, Xiang L, Yu P, Gao Z, Shim V, *et al.* Foot shape and plantar pressure relationships in shod and barefoot populations. Biomechanics and Modeling in Mechanobiology. 2020; 19: 1211-1224.
[153] Cifrek M, Medved V, Tonković S, Ostojić S. Surface EMG based muscle fatigue evaluation in biomechanics. Clinical biomechanics. 2009; 24: 327-340.
[154] Xiang L, Wang A, Gu Y, Zhao L, Shim V, Fernandez J. Recent machine learning progress in lower limb running biomechanics with wearable technology: A systematic review. Frontiers in Neurorobotics. 2022;16, 1-20.
[155] Figueiredo J, Santos CP, Moreno JC. Automatic recognition of gait patterns in human motor disorders using machine learning: A review. Medical engineering & physics. 2018; 53: 1-12.
[156] Eskofier BM, Federolf P, Kugler PF, Nigg BM. Marker-based classification of young–elderly gait pattern differences via direct PCA feature extraction and SVMs. Computer methods in biomechanics and biomedical engineering. 2013; 16: 435-442.
[157] Clermont CA, Osis ST, Phinyomark A, Ferber R. Kinematic gait patterns in competitive and recreational runners. Journal of Applied Biomechanics. 2017; 33: 268-276.
[158] Mundt M, Koeppe A, David S, Witter T, Bamer F, Potthast W, *et al.* Estimation of gait mechanics based on simulated and measured IMU data using an artificial neural network. Frontiers in Bioengineering and Biotechnology. 2020; 8: 41-57.
[159] Iwana BK, Uchida S. An empirical survey of data augmentation for time series classification with neural networks. PloS one. 2021; 16: e0254841-73.
[160] Nigg S, Vienneau J, Maurer C, Nigg BM. Development of a symmetry index using discrete variables. Gait & posture. 2013; 38: 115-119.
[161] Buckley C, O'Reilly MA, Whelan D, Farrell AV, Clark L, Longo V, *et al.* Binary classification of running fatigue using a single inertial measurement unit. *In* 2017 IEEE 14th International Conference on Wearable and Implantable Body Sensor Networks (BSN). IEEE 197-201.2017.
[162] Rashid KM, Louis J. Times-series data augmentation and deep learning for construction equipment activity recognition. Advanced Engineering Informatics. 2019; 42: 100944-100956.
[163] Liang S, Liu Y, Li G, Zhao G. Elderly fall risk prediction with plantar center of force using convlstm algorithm. *In* 2019 IEEE International Conference on Cyborg and Bionic Systems (CBS). IEEE. 2019. 36-41.
[164] Wahdow M, Alnaanah M, Fadel W, Adolf A, Kollod C, Ulbert I. Multi frequency band fusion method for EEG signal classification. Signal, Image and Video Processing. 2023; 17: 1883-1887.
[165] Wen J, Ding Q, Yu Z, Sun W, Wang Q, Wei K. Adaptive changes of foot pressure in hallux valgus patients. Gait & posture. 2012; 36: 344-349.
[166] Sherstinsky A. Fundamentals of recurrent neural network (RNN) and long short-term memory (LSTM) network. Physica D: Nonlinear Phenomena. 2020; 404: 132306-132334.
[167] Seth A, Hicks JL, Uchida TK, Habib A, Dembia CL, Dunne JJ, *et al.* OpenSim: Simulating

musculoskeletal dynamics and neuromuscular control to study human and animal movement. PLoS computational biology. 2018; 14: e1006223-e1006243.
[168] Reinbolt JA, Seth A, Delp SL. Simulation of human movement: applications using OpenSim. Procedia Iutam. 2011; 2: 186-198.
[169] Delp SL, Anderson FC, Arnold AS, Loan P, Habib A, John CT, *et al.* OpenSim: open-source software to create and analyze dynamic simulations of movement. IEEE transactions on biomedical engineering. 2007; 54: 1940-1950.
[170] Lerner ZF, DeMers MS, Delp SL, Browning RC. How tibiofemoral alignment and contact locations affect predictions of medial and lateral tibiofemoral contact forces. Journal of biomechanics. 2015; 48: 644-650.
[171] Hamner SR, Seth A, Delp SL. Muscle contributions to propulsion and support during running. Journal of biomechanics. 2010; 43: 2709-2716.
[172] Park S, Lee S, Yoon J, Chae S-W. Finite element analysis of knee and ankle joint during gait based on motion analysis. Medical engineering & physics. 2019; 63: 33-41.
[173] Mononen ME, Jurvelin JS, Korhonen RK. Effects of radial tears and partial meniscectomy of lateral meniscus on the knee joint mechanics during the stance phase of the gait cycle—A 3 D finite element study. Journal of Orthopaedic Research. 2013; 31: 1208-1217.
[174] Marangalou JH, Ito K, van Rietbergen B. A new approach to determine the accuracy of morphology–elasticity relationships in continuum FE analyses of human proximal femur. Journal of biomechanics. 2012; 45: 2884-2892.
[175] Godest A, Beaugonin M, Haug E, Taylor M, Gregson P. Simulation of a knee joint replacement during a gait cycle using explicit finite element analysis. Journal of biomechanics. 2002; 35: 267-275.
[176] Schnitzer TJ, Popovich JM, Andersson GB, Andriacchi TP. Effect of piroxicam on gait in patients with osteoarthritis of the knee. Arthritis & Rheumatism: Official Journal of the American College of Rheumatology. 1993; 36: 1207-1213.
[177] DeMers MS, Pal S, Delp SL. Changes in tibiofemoral forces due to variations in muscle activity during walking. Journal of Orthopaedic Research. 2014; 32: 769-776.
[178] Wang H, Chen T, Koff MF, Hutchinson ID, Gilbert S, Choi D, *et al.* Image based weighted center of proximity versus directly measured knee contact location during simulated gait. Journal of biomechanics. 2014; 47: 2483-2489.
[179] Liukkonen MK, Mononen ME, Vartiainen P, Kaukinen P, Bragge T, Suomalainen J-S, *et al.* Evaluation of the effect of bariatric surgery-induced weight loss on knee gait and cartilage degeneration. Journal of Biomechanical Engineering. 2018; 140: 041008-041019.
[180] Shu L, Yamamoto K, Yoshizaki R, Yao J, Sato T, Sugita N. Multiscale finite element musculoskeletal model for intact knee dynamics. Computers in Biology and Medicine. 2022; 141: 105023-105035.
[181] Julkunen P, Kiviranta P, Wilson W, Jurvelin JS, Korhonen RK. Characterization of articular cartilage by combining microscopic analysis with a fibril-reinforced finite-element model. Journal of biomechanics. 2007; 40: 1862-1870.
[182] Adouni M, Shirazi-Adl A. Evaluation of knee joint muscle forces and tissue stresses-strains during gait in severe OA versus normal subjects. Journal of Orthopaedic Research. 2014; 32: 69-78.
[183] Halonen K, Dzialo CM, Mannisi M, Venäläinen M, de Zee M, Andersen MS. Workflow assessing the effect of gait alterations on stresses in the medial tibial cartilage-combined musculoskeletal modelling and finite element analysis. Scientific Reports. 2017; 7: 17396.

[184] Shi X, Chen Z, Wang H, Yeung D-Y, Wong W-K, Woo W-c. Convolutional LSTM network: A machine learning approach for precipitation nowcasting. Advances in neural information processing systems. 2015; 28: 1-9.
[185] García-Pinillos F, Latorre-Román PÁ, Ramírez-Campillo R, Párraga-Montilla JA, Roche-Seruendo LE. How does the slope gradient affect spatiotemporal parameters during running? Influence of athletic level and vertical and leg stiffness. Gait & posture. 2019; 68: 72-77.
[186] Koblbauer IF, van Schooten KS, Verhagen EA, van Dieën JH. Kinematic changes during running-induced fatigue and relations with core endurance in novice runners. Journal of Science and Medicine in Sport. 2014; 17: 419-424.
[187]Borg G. Borg's perceived exertion and pain scales. Human kinetics. 1998.
[188] Matsas A, Taylor N, McBurney H. Knee joint kinematics from familiarised treadmill walking can be generalised to overground walking in young unimpaired subjects. Gait & posture. 2000; 11: 46-53.
[189] Enoksen E, Tjelta AR, Tjelta LI. Distribution of training volume and intensity of elite male and female track and marathon runners. International Journal of Sports Science & Coaching. 2011; 6: 273-293.
[190] Homyk A, Orsi A, Wibby S, Yang N, Nayeb-Hashemi H, Canavan PK. Failure locus of the anterior cruciate ligament: 3D finite element analysis. Computer methods in biomechanics and biomedical engineering. 2012; 15: 865-874.
[191] Song Y, Cen X, Chen H, Sun D, Munivrana G, Bálint K, *et al.* The influence of running shoe with different carbon-fiber plate designs on internal foot mechanics: A pilot computational analysis. Journal of Biomechanics. 2023; 153: 111597-111604.
[192] Chen TL-W, Wang Y, Peng Y, Zhang G, Hong TT-H, Zhang M. Dynamic finite element analyses to compare the influences of customised total talar replacement and total ankle arthroplasty on foot biomechanics during gait. Journal of Orthopaedic Translation. 2023; 38: 32-43.
[193] Strohrmann C, Harms H, Kappeler-Setz C, Troster G. Monitoring kinematic changes with fatigue in running using body-worn sensors. IEEE transactions on information technology in biomedicine. 2012; 16: 983-990.
[194] Rueterbories J, Spaich EG, Andersen OK. Gait event detection for use in FES rehabilitation by radial and tangential foot accelerations. Medical engineering & physics. 2014; 36: 502-508.
[195] Khandelwal S, Wickström N. Gait event detection in real-world environment for long-term applications: Incorporating domain knowledge into time-frequency analysis. IEEE Transactions on Neural Systems and Rehabilitation Engineering. 2016; 24: 1363-1372.
[196] Winiarski S, Rutkowska-Kucharska A, Kowal M. Symmetry function–An effective tool for evaluating the gait symmetry of trans-femoral amputees. Gait & posture. 2021; 90: 9-15.
[197] Fraser AM, Swinney HL. Independent coordinates for strange attractors from mutual information. Physical review A. 1986; 33: 1134.
[198] Kennel MB, Brown R, Abarbanel HD. Determining embedding dimension for phase-space reconstruction using a geometrical construction. Physical review A. 1992; 45: 3403.
[199] Xiang L, Mei Q, Wang A, Shim V, Fernandez J, Gu Y. Evaluating function in the hallux valgus foot following a 12-week minimalist footwear intervention: A pilot computational analysis. Journal of Biomechanics. 2022; 132: 110941-110950.
[200] Li L, Yang L, Zhang K, Zhu L, Wang X, Jiang Q. Three-dimensional finite-element analysis of aggravating medial meniscus tears on knee osteoarthritis. Journal of Orthopaedic Translation. 2020; 20: 47-55.

[201] LeRoux MA, Setton LA. Experimental and biphasic FEM determinations of the material properties and hydraulic permeability of the meniscus in tension. J. Biomech. Eng. 2002; 124: 315-321.
[202] Li G, Lopez O, Rubash H. Variability of a three-dimensional finite element model constructed using magnetic resonance images of a knee for joint contact stress analysis. J. Biomech. Eng. 2001; 123: 341-346.
[203] Weiss ND. Knee Ligaments: Structure, Function, Injury, and Repair. The Yale journal of biology and medicine. 1991; 64: 194.
[204] Song Y, Debski RE, Musahl V, Thomas M, Woo SL-Y. A three-dimensional finite element model of the human anterior cruciate ligament: a computational analysis with experimental validation. Journal of biomechanics. 2004; 37: 383-390.
[205] Gabriel MT, Wong EK, Woo SLY, Yagi M, Debski RE. Distribution of in situ forces in the anterior cruciate ligament in response to rotatory loads. Journal of Orthopaedic Research. 2004; 22: 85-89.
[206] Pena E, Calvo B, Martinez M, Doblare M. A three-dimensional finite element analysis of the combined behavior of ligaments and menisci in the healthy human knee joint. Journal of biomechanics. 2006; 39: 1686-1701.
[207] Griffin NL, Richmond BG. Cross-sectional geometry of the human forefoot. Bone. 2005; 37: 253-260.
[208] Arndt A, Ekenman I, Westblad P, Lundberg A. Effects of fatigue and load variation on metatarsal deformation measured in vivo during barefoot walking. Journal of biomechanics. 2002; 35: 621-628.
[209] Shiotani H, Mizokuchi T, Yamashita R, Naito M, Kawakami Y. Acute effects of long-distance running on mechanical and morphological properties of the human plantar fascia. Scandinavian Journal of Medicine & Science in Sports. 2020; 30: 1360-1368.
[210] Perry S, Lafortune M. Influences of inversion/eversion of the foot upon impact loading during locomotion. Clinical biomechanics. 1995; 10: 253-257.
[211] Lafortune M, Cavanagh P, Sommer III H, Kalenak A. Foot inversion-eversion and knee kinematics during walking. Journal of Orthopaedic Research. 1994; 12: 412-420.
[212] Mizrahi J, Verbitsky O, Isakov E. Fatigue-related loading imbalance on the shank in running: a possible factor in stress fractures. Annals of biomedical engineering. 2000; 28: 463-469.
[213] Gerlach KE, White SC, Burton HW, Dorn JM, Leddy JJ, Horvath PJ. Kinetic changes with fatigue and relationship to injury in female runners. Medicine and science in sports and exercise. 2005; 37: 657-663.
[214]Hay J. The biomechanics of sports techniques. Prentice-Hall. 1978.
[215] García-Pérez JA, Pérez-Soriano P, Llana S, Martínez-Nova A, Sánchez-Zuriaga D. Effect of overground vs treadmill running on plantar pressure: Influence of fatigue. Gait & posture. 2013; 38: 929-933.
[216] Anderson KG, Behm DG. Maintenance of EMG activity and loss of force output with instability. The Journal of Strength & Conditioning Research. 2004; 18: 637-640.
[217] Piorek M. Chaotic properties of gait kinematic data. *In* Computer Information Systems and Industrial Management: 14th IFIP TC 8 International Conference, CISIM 2015, Warsaw, Poland, September 24-26, 2015, Proceedings 14. Springer. 2015. 111-119.
[218] Gates DH, Dingwell JB. Comparison of different state space definitions for local dynamic stability analyses. Journal of Biomechanics. 2009; 42: 1345-1349.
[219] Granata K, Gottipati P. Fatigue influences the dynamic stability of the torso. Ergonomics. 2008;

51: 1258-1271.
[220] Dingwell JB, Cusumano JP. Nonlinear time series analysis of normal and pathological human walking. Chaos: An Interdisciplinary Journal of Nonlinear Science. 2000; 10: 848-863.
[221] Yoshino K, Motoshige T, Araki T, Matsuoka K. Effect of prolonged free-walking fatigue on gait and physiological rhythm. Journal of biomechanics. 2004; 37: 1271-1280.
[222] Asgari N, Sanjari MA, Esteki A. Local dynamic stability of the spine and its coordinated lower joints during repetitive Lifting: Effects of fatigue and chronic low back pain. Human movement science. 2017; 54: 339-346.
[223] Xiang L, Gu Y, Wang A, Mei Q, Yu P, Shim V, *et al.* Effect of foot pronation during distance running on the lower limb impact acceleration and dynamic stability. Acta of Bioengineering & Biomechanics. 2022; 24: 21-31.
[224] Jordan K, Challis JH, Newell KM. Long range correlations in the stride interval of running. Gait & posture. 2006; 24: 120-125.
[225] Lindsay TR, Noakes TD, McGregor SJ. Effect of treadmill versus overground running on the structure of variability of stride timing. Perceptual and motor skills. 2014; 118: 331-346.
[226] Willson J, Ratcliff O, Meardon S, Willy R. Influence of step length and landing pattern on patellofemoral joint kinetics during running. Scandinavian Journal of Medicine & Science in Sports. 2015; 25: 736-743.
[227] Dudley RI, Pamukoff DN, Lynn SK, Kersey RD, Noffal GJ. A prospective comparison of lower extremity kinematics and kinetics between injured and non-injured collegiate cross country runners. Human movement science. 2017; 52: 197-202.
[228] Brown AM, Zifchock RA, Hillstrom HJ. The effects of limb dominance and fatigue on running biomechanics. Gait & posture. 2014; 39: 915-919.
[229] DeFrate LE, Papannagari R, Gill TJ, Moses JM, Pathare NP, Li G. The 6 degrees of freedom kinematics of the knee after anterior cruciate ligament deficiency: an in vivo imaging analysis. The American journal of sports medicine. 2006; 34: 1240-1246.
[230] Zhang X, Li J, Ren C, Zhang P, Zeng Y, Zhang R, *et al.* Periodical assessment of four horns of knee meniscus using MR T2 mapping imaging in volunteers before and after amateur marathons. Scientific Reports. 2022; 12: 12093-12103.
[231] Guess TM, Razu S, Jahandar H, Stylianou A. Predicted loading on the menisci during gait: The effect of horn laxity. Journal of biomechanics. 2015; 48: 1490-1498.
[232] Wan C, Hao Z, Wen S. The effect of the variation in ACL constitutive model on joint kinematics and biomechanics under different loads: a finite element study. Journal of Biomechanical Engineering. 2013; 135: 041002-041011.
[233] Xiang L, Gu Y, Wang A, Shim V, Gao Z, Fernandez J. Foot Pronation Prediction with Inertial Sensors during Running: A Preliminary Application of Data-Driven Approaches. Journal of Human Kinetics. 2023; 87: 29-40.
[234] Powers CM, Witvrouw E, Davis IS, Crossley KM. Evidence-based framework for a pathomechanical model of patellofemoral pain: 2017 patellofemoral pain consensus statement from the 4th International Patellofemoral Pain Research Retreat, Manchester, UK: part 3. British journal of sports medicine. 2017; 51: 1713-1723.
[235] Briani RV, Pazzinatto MF, Silva DDO, Azevedo FM. Different pain responses to distinct levels of physical activity in women with patellofemoral pain. Brazilian Journal of Physical Therapy. 2017; 21: 138-143.

[236] James SL, Bates BT, Osternig LR. Injuries to runners. The American journal of sports medicine. 1978; 6: 40-50.
[237] Fulkerson JP. Diagnosis and treatment of patients with patellofemoral pain. The American journal of sports medicine. 2002; 30: 447-456.
[238] Dos'Santos T, Bishop C, Thomas C, Comfort P, Jones PA. The effect of limb dominance on change of direction biomechanics: A systematic review of its importance for injury risk. Physical therapy in sport. 2019; 37: 179-189.